Department of Precision and Microsystems Engineering

Actuator optimization for flatness correction of deformed surfaces

Sahil D. Bagwe

Report no	: 2022.058
Coach	: Dr. Ir. Matthijs Langelaar, Ir. Arnoud Delissen
Professor	: Dr. Ir. Matthijs Langelaar
Specialisation	: Structural Optimization Mechanics (SOM)
Type of report	: MSc. Thesis
Date	: September 28, 2022

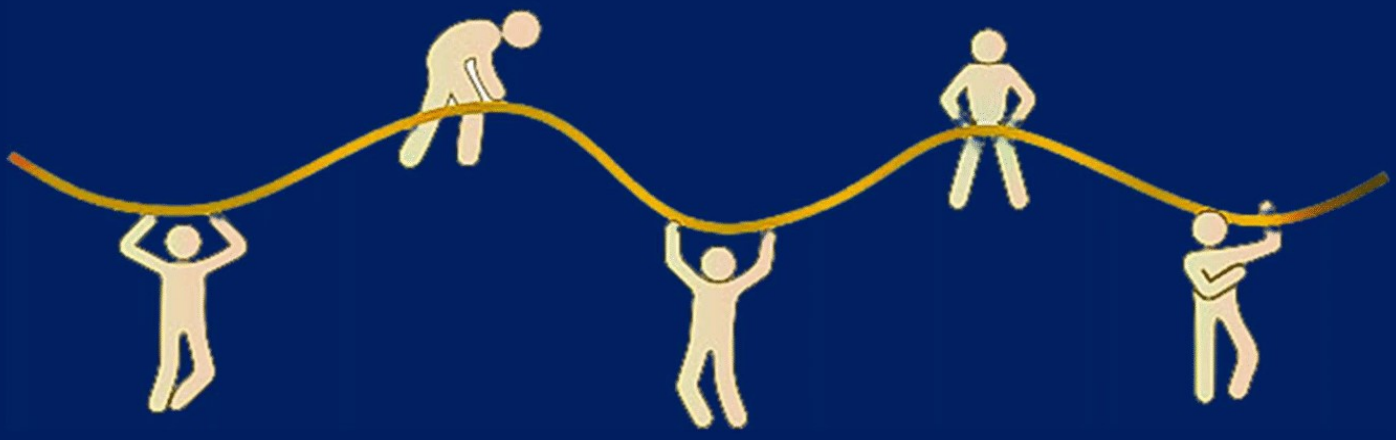

Actuator optimization for flatness correction of deformed surfaces

Structural optimization of the Advanced Long range Piezoelectric Wafer Stage (ALP-WS)

Master's Thesis
by

Sahil Dattatray Bagwe

in partial fulfilment of the requirements for the degree of Master of Science at Delft University of Technology,
to be defended publicly on September 28, 2022 - Wednesday at 0900 hrs.

Faculty of Mechanical, Maritime and Materials Engineering (3mE)

Student Number:	5264995
Project Duration:	July 19, 2021 - September 28, 2022
Thesis Committee:	Dr. Ir. Matthijs Langelaar (TU Delft)
	Ir. Arnoud Delissen (TU Delft)
	Dr. Hans Goosen (TU Delft)
	Dr. Ir. Micha Steur (ASML)
	Ir. Ron de Bruijn (ASML)

TU Delft ASML

उद्धरेदात्मनात्मानं नात्मानमवसादयेत्।
आत्मैव ह्यात्मनो बन्धुरात्मैव रिपुरात्मनः॥

Elevate yourself through your own efforts, and not degrade yourself. For, the mind can be the friend and also the enemy of the self.

-Bhagavad Gita Chapter 6, verse 5

ABSTRACT

By 2030, the global semiconductor industry is projected to hit the valuation of becoming a trillion-dollar industry. Advancements in electronic devices have gave rise to tougher requirements thereby requiring the manufacturers to push the limits of consistency. This has lead to a need to enhance the accuracy of the chip manufacturing process. ASML is the leading supplier of lithography systems that are used for the production of these advanced chips. Wafer flatness is one of the primary prerequisites for attaining high accuracy in integrated circuit manufacturing. The high accuracy is achieved by incorporating optical lithography in the development of circuits with small feature sizes. The current lithography machine requires precise estimation of wafer flatness on a sub-nanometer scale for the elimination of deviations between the exposed region and the plane of focus.

In this thesis, the point of focus is on the short stroke positioning system of a lithography machine. The short stroke positioning system is responsible for accurately placing the wafer to its desired location. The critical aspect of flatness is interpreted by performing scanning operations on a wafer table surface. These operations provide an estimation of the types of deformations the wafer is subjected to. The wafer table acts as a wafer carrier, which undergoes lithography operations. Therefore, it becomes very critical to examine the nature of the wafer table. After performing scans for surface deformations, an optimization problem is formulated which involves placing piezoelectric actuators under the wafer table. The role of the piezoelectric actuators is to correct the wafer table thereby enhancing its flatness property.

Through this research, the optimization yields to give a better estimation of flatness by placement of actuators. The problem formulation and the solution proposed are able to correct the flatness by approximately 95% of the initial deformation value. The work done in this research can be extended from an application point of view and can be utilized in estimating and correcting the deformations of any given structure. Since this research involved working in a 2-dimensional domain, the further implications of this research involve extending the proposed flatness correction technique to a 3-dimensional domain.

ACKNOWLEDGEMENT

This thesis was done in collaboration between the Department of Precision and Microsystems Engineering at the Delft University of Technology and the Mechatronics and Control group at the Research department at ASML. It has been written to fulfill the graduation requirements of the Master of Science in Mechanical Engineering at the Delft University of Technology.

This thesis concludes my time as a master's student at the Delft University of Technology. The two years of my student life in the Netherlands have been a humdinger of a journey where I take back some amazing connections of professionals and friends along with a graduation degree.

To start with, I would like to thank Matthijs Langelaar and Arnoud Delissen for allowing to take up this project and do my graduation thesis at ASML. Their advice, feedback, and support have helped me to push myself a bit harder and make this project a reality. A special mention to Arnoud for his time and patience throughout the year, be it solving my errors or encouraging me to explore more. I would also like to thank Micha Steur and Ron de Bruijn from ASML for their close involvement and for providing me with counsel and good advice. Both Micha and Ron made sure that there were no delays in getting my doubts solved and also made sure the administrative part at ASML was carried out smoothly. I hope I didn't take much time from Arnoud and Ron who were also doing their Ph.D. at TU Delft and ASML respectively around the same time.

I would also like to thank my friends who have been a part of my ups and downs of this memorable journey. Back in the year, I happened to dislocate my shoulder. This was one of the most difficult time in my Master's education, a big Thanks to all the people who were with me during that time, who helped me get out of that challenging phase.

Finally, I would like to express my gratitude to my parents and my little sister for standing by my side and supporting my decision to pursue my Master's education in a foreign land during the difficult times of the pandemic. This would not have been possible without them. I am taking back more than just a degree, something that will remain with me for the rest of my life.

Enjoy the read.

- S. D. Bagwe
Delft, June 2022

NOMENCLATURE

SYMBOLS

f_o	Optimization objective
ρ_e	Element density (Design variable)
E	Young's Modulus
p	Penalty factor
ρ_c	Density of Cordierite
$\rho_s c$	Density of Silicon Carbide
f_c	Compliance objective
f_{ef}	Eigenfrequency objective
w_c	Multi-objective weight - Compliance
w_{ef}	Multi-objective weight - Eigenfrequency
$\mathbf{K}$	Stiffness Matrix
$\mathbf{u}$	Displacement vector
$\mathbf{f}$	Load vector
$\mathbf{M}$	Mass Matrix
λ	Eigenvalue
ω	Eigenfrequency (rad/s)
v_f	Volume fraction
m_{max}	Maximum weight of Intermediate body
Δx_n	LSF incrementor
ΔZ_i	Deformation error of sampling point
y_{max}	Maximum deformation amplitude
w_{ef}	Multi-objective weight - Eigenfrequency
K^k	Distance between two nodes
x^k	Distance of intermediate point from one node
F_a	Actuator force
η, ξ	Natural coordinates
l_i	Actuator distance (Design variable)
F_i	Actuator force (Design variable)
F_{max}	Maximum actuator force
F_m	Middle actuator
A, B, C, D	Actuator location reference (2 actuators per half)
X, Y, Z, W	Actuator location reference (3 actuators per half)

ABBREVIATIONS

TO	Topology Optimization
InB	Intermediate Body
WT	Wafer Table
W	Wafer
WS	Wafer Stage
SO	Structural Optimization
SQP	Sequential Quadratic Programming
MMA	Method of Moving Asymptotes
FEM	Finite Element Method
SIMP	Solid Isotropic Material with Penalization
LSF	Local Surface Flatness
MZ	Minimum Zone
DUV	Deep ultraviolet
EUV	Extreme ultraviolet

List of Figures

List of Tables

CONTENTS

1

INTRODUCTION

Smart structure design is a novel engineering discipline aiming at incorporating active members like sensors, actuators, and control circuit elements into a single system, thereby enabling it to respond to environmental changes [1]. Smart structures have played an important role in improving the performance of applications in fields such as aerospace engineering, automobile manufacturing, precision instruments and machineries, and so on. The potential advantages of smart structures have drawn the attention of the semiconductor industry to improve chip performance at sub-micron-level precision. ASML is the leading supplier of lithography systems in the semiconductor industry. A lithography machine includes a wafer stage system comprising of a light source, reticle handler, lens, wafer handler, metrology frame, long stroke system, and short stroke system. The architecture of a dual-stage wafer machine is shown schematically in Figure 1.1.

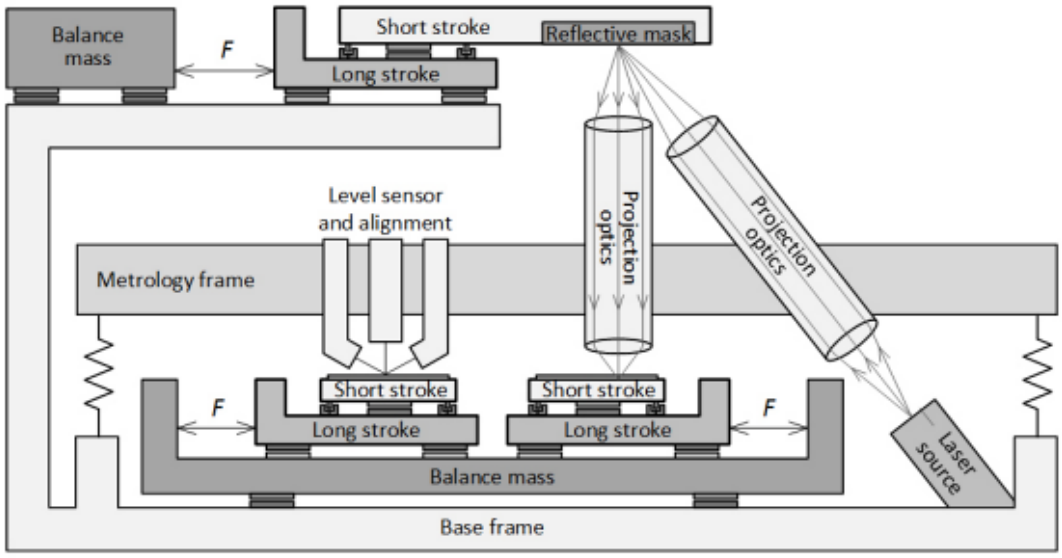

Figure 1.1: Dual-stage wafer system architecture | *Image adapted from [2]*

The photolithography process includes either shifting of the light source or motion of the wafer stages. Due to the high-cost factor encountered in the movement of the light source, it is kept constant and the wafer stage is set to motion. The light source emits laser light on the wafer surface which records a height map of the entire domain. If a fluctuation is encountered in the height map recordings, the wafer is adjusted by the actuation of actuators. The actuators are active members of a machine and are responsible for the positioning of the wafer table. A long stroke and a short stroke system carry the silicon wafer and are responsible for the movement of the wafer stage subsystem. The long stroke system is responsible for coarse positioning of the wafer stage with an accuracy of micrometers. A short stroke system is responsible for its fine positioning with an accuracy of nanometers. It positions the wafer stage to the desired area which is to be illuminated by the light source. A wafer stage is a 6 DoF positioning system consisting of active

components like leveling and alignment sensors, positioning actuators, fine positioning body, wafer table, and wafer. The motion of the fine positioning body ensures that the desired surface on a wafer is illuminated by the light source. The role of the actuators is to not only locate the wafer to the desired position but also correct any deviations recorded on the height map of the top surface.

Flatness is a critical parameter when handling silicon wafers. The measurement of surface flatness becomes an essential process for both wafer and device manufacturers. Scanning probe instruments are promising tools for measuring large flat surfaces. ASML's wafer-scanners are based on the scanning concept in which both the wafer and the reticle move relative to a stationary light stripe on which the demagnifying lens of the wafersteppers is attached. The scanning of the surface occurs by exposing a part of the wafer to a slit. This is referred to as site/local flatness, where a small part of the entire domain is considered and the surface error of that site domain is recorded. If the wafer is deformed, the scanning data records the error, which is the difference between the exposed warped surface and the flat scanning surface [3]. A deformed wafer surface causes erroneous imprinting on the wafer resulting in *"Overlay errors"*. Overlay is defined as the relative position of any pattern layer with respect to other layers [4]. Overlay errors affect both the electrical properties of the contacts and the insulation, potentially resulting in short circuits [4].

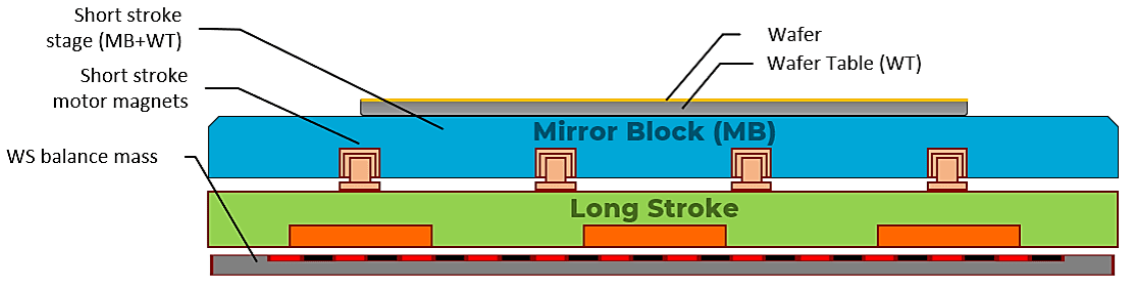

(a) Electro-magnetic wafer stage concept

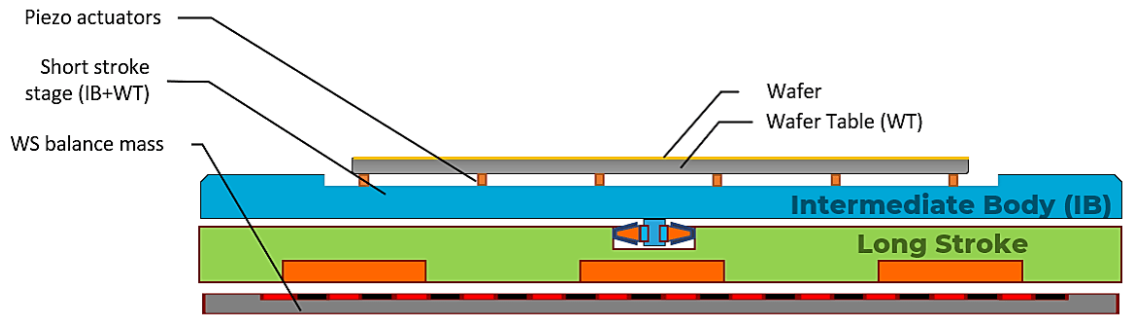

(b) Piezoelectric wafer stage concept

Figure 1.2: Comparison of the wafer stage architecture

The current wafer stage includes a dual-stage concept with electromagnetic actuators for wafer positioning, as shown in Figure 1.2a. Considering the sub-nanometer resolution, the electromagnetic actuated stage do not compensate for finer adjustments of the wafer table. It includes the motion of a long stroke system for coarse positioning, and a short stroke system for fine positioning. In order to obtain finer resolution in the positioning of the wafer table, piezoelectric actuators are incorporated into the wafer stage system as shown in Figure 1.2b. The design consists of actuators which account for finer displacements of the wafer table in addition to a long stroke and a short stroke system displacements. As previously mentioned, the role of the piezoelectric actuators is not only to position the wafer table but also to maintain top surface flatness of the wafer table.

A PROBLEM STATEMENT

The objective of this thesis is to perform structural optimization of the short stroke system with a focus on topology optimization (TO) of the fine positioning body (intermediate body). This is then followed by the next objective of flatness correction of the wafer table by optimizing for the actuator positions and also their corresponding forces. For optimal exposure, the wafer table is aimed to be perfectly flat during exposure. However, in actual case, the wafer table is never perfectly flat due to irregularities, deformations, manufacturing tolerances, and so on. Manufacturing defects are the fundamental reason for the occurrence of irregularities on a wafer table. Since these irregularities get transferred to the wafer resulting in handling and process issues, it is critical to further reduce these irregularities. During wafer operations, they can further propagate leading to internal residual stress resulting in wafer cracking.

The structural optimization of the intermediate body includes the formulation of a topology optimization problem. The optimization objective is to perform multi-objective optimization with compliance and eigenfrequency as the objective functions. The intermediate body must adhere to the weight and eigenfrequency requirements, also the volume of the structure must be restricted within a specified bounding box.

Another important problem statement addressed in this thesis includes the determination of actuator locations under the wafer table. The actuators act as interacting components between the intermediate body and the wafer table, wherein the wafer table is subjected to deformations. The objective is to determine the optimal location of actuators on the intermediate body to minimize the deformations of the top surface of the wafer table, thereby attaining a globally flat surface for the wafer to be positioned on.

B RESEARCH GOALS

From the problem statement mentioned in Section A, the main research aim of this thesis is defined as the following:

To design the intermediate body of a short stroke system and optimize for actuator placement under the wafer table to ensure global flatness of the top surface.

The implementation of the optimizations for structural design and actuator position is carried out in a 2-dimensional domain. To achieve the defined research goal, it has been divided into smaller research objectives that are defined as the following:

1. **Topology optimization of intermediate body**

   The optimization is aimed at estimating the stable dynamic performance of the structure. This goal involves implementing topology optimization involving multi-objective formulation with compliance and eigenfrequency as the objectives. The formulation of the problem involves mass, and eigenfrequency as constraints to the optimization.
   Assumption:
   The effect of self weight of the structure on the design outcome is not considered in this optimization.

2. **Scanning of deformed surfaces and recording scanning error**

   The second goal involves an analysis of the flatness property of a deformed surface by performing surface scanning. The scanning data is to be stored based on an in-plane incremental motion of a surface scanning slit over the entire domain. The recorded errors of the surface will include the implementation of global scanning and local scanning methods.
   Assumption:
   The wafer is considered to not have any deformations and is assumed to have a shape that matches the top surface of the wafer table.

3. **Optimization of deformed surface to attain global flatness with actuator placement**

   The third goal involves estimating the location and force of the actuators based on the errors recorded. The objective here will be to optimize the actuator location and force that can be applied to the wafer table. The motive of the optimization is to attain a globally flat surface.
   Assumption:
   The wafer table is to be mounted on the top of the intermediate body. However, in this optimization, it is assumed that the intermediate body is infinitely stiff. Also, the actuators are modelled such that they apply vertical force only.

C READER'S GUIDE

The thesis outline consists of five chapters that are aligned in accordance with the research goals addressed in Section B. Chapter 2 includes topology optimization of the intermediate body. The design domain of the structure along with the necessary boundary conditions is defined in this chapter. This chapter includes structural optimization of the structure as per the objective and constraint formulations.

Furthermore, the surface scanning algorithm is discussed in detail in Chapter 3. It focuses on scanning the top surface of the wafer table subjected to deformations, and recording the scanning data over over the entire domain. The surface deformations are quantified by incorporating 2 scanning algorithms, which are discussed here in detail. The scanning algorithms provides data useful for estimating local and global surface flatness. A peak to base algorithm is implemented to achieve information of the global flatness of the surface. Further, the actuator locations are varied over the entire domain to record their effect on the surface flatness. Based on the readings obtained from the scanning algorithm and global flatness algorithm, the location of the actuators are defined to correct the deformations that were initially recorded.

Next, Chapter 4 includes a study of the behavior of the surface flatness by defining an optimization problem to find the optimum actuator properties. The flatness correction of the top surface is achieved by optimizing the actuator location and its applied force. The actuator force optimization is carried out simultaneously with location optimization with an intent of achieving optimum global flatness.

Finally, the concepts implemented in the mentioned chapters and the results obtained are summarized in Chapter 5, which includes conclusions drawn based on the obtained results. Further, the chapter includes recommendations for future research to extend the implementations of the study in a three-dimensional domain.

2

TOPOLOGY OPTIMIZATION

In this chapter, the basic building blocks of topology optimization are covered in detail. It entails the implementation of topology optimization concepts in the structural design of an intermediate body. The second section of this chapter includes thee problem definition of the structure wherein the objective and constraints are briefly defined. The chapter concludes with a discussion of model specifics and the optimization results, which is then followed by a short discussion of the results. The final chapter includes conclusions drawn from the optimization.

A INTRODUCTION

The inclusion of structural optimization in the design phase play a critical role in enhancing its structural properties. The optimization method seeks to find the optimum solution when the design domain is subjected to a defined objective, boundary conditions, and constraints. The process of finding an optimal solution undergoes an iterative design process depending on the chosen performance criteria. A standard structural optimization problem is represented as:

$$\mathrm{SO} = \begin{cases} \text{minimize } f_0(\mathbf{x}) \text{ with respect to } \mathbf{x} \\ \text{subject to} \begin{cases} \text{design constraints on } \mathbf{x} \\ \text{equilibrium constraints} \end{cases} \end{cases} \tag{2.1}$$

where f_0 is a minimization objective function, $\mathbf{x}$ act as a design variable that define the objective function. The optimization process entails specifying a set of constraints that must be satisfied during the optimization cycle as a function of the design parameters. The concept of structural optimization is subdivided into three major categories: shape optimization, sizing optimization, and topology optimization; as shown in Figure 2.1 [4].

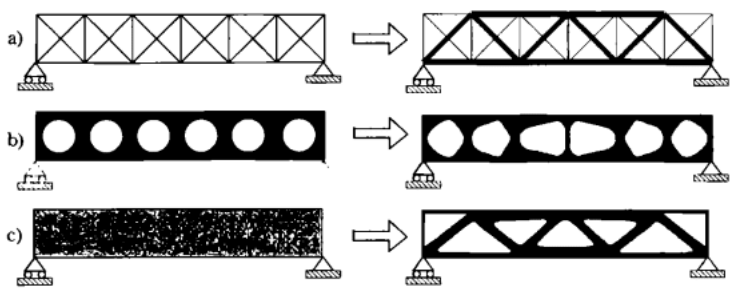

Figure 2.1: Structural Optimization Categories - a) Sizing, b) Shape, c) Topology | *Image adapted from [4]*

The purpose of a common size problem is to identify the best thickness distribution over a structure's domain. Whereas, shape optimization identifies the shape of a structure, which is the design variable in the optimization procedure. The number, placement, and form of holes, as well as the domain's connectivity are all factors to consider while optimizing the topology of solid structures

[4]. A standard topology optimization problem includes having density of each element ρ_e as an optimizing parameter which affects the stiffness of the structure. During optimization, the element densities are adjusted to represent either a solid $(\rho_e = 1)$ or void $(\rho_e = 0)$ material, resulting in an optimized solution with improved performance of the structure. As shown in Figure 2.1, the sizing, and shape optimization require a starting point to make the objective converge to a possible optimal solution, whereas topology optimization just requires a definition of a blank design space.

The potential of topology optimization can only be realized by employing gradient-based optimization which reduces computing effort by orders of magnitude while allowing for fine design resolution [5]. The gradient based approaches require sensitivities of the response functions with respect to the design variables. The purpose of employing sensitivities is to limit the number of function evaluations based on estimation of how the objective function is affected by a minimal variation of the design variable. The gradient-based approaches ensure smooth, differential problems that can be efficiently solved using optimality criteria, Sequential Quadratic Programming (SQP), steepest descent method, and Method of Moving Asymptotes (MMA) [6]. In this project, the density-based approach in combination with the MMA optimization routine has been used.

Density-based approach is the most commonly used method for solving a structural optimization problem. The design domain is modeled using a finite element method (FEM), wherein the design domain is discretized into small elements. Here, each element carries an identity wherein the density of an element is the design variable in the optimization. During an optimization cycle, each element's displacement and stress gradient are calculated, and the new design of the structure is based on the constraints and design sensitivities. The sensitivity analysis is performed at each iteration to determine the influence of the element density on the objective function and the constraints, after which the element densities are changed until a final convergence is achieved [4]. The final converged solution includes elements that carry either 0 (void) or 1 (solid) material density value. The *SIMP* (Solid Isotropic Material Penalization) [7] approach ensures that the elements which are assigned intermediate density values are penalized with a penalty factor to attain either 0 or 1 state. The penalization of the elements is based on the power law, as shown in Equation 2.2.

$$E_e = (\rho_e)^p E_o; \quad 0 \leq \rho_e \leq 1 \tag{2.2}$$

In order to avoid a singular system matrix, Equation 2.2 can be modified to Equation 2.3.

$$0 \leq \rho_{min} \leq \rho_e \leq 1 \tag{2.3}$$

where ρ_e is the design density of an element that acts as a variable, and p is the penalizing factor. The Young's modulus is defined with E_0, and penalization is applied to ρ_e. Here, E_e is the Young's modulus of a single element which depends on density of the element. In order to bound the Young's modulus between limits, the element density is bounded between ρ_{min} and 1, where the value of ρ_{min} is assigned a very small value. If the density is bounded between 0 and 1, then the element with 0 density will have the Young's modulus E_e to be zero. This will cause the problem of singular matrix.

The SIMP method stated above generates a non-existential design, wherein the elements are connected with nodular contact with each other leading to checkerboard pattern. Another design problem includes generation of a perforated structure with excess number of holes leading to complications in the obtained model. When a finer finite element mesh is used in computational implementations, this impact causes numerical instability where a higher number of holes are generated leading to mesh-dependent models. To avoid this, filtering methods are used wherein the user sets a threshold value, which creates a convolution kernel, and the values outside the convolution kernel are deleted. 1) Density Filtering, 2) Sensitivity Filtering, and 3) Greyscale Filtering are the three most prevalent filtering methods employed in structural optimization [8]. This work uses penalization along with the implementation of density filtering. A SIMP method is implemented on the structure as the optimal solution is found using a gradient based MMA optimizer.

The MMA optimizer includes gradient based approach to systematically discover the best solution for the optimization problem. For each iteration, the MMA optimizer generates an approximated

sub-problem. The sub-problem is mostly dependent on gradient information, but it also relies on the 'moving asymptotes' which are a collection of parameters that are modified with each iteration. During this optimization, the move limit of the optimizer was set to 0.1, and the convergence tolerance was set to 10^{-4} depending on the change in the design variable.

B DESIGN DOMAIN & REQUIREMENTS

The piezoelectric wafer stage architecture, as represented in Figure 1.2b, shows an intermediate body carrying a wafer table, and a wafer. In this thesis, we aim for topology optimization of the intermediate body considering eigenfrequency, and weight constraints. The layout of the intermediate body is schematically shown in Figure 2.2.

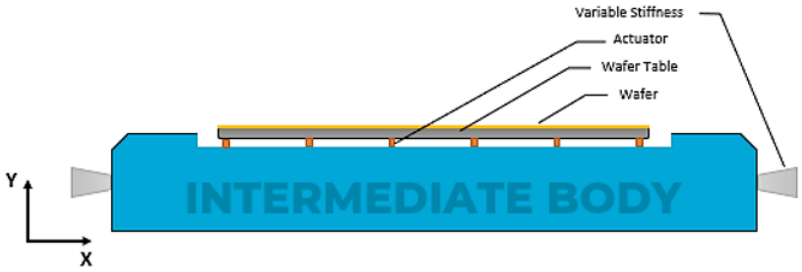

Figure 2.2: Schematic representation of intermediate body

The structure is supported by two variable stiffness components. It consists of piezoelectric actuators mounted on top of it. These actuators support the wafer table, and act as connecting members between the intermediate body and the wafer table. To perform topology optimization, the design domain can be represented, as shown in Figure 2.3.

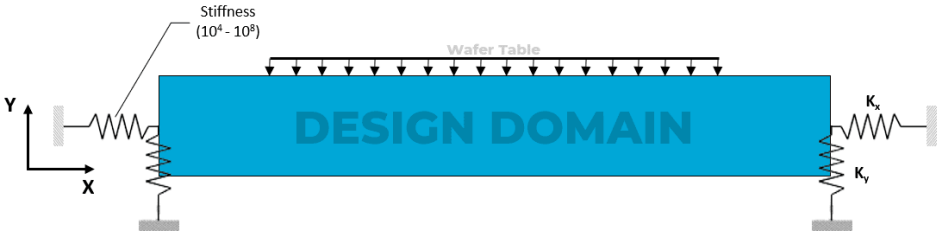

Figure 2.3: Design domain - Topology Optimization

The variable stiffness component is an On/Off state stiffness device with an on-state stiffness of 10^8 N/m and an off-state stiffness of 10^4 N/m. The stiffness component provide a stiffness of $10^4 - 10^8$ N/m in X-direction, and have a high stiffness value of 10^{14} N/m in Y-direction. Since, the actuator locations are not determined, the loading condition of the wafer table is represented with a uniformly distributed load (UDL) as indicated in Figure 2.3. The actuators can be placed at any location in the specified UDL region. Since, there is no information of actuator locations, the region underneath the loading is considered as a non-design domain. Therefore, from the representation, loading of the wafer table is done on a flat top surface of the intermediate body. The intermediate body comprises of a single ceramic material whose material specifications are shown in Table 2.1.

Property	Specification
Modulus of elasticity (E_c) (GPa)	145
Density (ρ_c) (Kg/m^3)	2550
Poisson's Ratio	0.3

Table 2.1: Material specification - Intermediate Body

The intermediate body supports the wafer table through piezoelectric actuators. Therefore, force exerted by the uniformly distributed load is the self-weight of the wafer table. In a 2-dimensional setting, the wafer table is represented by a rectangular plate. The material specifications of the wafer table are shown in Table 2.2. These specifications are used to calculate the force applied by the UDL on the intermediate body.

Property	Specification
Modulus of elasticity E_{sc} (GPa)	380
Density (ρ_{sc}) (Kg/m^3)	3070
Poisson's Ratio	0.18

Table 2.2: Material specification - Wafer Table

In this thesis, the diameter of the wafer table is 310 mm, and the thickness of the wafer table can be changed depending on the requirement as per a weight ratio between the intermediate body and the wafer table. The thickness of the wafer table can be any value ranging from 5 mm to 10 mm depending on the choice specified by the designer. The design requirements of the intermediate body include having the first non-rigid body eigenfrequency greater than 1500 Hz and a bounding volume of $450 \times 450 \times 100$ mm. The mass criteria of the intermediate body includes maintaining the mass ratio between the wafer table and the intermediate body to $1:4$, as represented by Equation 2.4.

$$\frac{WT + W}{InB} = \frac{1}{4} \tag{2.4}$$

Where WT is weight of the wafer table, W is weight of the wafer and InB is weight of the intermediate body. Along with the weight ratio requirement, an additional specification of the design includes, having the approximate total weight of the intermediate body and the wafer table around 8 kg. However, this requirement of the total weight is not a strict constraint but an attempt to meet this requirement is made in this optimization. The weight ratio specified in Equation 2.4 depends on the weight of the intermediate body. The intermediate body acts as a balanced mass which compensates for the vibrations transferred from the long stroke system. These compensations can be utilized to reduce the stroke of the actuators thereby actuating the wafer table in a sub-nanometer level precision. The ratio specification can however be altered to be $1:5$, but this will lead to the change in the weight of the intermediate body and the wafer table, which might ultimately depend on the amount of transmissibility of the disturbances.

C PROBLEM FORMULATION

As shown in Figure 1.2a, the current short stroke system with electromagnetic actuators include a Mirror Block along with a wafer table with a combined weight of 20 kg. The shift to a piezo-actuated wafer stage includes benefits in precision positioning of wafer to the desired location. The design domain and the boundary conditions of the intermediate body are defined in Section B. The weight of the intermediate body is 4 times that of the wafer table. In this optimization, the self weight of the intermediate body is not taken into consideration.

The design of an intermediate body is formulated using a weighted sum approach for multi-objective optimization problem [9] wherein the goal is to minimize the compliance and maximize

the eigenfrequency of the structure. In this formulation, the density of an element is the design variable. The two objectives are aggregated into a single global objective via linear scalarization, as represented in Equation 2.5.

$$\begin{aligned} f_0 &= w_c f_c' + w_{ef} f_{ef}' \\ w_c &+ w_{ef} = 1 \end{aligned} \tag{2.5}$$

In order to incorporate the multi-objective formulation, scaling of the objective functions is required. Here, f_c' and f_{ef}' illustrate scaled value of compliance and eigenfrequency objectives respectively. In this case, the initial objective value was assigned a scaled value of 100, and as the objective value changed through the optimization cycle, the current state objective iteration value was scaled with reference to the initial objective value scaling of 100. In Equation 2.5, w_c is the weight factor of compliance objective, and w_{ef} is the weight factor of eigenfrequency objective. During implementation of weighted sum multi-objective optimization, the sum of all the objective function weights must be equal to 1. The compliance objective formulation is represented in Equation 2.6.

$$\begin{aligned} \min_{\rho_e} \quad & f_c \\ \text{such that: } & f_c = \mathbf{f}^{\mathbf{T}}\mathbf{u} \\ & \mathbf{K}(\rho_e)\mathbf{u} = \mathbf{f} \\ & \kappa = (1-w)\rho_e^p + w\rho_e \\ & \mathbf{K}(\rho_e) = \textstyle\sum_{e=1}^{N} \kappa_e \mathbf{K}_{\mathbf{el}}^{(\mathbf{e})} \end{aligned} \tag{2.6}$$

Here $\mathbf{u}$ and $\mathbf{f}$ are displacement and load vectors respectively. κ is the stiffness scaling factor, $\mathbf{K}$ is the global stiffness matrix, p is the penalty factor ($p = 3$), and ρ_e is density of the element that acts as a design variable. $\mathbf{K_{el}}$ is the element matrix.

The general eigenvalue problem formulation is represented in Equation 2.7.

$$\begin{aligned} \min_{\rho_e} \quad & f_{ef} \\ \text{such that: } & (\mathbf{K}(\rho_e) - \lambda_j \mathbf{M}(\rho_e))\phi_j = 0 \\ & \phi_j^T \mathbf{M}(\rho_e)\phi_k = \delta_{jk} \\ & \mu = \rho_e \\ & \mathbf{M}(\rho_e) = \textstyle\sum_{e=1}^{N} \mu_e \mathbf{M}_{\mathbf{el}}^{(\mathbf{e})} \end{aligned} \tag{2.7}$$

where λ is the eigenvalue of the structure, ϕ represents the eigenmodes, μ is mass scaling factor, $\mathbf{M}$ is the global mass matrix of the structure, and $\mathbf{M_{el}}$ is the element matrix. In this thesis, 4 eigenmodes are considered. Therefore, the value of j and k will range from 1 to 4. Equation 2.7 includes minimization of the eigenvalue subject to state equations of the eigenvalue problem and the mass orthogonality of eigenmodes, respectively. Eigenvalue maximization as an objective function includes optimizing multiple eigenfrequencies simultaneously. If the objective function contains the maximization of a single eigenfrequency, the objective function's sensitivity may be discontinuous, resulting in oscillation and divergence throughout the optimization process. To address this issue, a multi-frequency objective function is defined in Equation 2.8 [10].

$$f_{ef} = \lambda_t + \sum_{i=1}^{N} w_i \left(\sum_{i=1}^{N} \frac{w_i}{\lambda_i(\rho_e) - \lambda_t} \right)^{-1} \tag{2.8}$$

where λ_i is the system's i^{th} eigenvalue and w_i are the associated weighting factors. When all weighting factors are identical, the parameter λ_t decides which value is being optimized. This is done since eigenvalues near to λ_t have the greatest contribution to the objective value λ [10]. The eigenvalue closest to λ_t will be optimized in such instance.

In this thesis, the fundamental eigenfrequency of the structure is to be maximized. In order to do so, the value of λ_t is assigned to be 0. This would mean that, the smallest eigenvalue has greatest contribution to the mean-eigenvalue, thereby optimizing for the smallest eigenvalue. Also,

each eigenvalue is given the same weighting factor, $w_i = 1$. Equation 2.8 can then be represented by the following:

$$f_{ef} = \left(\sum_{i=1}^{N} \frac{1}{\lambda_i(\rho_e)} \right)^{-1} \tag{2.9}$$

Equation 2.9 can be substituted in Equation 2.7 as a minimizing objective function for optimization of the intermediate body.

Equation 2.6 and Equation 2.9 are substituted in the multi-objective function stated in Equation 2.5. The minimization of the multi-objective function depends on the weights of compliance and eigenfrequency functions represented by w_c and w_{ef} respectively. In order to check the effect of objective functions weights on the results, the optimization problem was solved by varying the weights and recording the response obtained after convergence. A graphical representation of the results is shown in Figure 2.4, where the effect of weight on compliance and eigenfrequency objective is plotted.

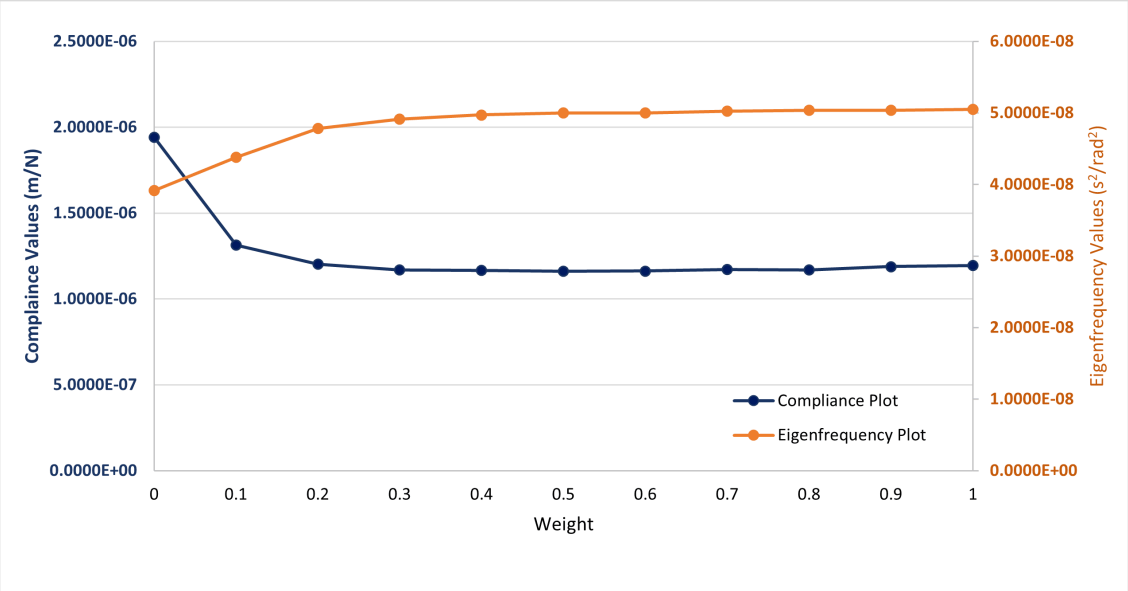

Figure 2.4: Effect of weight in the multi-objective formulation

Figure 2.4 represents the behaviour of compliance and eigenfrequency objectives with their corresponding change of weights. As previously mentioned, during a weighted multi-objective optimization cycle, the summation of weights of the objective functions must be equal to 1. The data obtained from Figure 2.4 show that the value of the objective functions does not change when the weight of the compliance function increases from 0.4 to 1. This trend occurs as a result of the mass constraint and also due to scaling issues of the objective functions, wherein one objective dominates the optimization cycle. The effect of weights on compliance and eigenfrequency, along with a brief discussion on the scaling issues is shown in Appendix A. To tackle the issues of scaling functions, ϵ-constraint method is implemented wherein, the objective of compliance minimization is considered and the eigenfrequency objective is converted into a constraint thereby restricting it to a user-specific eigenfrequency requirement [11]. Here, an eigenfrequency constraint is formulated to satisfy the eigenfrequency requirement of ($\lambda_1 \geq 1500$ Hz) of the structure. The final problem definition includes compliance minimization as an objective function as represented in Equation 2.6.

The intermediate body must satisfy certain requirements on eigenfrequency and weight properties of the structure. In order to achieve this, necessary constraints must be assigned to the optimization problem. During optimization, the optimum solution will be found by continually modifying the design variables until the minimum value objective function is computed, while it is still subjected to the constraints. The two constraints imposed in the optimization are:

1. **Eigenfrequency Constraint** (c_1)
   The equation of the eigenfrequency constraint is as per the lower bound formulation, wherein a scalar variable ω_{min} acts a lower bound [12]. The bound formulation is implemented on the constraint to avoid issues of eigenfrequency multiplicity. The formulation is represented in Equation 2.10.
   $$\omega_{min} - \omega_j \leq 0 \tag{2.10}$$
   In this optimization, ω_{min} refers to the minimum required eigenfrequency i.e. ($\omega_{min} = 2\pi\lambda_{min}$) rad/sec, and ω_j is the j^{th} eigenfrequency (In this case j = 1). Here $\lambda_{min} = 1500$ Hz is the minimum required fundamental non-rigid body frequency of the structure. The eigenfrequency constraint is applied to get a desired fundamental eigenfrequency λ_1. The representation of the constraint in negative null form is as shown in Equation 2.11.
   $$\frac{\omega_{min}}{\omega_1(\rho_e)} - 1 \leq 0 \tag{2.11}$$
   where ω_1 is the first non-rigid body mode eigenfrequency that can be calculated as $\omega_1 = 2\pi\lambda_1$ and ω_{min} is the minimum permissible eigenfrequency.

2. **Weight Constraint** (c_2)
   The objective of performing topology optimization on the intermediate body is to design a lightweight structure to avoid the transmissibility of disturbances to the wafer table. In order to achieve this and to meet the requirements as mentioned in Equation 2.4, weight constraint is imposed in the optimization. The formulation of the constraint is as shown in Equation 2.12
   $$\frac{\rho_c V_t v_f(\rho_e)}{m_{max}} - 1 \leq 0 \tag{2.12}$$
   where V_t is total volume of the structure and v_f is volume fraction. In this constraint formulation, the value of m_{max} is assigned to be 6.5 kg. The calculation of m_{max} is shown in Appendix A.

The optimization problem is therefore defined as:

$$\begin{aligned} \min_{\rho_e} \quad & \mathbf{f^T u} \\ \text{subject to: } & \tfrac{\omega_{min}}{\omega_1(\rho_e)} - 1 \leq 0 \\ & \tfrac{\rho_c V_t v_f(\rho_e)}{m_{max}} - 1 \leq 0 \\ & \rho_e^{min} \leq \rho_e \leq 1 \end{aligned} \tag{2.13}$$

D CONVERGENCE & RESULTS

Based on the design domain and necessary boundary conditions as represented in Figure 2.3, the topology optimization for compliance minimization has been carried out. The motive of the optimization was to design a structure that satisfies an eigenfrequency constraint. The constraint included having the fundamental eigenfrequency of the structure greater than 1500 Hz. Along with the eigenfrequency requirement, a weight constraint was also imposed on the structure as formulated in Equation 2.12. The weight constraint includes having a weight ratio between the intermediate body and the wafer table of 1 : 4, and the total weight of the structure to be around 8 kg. As previously mentioned in Section B, thickness of the wafer table can be assigned any value between 5 mm to 10 mm. Based on the choice of thickness value, the weight of the intermediate body can be varied as shown in Figure 2.8. This variation in weight of the intermediate body will have an effect on the weight constraint of the optimization, thereby resulting in a possible alternative design. In an attempt to meet the weight requirements, the thickness of the wafer table was chosen to be 6.47 mm resulting in the total weight of the wafer table to be approximately 1.5

kg. The calculation of this estimation is shown in the Appendix A. Based on the values obtained, the expected weight of the intermediate body must be around 6.5 kg. The obtained final structure of the intermediate body is represented in Figure 2.5.

Figure 2.5: Optimal structure - Intermediate body

The convergence plot of the structure is represented in Figure 2.6. Here, X-axis indicates the number of iterations taken by the optimizer for convergence, and Y-axis indicates scaled value of the objective function. The figure also includes the behavior of constraint values as the optimization attains convergence.

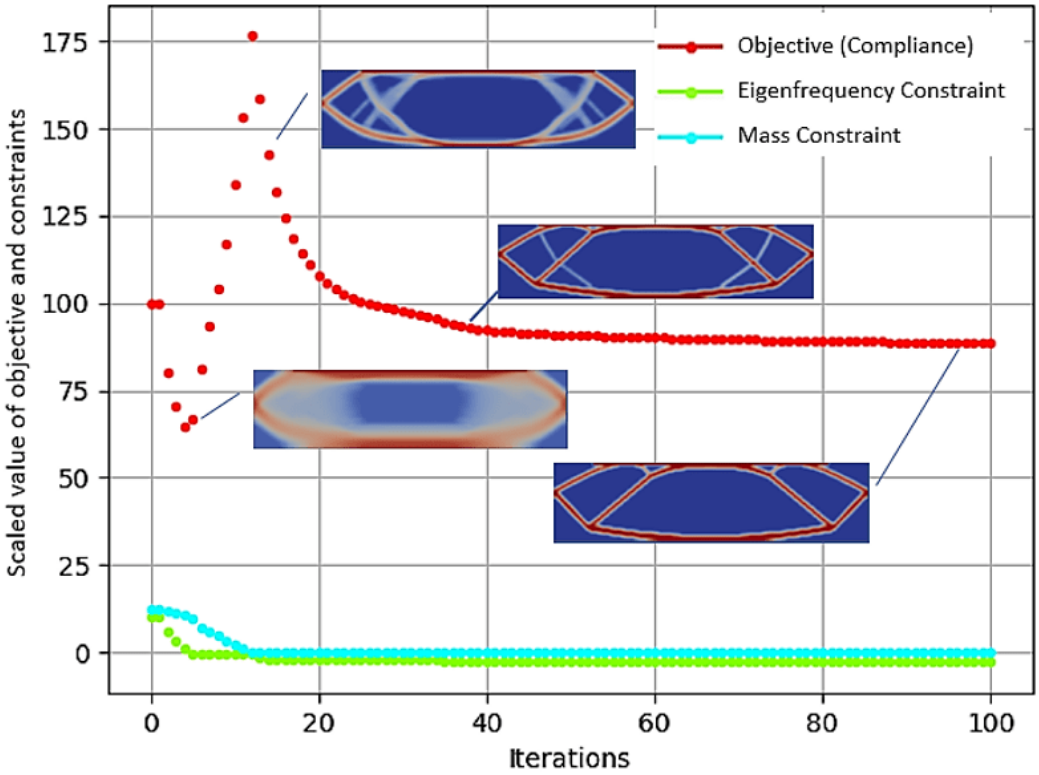

Figure 2.6: Convergence Plot - Intermediate body

Based on the results obtained from topology optimization, the structure satisfied all specified requirements. A comparison of the required values and the obtained values is shown in Table 2.3.

Property	Required	Obtained
λ_1 (Hz)	$\geq$ 1500	1775.550
Weight InB (kg)	$\leq$ 6.5	6.499
WT + InB (kg)	$\approx$ 8	7.999
Compliance (m/N)	–	1.19×10^{-6}

Table 2.3: Comparison of the results - Intermediate Body

The constraint on eigenfrequency of the structure was set to 1500 Hz. However, the optimum eigenfrequency value obtained is much greater than 1500 Hz. This means that, the eigenfrequency constraint is inactive and the optimization problem is based on the value of m_{max} set for weight constraint. A representation of mode shapes of the structure at their respective eigenfrequencies is shown in Figure 2.7. The first four eigenmodes are plotted and corresponding behavior of the structure is represented. Although, in this optimization only the first eigenmode was been considered, the next three eigenmodes along with their respective eigenfrequencies are illustrated for representation purposes.

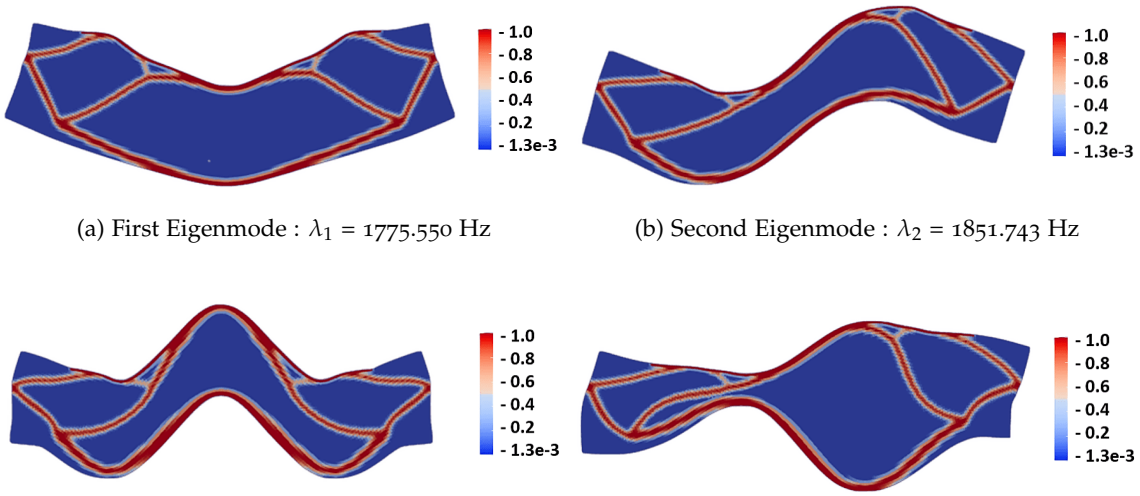

(a) First Eigenmode : λ_1 = 1775.550 Hz

(b) Second Eigenmode : λ_2 = 1851.743 Hz

(c) Third Eigenmode : λ_3 = 3435.569 Hz

(d) Fourth Eigenmode : λ_4 = 4082.977 Hz

Figure 2.7: Non-rigid body eigenmodes - intermediate body

This section included the results obtained from topology optimization. The intermediate body design satisfied all the requirements set by the designer. The eigenfrequency, and weight constraints were satisfied. However, based on the results, there are some aspects that need to be focused on; one of them being the effect of thickness of the wafer table on weight constraint parameters, another being the effect of weight of the structure on the compliance of the design.

E DISCUSSION

The design obtained satisfied all constraints imposed in the optimization. The weight of the intermediate body satisfied the requirements as per Equation 2.4, and also as per the constraint set in Equation 2.12, The maximum allowable weight of the structure depended on an assumed thickness of the wafer table, which in this case was chosen to be 6.47 mm. The thickness of the wafer table can be ranged from 5 mm to 10 mm. Depending on the range, the weight of intermediate body is linearly dependent on the thickness, as shown in Figure 2.8. The allowable weight of the intermediate body will range from 5.68 kg to 6.84 kg.

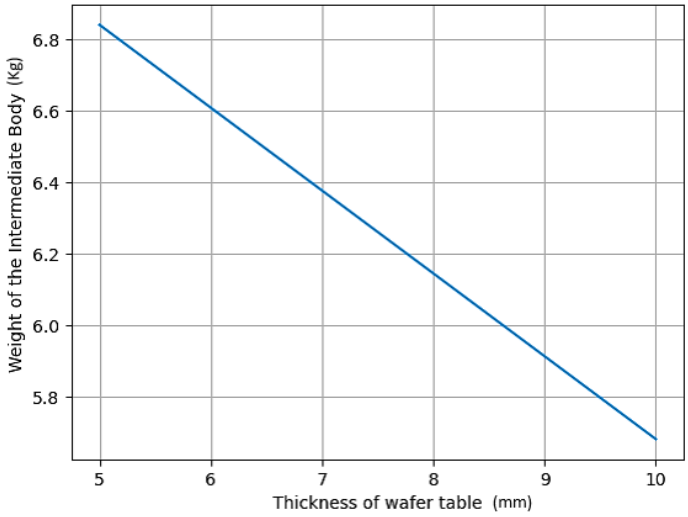

Figure 2.8: Effect of wafer table thickness on weight of the Intermediate body

The effect of wafer table thickness on the compliance of intermediate body is shown in Appendix A. Considering the thickness of wafer table as 6.47 mm and restriction of the total weight of the structure around 8 kg, the weight of the intermediate body was calculated to be 6.5 kg (m_{max}). In order to check the effect of weight on the compliance of the structure, the optimization cycle was run with 3 different values of m_{max}. Figure 2.9 represents behaviour of the final design of the intermediate body when maximum permissible weight is specified to 8 kg, 10 kg,and 12 kg respectively.

(a) 7.99 kg structure

(b) 9.99 kg structure

(c) 11.99 kg structure

Figure 2.9: Structural design behavior with different weight constraint

The data showing the effect of maximum allowable weight on compliance is tabulated in Table 2.4.

Weight of the structure (kg)	**compliance (m/N)**
6.5	1.19×10^{-6}
8.0	8.901×10^{-7}
10.0	6.715×10^{-7}
12.0	5.446×10^{-7}

Table 2.4: Effect of m_{max} on compliance

The results obtained illustrate the designs of the structure for multiple weight requirements. It is observed that, as the weight of the structure increases, the thickness of the design increases thereby increasing the stiffness of the structure. Apart from the increased thickness, there are additional

support members generated at the lower corner edges. The generation of these support members causes the base of the structure to flatten as compared to the curved base in Figure 2.5. Also, the structures obtained in Figure 2.9 have a thicker support to the top surface where the wafer table is to be mounted as compared to the support obtained in Figure 2.5.

F CONCLUSION

This chapter focused on topology optimization of an intermediate body of a wafer stage system. A multi-objective weighted sum problem was formulated with compliance and eigenfrequency as objectives. However, due to scaling issues in the objective functions, an alternative approach of ϵ constraint method was implemented. A brief explanation of the issues posed due to weighted sum multi-objective approach is available in Appendix A. Apart from the scaling issues, the outcome of the optimization largely depends on the weights assigned to the objective functions. Therefore, a critical decision making must be followed while deciding the weights in the multi-objective function. In this approach, the eigenfrequency objective was converted to a constraint, thereby converting the problem into single objective function. The structure was optimized with an objective to minimize compliance, and was subjected to eigenfrequency and weight constraints. The result obtained from this optimization matched the necessary requirement under which the intermediate body will be operating. However, from the results tabulated in Table 2.3, the eigenfrequency constraint is inactive and is not causing any limitation on the optimum design.

A further look into the effect of change in mass parameters on the compliance of the structure was studied. The results obtained showed that as the value of m_{max} increases, the stiffness of the structure increases. From Table 2.4, it can be observed that changing the maximum allowable weight to 8 kg improves the compliance of the structure. However, after the value crosses 10 kg, there is no significant improve in compliance. Therefore, the choice of maximum weight of the structure can be adjusted to be around 8 kg. Taking into consideration the effect of change in maximum weight m_{max} of the structure, the choice of weight to be considered depends on the designer. This choice must be based on the amount of transmissible disturbances from the intermediate body to the wafer table. This effect of disturbances can be estimated by varying in the weight ratio between the intermediate body and wafer table. Also, in cases where the weight of the structure is of priority then the designer can set a lower maximum permissible weight, and if stiffness of the structure is the priority then setting a higher value of maximum permissible weight is preferable. Another important aspect that remains to explore is the effect of self-weight of the intermediate body on the design. It will be interesting to investigate the effect of self weight as it will involve the inertial forces of the structure when it is set in motion. The study of effect of vibration on the structural design, and self weight optimization is subjected to future work.

3

SURFACE SCANNING

This chapter contains a coarse explanation covering the significance of the flatness property of a deformed surface. It entails the execution of surface scanning algorithms on a deformed wafer table. The second section of this chapter explains an algorithm for estimation of global flatness of the surface. Section 3 covers the non-correctable exposure flatness metric for estimating local surface flatness. Section 4 covers the influence of actuators on global flatness and local flatness of the deformed surface. The chapter concludes with a discussion on the results obtained and the significance of the local surface flatness score. The final section covers the conclusions drawn from this approach followed with a possibility of expansion of this method in a 3-dimensional domain.

A INTRODUCTION

Wafer flatness is one of the primary prerequisites for attaining high accuracy in integrated circuit manufacturing. The high accuracy is achieved by incorporating optical lithography in the development of circuits with small feature sizes [3]. Current lithography machines require precise determination of wafer flatness on a sub-nanometer scale for elimination of deviations between the exposed region and plane of focus. As explained in Chapter 1, a wafer table supports the wafer and positions it as per the desired region to be exposed. As a result, wafer table flatness play a crucial role in effective patterning performance, especially in the sub-nanometer domain. Surface imperfections can impair the wafer capabilities of numerous device production processes, including etching, bonding, and lithography. During operation, the back of the silicon wafer is in direct contact with the top surface of the wafer table. Therefore, the top surface of the wafer table must ideally be perfectly flat. However due to manufacturing defects or exposure to thermal conditions, the wafer table is deformed thereby affecting its flatness [13]. This leads to overlay errors which affects the accuracy of the lithography process. Overlay refers to a lithography system's capacity to print precise features on each layer exactly where they should be. Tiny alignment marks are present on the wafer to print the features on the surface. During the lithography process, the wafer stage and the reticle aligns themselves with reference to the alignment marks. When the surface is deformed, the alignment of the wafer and the reticle is distorted leading to misaligned printing of the mask affecting both electrical properties of the contacts and also its insulation [14]. This misalignment in printing potentially leads to short circuits. In order to quantify the deformations in the wafer table and avoid overlay errors, the top surface of the wafer table is scanned and the deformations are recorded.

Flatness of a wafer table surface can be described by a global flatness or as a maximum error from local/site flatness. Global flatness is measured considering the entire surface domain at once and calculating the deformations of the surface with respect to a reference plane. In the case of site flatness, entire surface domain is split into small sub-domains and each sub-domain is exposed to a reference surface. The site flatness of the exposed region is characterized as a scanning error with respect to the reference plane. The reference plane is positioned using a least-squares fit on the exposed area. The errors recorded during this exposure are the distances from the deformed sub-domain surface to the reference plane. The scanning process includes a slit of specified dimension that aligns itself to best match the exposed surface. The surface is aligned

by titling the entire wafer stage such that the desired exposed region best orients with the slit. A comparative representation of global flatness measurement and local flatness measurement is shown in Figure 3.1.

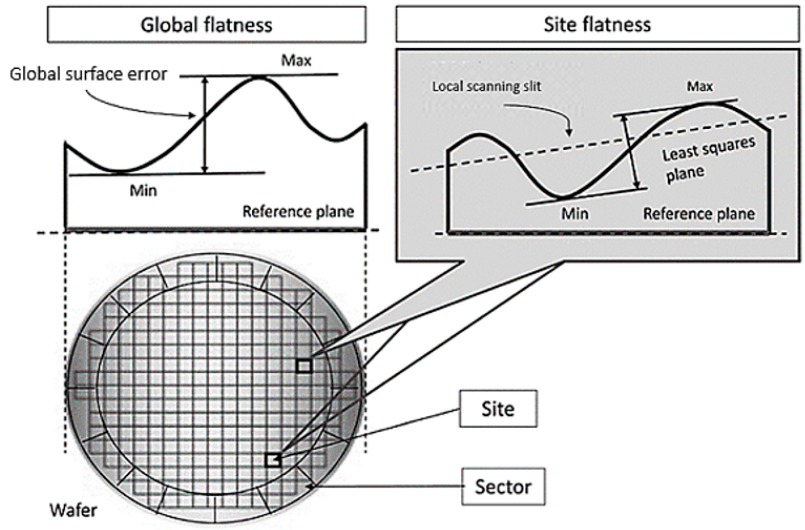

Figure 3.1: Methods of flatness measurement | *Image adapted from [15]*

Figure 3.1 consists of representation of global and local flatness measurements. In global flatness measurement, the entire wafer surface is examined at once and the deformation in the surface is calculated based on maximum and minimum value. The deformation recorded between the maximum value and minimum value is termed as global surface error. In local flatness measurement, the surface is sub-divided into grids and the deformations in each grid are compared to a least square fit plane. The value obtained from this comparison is quantified as local surface error of that grid domain.

In this thesis, the scanning of the wafer surface is done in a 2-dimensional domain. A local flatness scanning method is briefly explained in Section C, wherein the scanning errors recorded per scan are quantified based on local surface scan.

B MINIMUM ZONE METHOD

The minimum zone method for flatness estimation is used for evaluating the global flatness of a deformed surface. In this method, the deformed surface is constrained between 2 horizontal parallel planes, one of which covers the upper extreme of the deformation and the second plane covers the lower extreme [16].

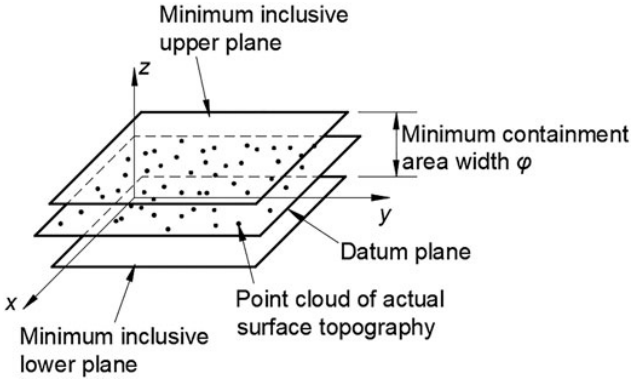

Figure 3.2: Minimum zone estimation | *Image adapted from [16]*

The positioning of planes is done by selection of sampling points of the deformed surface. The selection of points and the placement of the plane is shown in Figure 3.2. The points included in the plane must match one of the three criterion, namely; 1) Triangle criteria, 2) Intersection criteria, and 3) Straight line criteria [16]. The distance between these two planes is used for interpretation of global flatness of a surface.

1. Triangle Criteria

   The triangle criteria includes locating total 4 points on the parallel planes. The allocation of these points must be such that one plane consists 3 points and the other consists a single point.

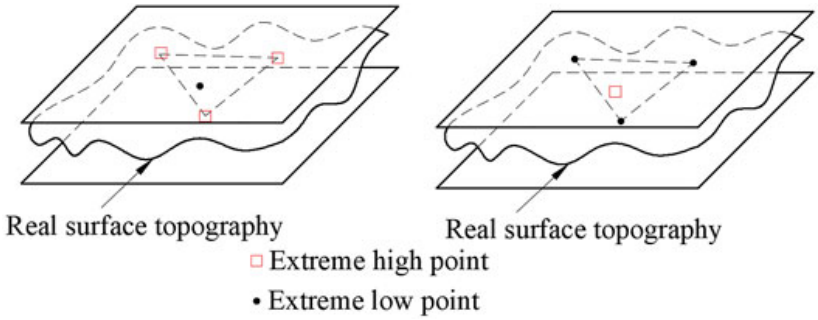

Figure 3.3: Triangle criteria - Minimum zone method | *Image adapted from [16]*

   As shown in Figure 3.3, the allocation of the 3 points can either be on the upper extreme plane or on the lower extreme plane. However, the other 1 point must be selected such that, when projected it should lie on the inner side or edge of the triangle formed by the 3 points.

2. Cross Criteria

   The cross criteria also includes locating total 4 points on the parallel planes. However in this case, the allocation of these points must be such that each of the two planes consists 2 points each.

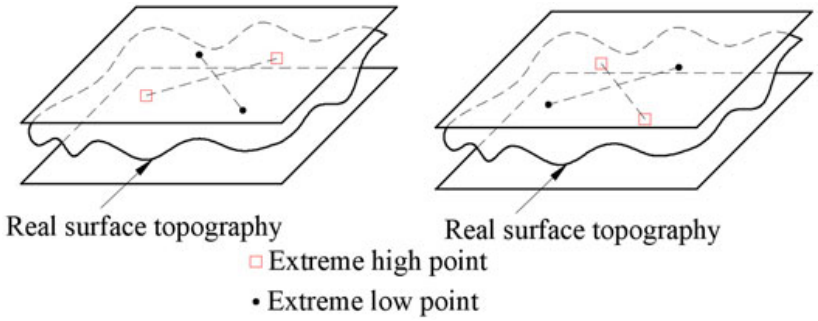

Figure 3.4: Cross criteria - Minimum zone method | *Image adapted from [16]*

   As shown in Figure 3.4, the allocation of the 2 points must be in such a way that the two virtual line must be intersecting with each other.

3. Linear Criteria

   The linear criteria includes locating total 3 points on the parallel planes. In this case, the allocation of these points must be such that one plane consists 2 points and the other consists of a single point.

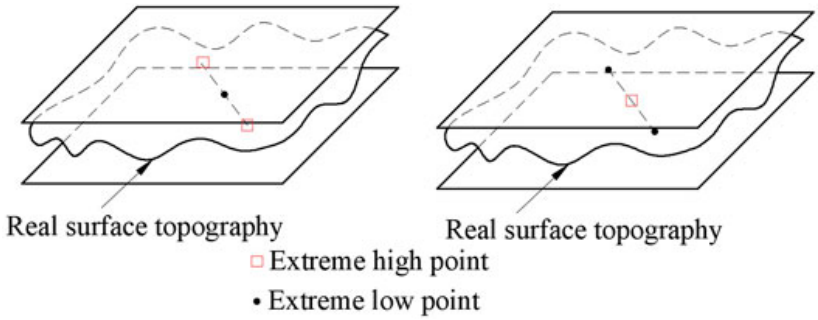

Figure 3.5: Linear criteria - Minimum zone method | *Image adapted from [16]*

As shown in Figure 3.5, the allocation of the 2 points can either be on the upper extreme plane or on the lower extreme plane. The other 1 point must be selected such that, when projected it should lie on the virtual line formed by the 2 points either on the upper extreme plane or on the lower extreme plane.

The selection of the multiple sampling points on a surface is best suited when this method is implemented in a 3-dimensional domain. In this thesis, the wafer table surface is realized in 2-dimensional domain. In 2D, the upper plane and the lower plane are placed at the maximum and the minimum values of the surface deformation. Involving more than one deformation point to place the planes might include complexities in defining an asymmetric deformation curve. This might result in false interpretation of surface flatness. Therefore, the minimum zone value of a 2-dimensional curve involves taking the peak to base deformation. The formulation for global flatness estimation using minimum zone method is represented in Equation 3.1.

$$\text{MZ} = \max(\text{deformation}) - \min(\text{deformation}) \tag{3.1}$$

The minimum zone value is confined between two parallel planes placed at the maximum deformation value and at the minimum deformation value.

C LOCAL SURFACE FLATNESS (LSF)

In this thesis, a Local Surface Flatness (*LSF*) scanning algorithm is implemented for estimating the local flatness of a deformed surface. The estimation is been carried out using a scanning slit of fixed dimension that acts as a reference plane. The scanning of a deformed surface is done by considering a local domain wherein the scanning slit is aligned as per a deformed area. This process of alignment and scanning is carried out over the entire domain and the corresponding scanning errors are recorded. The scanning methodology of the surface is represented in Figure 3.6. The error value per slit depends on the number of sampling points the surface is divided into. The number of error values per slit can be increased by increasing the number of sampling points. Each sampling point will record error with respect to the scanning slit.

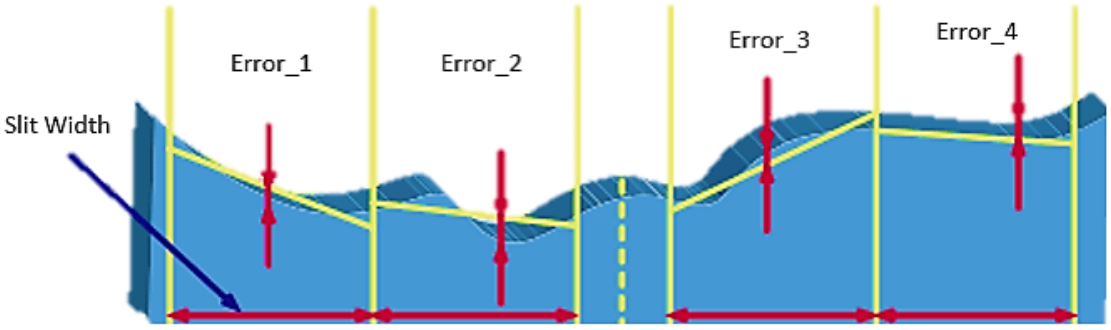

Figure 3.6: Local surface scanning and error estimation

Figure 3.6 illustrates the scanning algorithm implemented in this thesis. A critical aspect of this algorithm is the definition of a x-incrementor. This incrementor is used to define the starting point of the scanning procedure and is dependent on the length of the slit. The significance of having an incrementor is to be flexible for all types of lithography machines. The incrementor will enable the algorithm to perform flatness estimation for all field sizes of chip design on the silicon wafer. In a 2-dimensional setting, the wafer surface is scanned along the X-axis, therefore the incrementor is defined in x-direction. In this thesis, the length of the scanning slit is 26 mm and the value of the x-incrementor is 1.5 mm. Based on the value of the x-incrementor, the surface scanning will have a set number of starting points as per Equation 3.2.

$$\text{Number of starting points} = \frac{\text{Slit dimension}}{\text{x-incrementor}} \tag{3.2}$$

In scenarios where the dimension of the slit is not completely divisible by the user-specified incrementor, the closest lower whole number signifies the number of starting points of the scan. A representation of definition of starting points is illustrated in Figure 3.7.

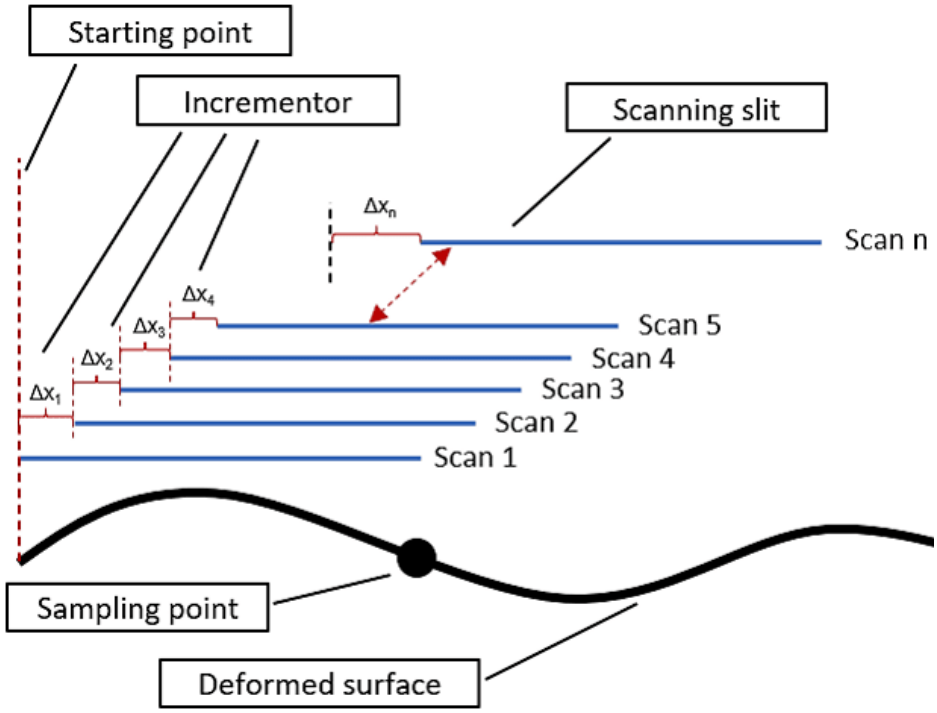

Figure 3.7: Definition of multiple starting points of scanning

Figure 3.7 indicates the scanning of a single sampling point and the slits that cover the point during different starting locations. Here, Δx_1 indicates the incrementor added to the initial starting point, Δx_n indicates the final incrementor added and the final slit location that covers the sampling point. The value of Δx_n is $(n \cdot \Delta x_1)$, where n is the number of starting points. After addition of each incrementor the new starting point of the slit becomes the starting point of the scan. The number of starting points depends on the dimension of the scanning slit and also on the incrementor value. Since there exists n starting points, the surface will be scanned n number of times, each time with from different start location. As per Equation 3.2, the number of starting points in X-axis will be 17, since 26/1.5 gives 17.3333. The rounding-off of the number is done to a lower value to keep the errors recorded for the scans as per the dimension of the slit. In the case of X-axis scanning the starting points will be at $0.0, 1.5, 3.0, 4.5, \ldots\ldots, 25.5, 26.0$ mm. The difference in the last two starting locations of the X-axis scanning is 0.5 mm, this is due to the fact that the after 25.5 mm, the next starting point will be from 27.0 mm which is greater than the slit dimension. In such a situation, the value of the next starting point involves assignment of the maximum slit dimension i.e. 26.0 mm.

The initial scan starts from 0.0 mm as the starting point and after each scan, incrementors are added which shifts the starting point of the next scan. The shift in the starting point can be applied either in $+X$-direction or in $-X$-direction. If this shift is added to just one direction it will lead to asymmetric scanning error pattern which will make flatness estimation more complex, thereby making the results of the scan ambiguous for interpretation. To compensate this asymmetry the entire surface is scanned in backward direction with the same incrementor applied in $-X$-direction. A representation of the forward and backward scanning is shown in Figure 3.11. The X-axis scanning includes 17 starting points, which means that the surface will be scanned 17 times in forward direction. Due to the introduction of backward scanning, the surface will also be scanned for additional 17 times in $-X$-direction thereby making the total number of scans equal to 34. Depending on whether the sampling point lies under the slit during those 34 scans, the scanning error of each point will be recorded. This scanning and error recording is shown in Figure 3.8.

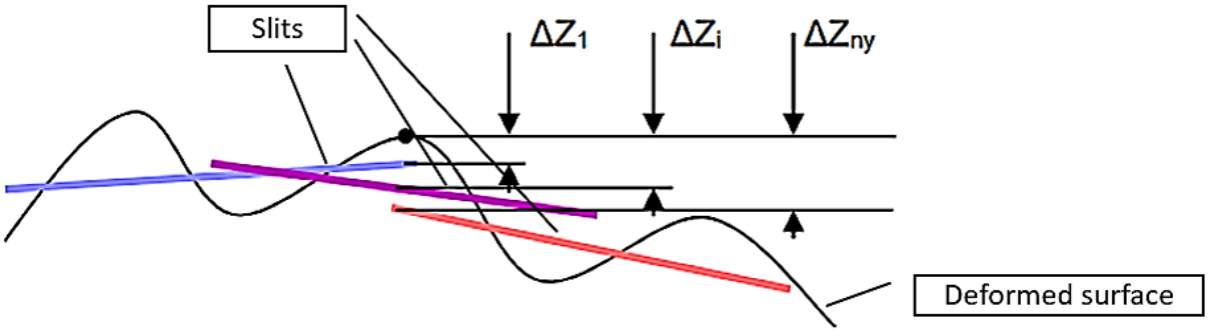

Figure 3.8: Local surface scanning with moving slit

Here ΔZ_i denotes the error recorded from each of the scans for a single sampling point, where i denotes number of scans for each sampling point. The more the number of sampling points, the more are the errors recorded per scan. After performing the scans, each sampling point has distinct error value obtained from each of the scan. Out of obtained error values for a single sampling point, the maximum absolute error value is considered and that value signifies the maximum possible error of that point in a specific deformation curve. It signifies that, the error value of that particular sampling point cannot exceed that specific value. This process is carried out for all the sampling points, as every sampling point is assigned its respective maximum absolute value from its corresponding error values obtained from the scan. A schematic representation of the flow of the algorithm is shown in Flowchart 3.9.

With reference to Figure 3.8, the results obtained from the algorithm will include $n \cdot 34$ number of error values, where n denotes the number of sampling points the surface is subdivided into. The number of error values for each of the sampling point will depend on whether or not the point lies under the slit after the incrementor is added. Therefore, the maximum number of error values a single sampling point can have is 34. Now the surface will have "n" maximum absolute values for n sampling points. However, the representation of the flatness property of a surface can best be defined with a single value. This can be beneficial for the designer for better interpretation of the local surface scanning flatness. Therefore, out of those "n" maximum absolute values, the maximum absolute value is chosen. This value is the maximum absolute value obtained from the maximum absolutes that were previously obtained from each of the scans and is denoted as the *"LSF score"* of the surface. This LSF score denotes the local scanning flatness of the surface and is further taken into consideration for evaluation and/or flatness correction purposes.

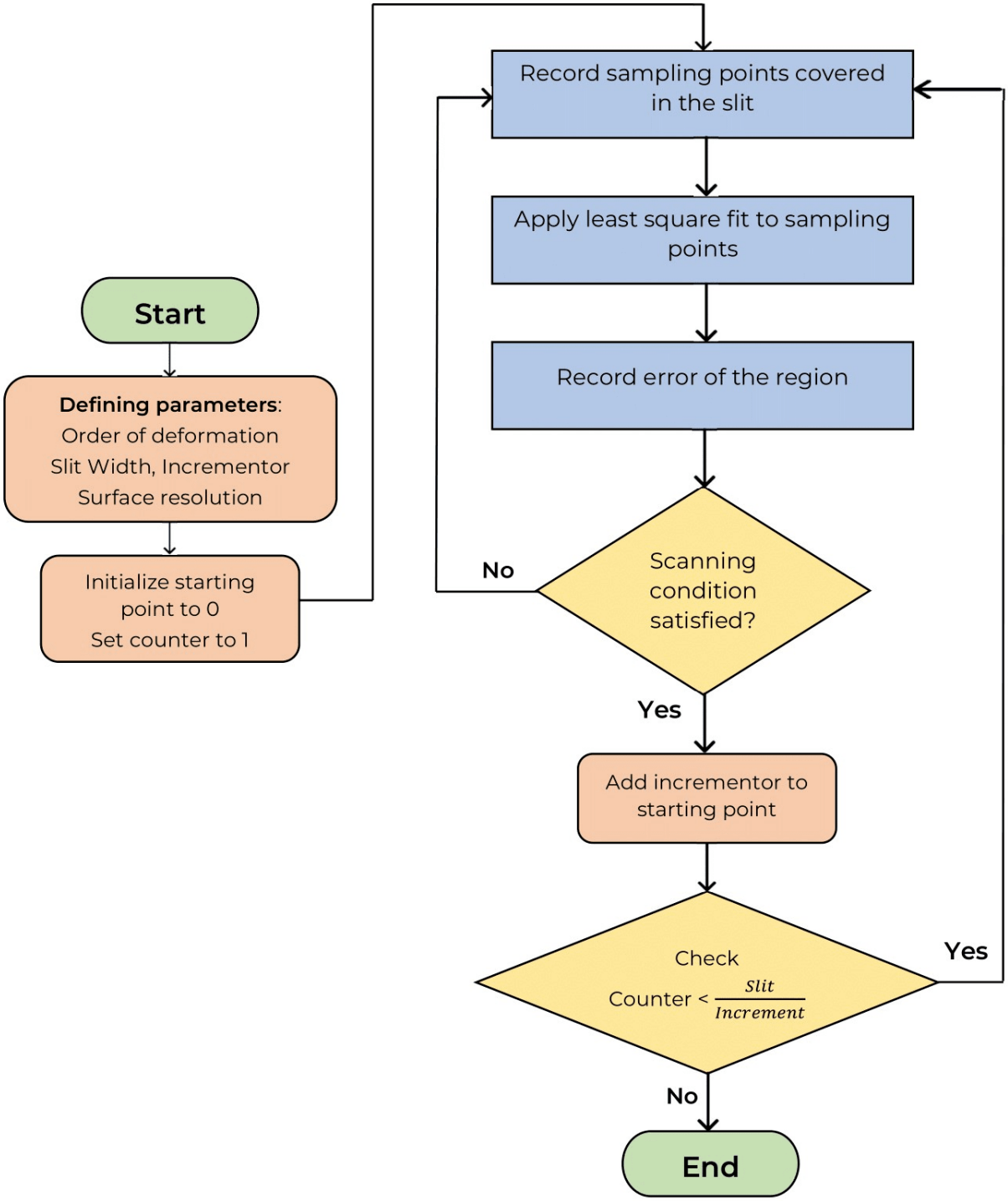

Figure 3.9: LSF algorithm

This thesis considers scanning of the wafer table subject to deformation superimposed on the top surface. The shape of the wafer matches the profile of the top surface of the wafer table. The deformation superimposed on the top of the wafer surface has a maximum deformation amplitude of 500 nm. For illustration purposes, the wafer table is subject to a cosine deformation as illustrated in Figure 3.10. The equation of deformation is formulated in Equation 3.3.

$$y = \frac{y_{max}}{2} - \frac{y_{max}}{2}\cos(\frac{2\pi x}{D}) \tag{3.3}$$

where D denotes diameter of the wafer table, y_{max} is the maximum deformation of the shape = 500 nm, and y denotes the deformation value depending on corresponding x values.

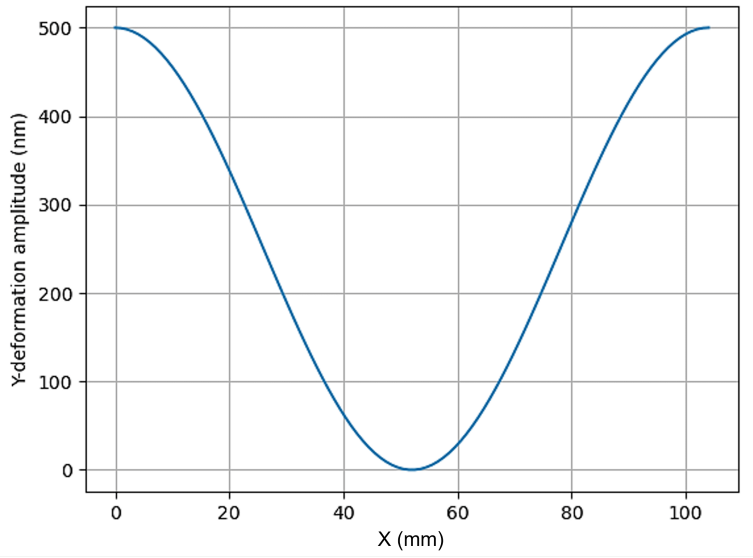

Figure 3.10: Wafer Table surface deformations - Cosine

The deformation shown in Figure 3.10 shows a maximum deformation of y_{max} = 500 nm and minimum deformation of y_{min} = 0 nm.

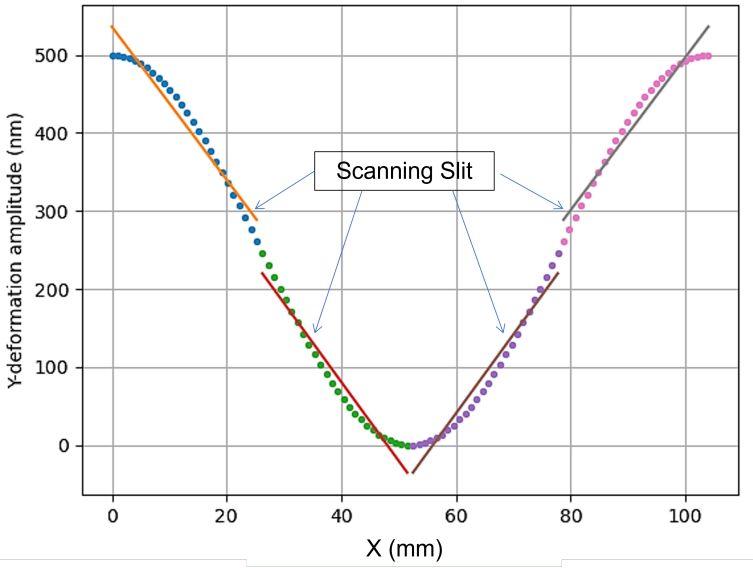

Figure 3.11: Surface deformation scanning - 1^{st} scan out of 34

Figure 3.11 illustrates the scanning of the surface subjected to cosine deformation. The illustration includes scanning from the initial scanning position which signifies the 1^{st} scan out of the 34 scans. Later on, as shown in Figure 3.7, the surface is scanned multiple times by changing the start point based on the incrementor specified. For better visualization of the scanning plots per scan, a wafer table of 104 mm diameter is considered in Figure 3.11. The LSF scanning error plot is represented in Figure 3.12.

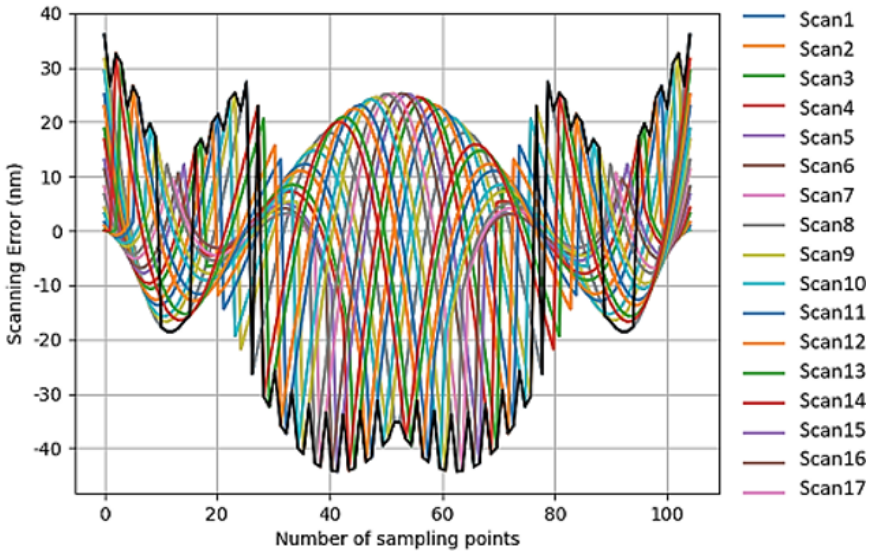

Figure 3.12: LSF scanning error plot

In Figure 3.12, each of the colored plot represents the scanning error for the sampling points in the deformation. Out of the total recorded error values for each sampling point, the maximum absolute value is assigned which represents the maximum possible scanning error that specific point can have. This is shown in Figure 3.12 with solid black LSF plot. However, the solid black LSF plot shown in Figure 3.12 consists of certain sampling points having negative error values as well. The sampling points with negative error values are considered for their magnitude and the final LSF error extract plot contains the magnitude of those negative error values as illustrated in Figure 3.13.

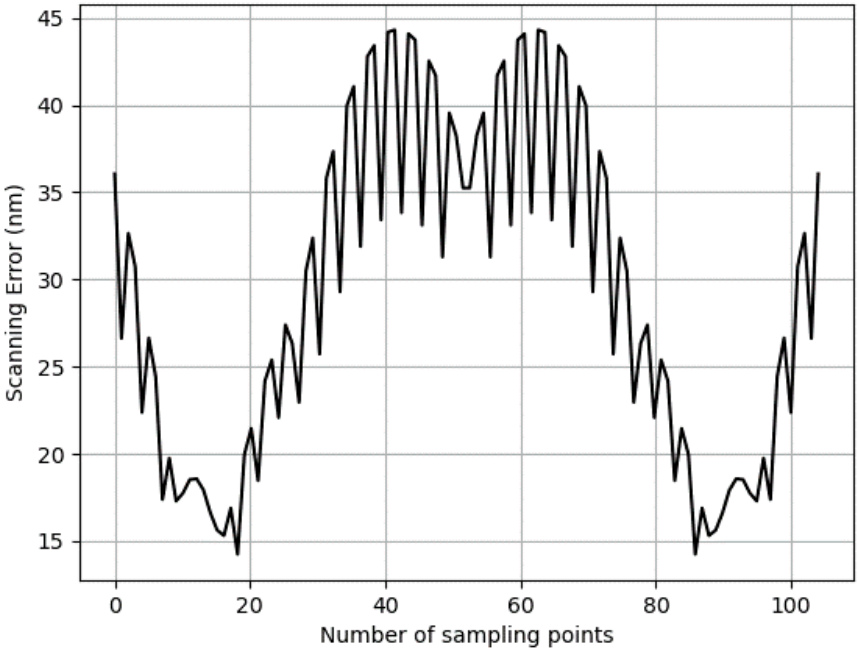

Figure 3.13: Nodal LSF error extract plot

The maximum absolute error value obtained from Figure 3.13 is 44.3048 nm. This value is the assigned LSF score of a 104 mm diameter wafer table with cosine deformation. In this thesis, the diameter of the wafer table is 310 mm. The LSF error plots along with the LSF error extract plot of a 310 mm wafer table with cosine deformation is included in the Appendix B with their corresponding LSF score.

For the cosine deformation visualized for 310 mm wafer table, the LSF score is 5.0751 nm. However, this local error value was based on scanning the deformation with a slit of length 26 mm. The same cosine deformation was scanned by changing the dimension of the slit and recording its effect on the LSF score. The representation of this effect is shown in Figure 3.14.

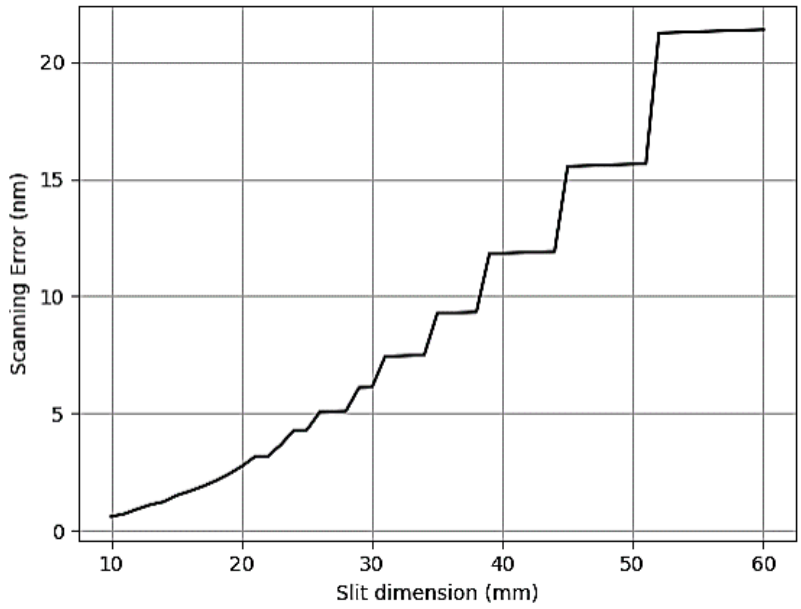

Figure 3.14: Effect of dimension of scanning slit on local scanning error

The trend observed in Figure 3.14 shows that, smaller the slit length, lower is the LSF score. As the LSF score decreases, the overlay errors in the lithography process are reduced. In this thesis, the length of the slit is taken to be 26 mm.

Apart from the slit length, the LSF score also depends on nature of the deformation curve. The effect of LSF score depending on different deformation types is represented in Table 3.1.

Deformation type	Equation of the curvature	LSF score
2^{nd} order	$y = y_{max}(\frac{x}{R})^2$	2.0678 nm
3^{rd} order	$y = y_{max}(\frac{x}{R})^3$	5.7964 nm
4^{th} order	$y = y_{max}(\frac{x}{R})^4$	10.8458 nm

Table 3.1: LSF scores for curve types

Table 3.1 shows the LSF score of different deformation curves when scanned with a slit of length 26 mm. The values obtained show that as the order of the deformation curve increases, the LSF score increases. This increase in the LSF score makes lithography process more prone to overlay errors, thereby making the wafer table unfit for use.

D ACTUATOR LOCATION - BRUTE FORCE METHOD

The scanning algorithm explained in Section C is used for estimating the amount of scan error of a deformed wafer table. This estimation is based on the LSF score. The obtained value of the surface must be corrected to improve the surface flatness. This correction is achieved by incorporating actuators under the wafer table that apply either a push or a pull force to reduce the maximum

deformation amplitude to a lowest optimum value.

In this thesis, the flatness property of a wafer table of 310 mm diameter and 7 mm thickness is evaluated in a 2-dimensional domain. In Section C, a cosine deformation was implemented on the wafer table for illustration purposes. However, in this thesis, the wafer table surface is subjected to 2^{nd} order parabolic deformation with maximum deformation amplitude of 500 nm. In addition to the deformation, the wafer table includes sagging due to its self-weight which is also superimposed on the surface. The LSF plots of the 2^{nd} order deformation is included in the Appendix B. The illustration of a 2^{nd} order parabolic deformation in addition with self-weight sag is represented in Figure 3.15. The nature of the self-weight sag curve is due to the placement of the actuators at arbitrary locations. The figure also illustrates the effect of actuator force on the total flatness of the surface.

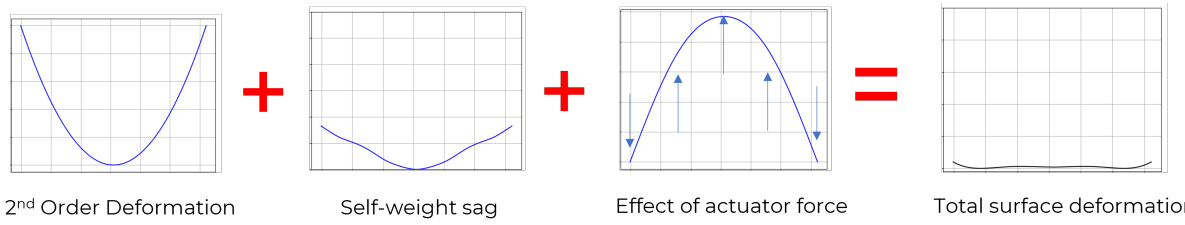

Figure 3.15: Total deformation of the top surface

Figure 3.15 shows that, the deformation due to self weight sag is very less as compared to the superimposed deformation curve. It means that the actuator forces play an important part in reducing the surface deformations. The wafer table is modelled using a plane-strain FEM approach where the entire domain is subdivided into elements depending on the size of the mesh. As mentioned in Chapter 2, the mass of the wafer table is 1.5 kg and the material properties of the part are shown in Table 2.2. This mass is distributed over the entire structure in the FEM domain to model the self-weight of the structure. The total surface deformation is corrected by incorporating piezoelectric actuators placed under the wafer table. The piezoelectric actuators are a push/pull type of actuators with different stiffness in x and y direction. The maximum force of the actuator depends on the choice of the actuator and its corresponding force properties.

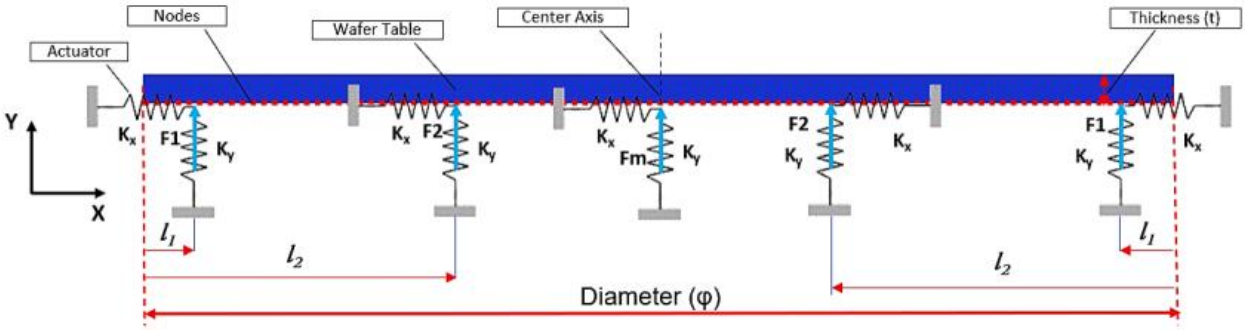

Figure 3.16: Actuator placement illustration

This section includes placement of piezoelectric actuators for correction of deformations on the wafer table surface. The actuator properties are tabulated in Table 3.2.

Actuator properties	Value
X-stiffness (K_x^a)	10^5 N/m
Y-stiffness (K_y^a)	10^8 N/m

Table 3.2: Properties of piezoelectric actuators

The wafer table is visualized as a FEM model with 310 elements in X-direction and 7 elements in Y-direction. The actuators are represented in the form of spring members with a force. Initially, two actuators are placed per half side of the wafer table. Apart from those 4 actuators, 1 actuator is also placed at the centre of the wafer table. By placing this center actuator the eigenfrequency of the wafer table is improved, as this middle actuator provides stability to the entire structure. The actuator placement model is illustrated in Figure 3.16, where the location of the actuators is represented by l_1 and l_2, and the actuator force is represented by F_1 and F_2 respectively. The distance l_1 and l_2 of the actuators are measured from the extreme left side of the wafer table. Since the deformation is symmetric, the location of the actuators is mirrored on the right side of the axis. The location on the right side is same as that to the left side. Based on the actuator placement, the corresponding effect on the flatness property is evaluated. This evaluation is based on the global and the local flatness score obtained by placement of the actuators, where the quantification of the score is done by implementing all possible combinations of the actuator placement. This method of evaluation is called the Brute force method of solving the problem which includes exhaustive search of results in solving a problem wherein the results are based on sheer computing power. The results obtained from the brute force method will be used to study the behaviour of a deformed surface based on the global and local flatness values. It will enable the designer to understand the influence of actuators on the flatness of a deformed surface.

E ANALYSIS

In order to explore the behavior of this problem, the actuator forces are assigned a fixed value, were the first actuator is assigned a force of -30 N, second actuator is assigned 20 N, and the middle actuator is assigned a value of 20 N. These values of actuator forces are an assumption and is purely based on designers choice which can be changed as per the requirement. An important aspect to keep in mind is that, at all points the summation of all the actuator forces must be zero. This check ensures that the structure is not into any form of acceleration due to the forces and is maintained at static equilibrium. In the force condition, the effect of gravity is left out, since it does not have a significant influence on the equilibrium of the system as compared to actuator forces. A bowl type of deformation was realized on the wafer table. Initially, 2 actuators per half are modelled, wherein the actuators are placed at all possible combinations of sampling points. The location of the center actuator remains fixed throughout the analysis. The actuator at location l_1 is assigned a pulling force of value $-F_1$, the actuator at location l_2 is assigned a pushing force of value $+F_2$, and the center actuator is assigned a force of $+F_m$. For each of the location combination, the MZ value and LSF score is recorded. Since, the wafer table structure with 310 mm diameter is modelled with 310 elements, resulting in 155 elements per half, the total number of combinations to locate 2 actuator would be $155 \times 155 = 24025$.

The results obtained from the Brute force method are illustrated in Figure 3.17. Figure 3.17a represents the MZ value results obtained from different combinations of the actuator locations, and Figure 3.17b represents the corresponding LSF score from those combinations. Figure 3.17b shows that the LSF score is optimum when actuator 1 is located between 0 to 5 mm, and actuator 2 is located between 25 to 42 mm. If the actuators are placed in the LSF optimum locations, then the MZ value is compromised wherein for those actuator location, Figure 3.17a show a gradient change from 100 nm to 300 nm.

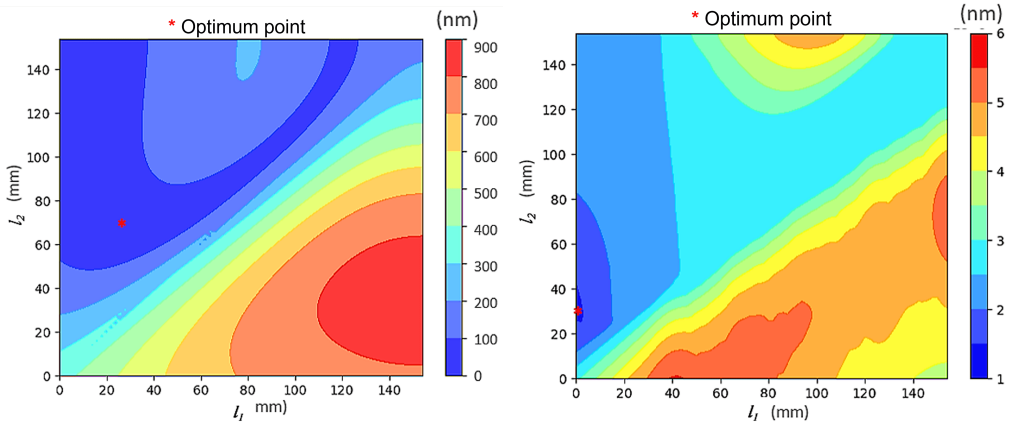

(a) MZ value contour plot (b) LSF score contour plot

Figure 3.17: Effect of actuator placement on MZ and LSF value

From the optimum patch obtained in Figure 3.17, the optimum location of actuators for minimum MZ value and LSF score is tabulated in Table 3.3.

Property	**Optimum value (nm)**	**Actuator1 location- l_1 (mm)**	**Actuator2 location- l_2 (mm)**
MZ value	24.8761	24	70
LSF score	1.4021	0	32

Table 3.3: Properties of piezoelectric actuators

The local and global flatness have different optima depending on the LSF score and MZ value respectively. However, the decision of the actuator placement depends on the choice of the objective. For each of the 24025 iterations, the LSF scores and MZ values are plotted using a Pareto plot. The decision for the actuator location can be interpreted from Pareto front representing local and global flatness values, as illustrated in Figure 3.18.

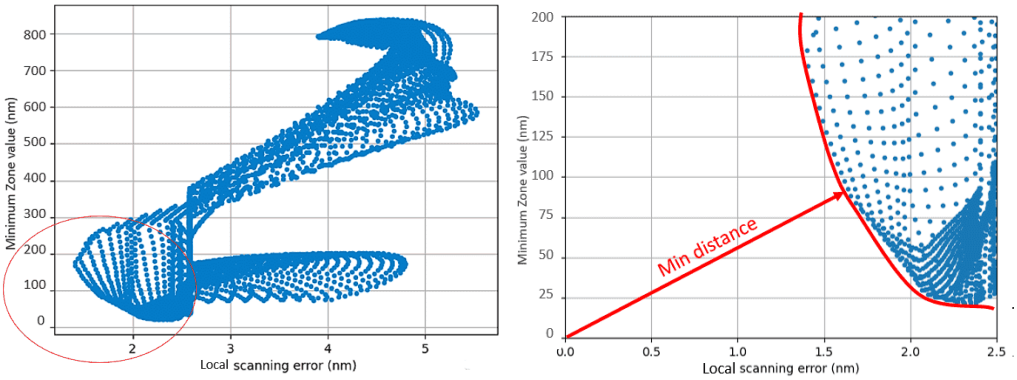

(a) Local error v/s Global error (b) Pareto front

Figure 3.18: Pareto plot

From the Pareto front plot, the local and global flatness value obtained is as follows:

Actuator1 - l_1 (mm)	**Actuator2 - l_2 (mm)**	**MZ value (nm)**	**LSF score (nm)**
0	54	97.56	1.617

Table 3.4: Properties of piezoelectric actuators

If the local flatness of the surface is of the priority then taking the actuator location with lowest LSF score will be ideal. If the global flatness of the surface is of the priority then the actuator locations with lowest MZ value will be ideal.

F DISCUSSION

The results obtained from the brute force method in actuator placement provided an estimation about the influence of actuators on the local flatness (LSF score) and global flatness (MZ value) of a deformed surface. From the results obtained, the following points must be taken into consideration.

1. Dependency of local scanning errors on the dimension of the scanning slit

   The dimension of the slit play a vital role on the LSF score of the deformation. From Figure 3.14, it is clear that the slit dimensions affects the outcome of local scanning. The smaller the slit dimension, better is its alignment with respect to the deformation, and the lower is the LSF score. However, the trend observed in the curve is subject to further investigations. It might be interesting to further look into the reason for the sudden jumps in the LSF score after the slit crosses a certain dimension.

2. Placement of actuators in intermediate locations between two sampling points

   The brute force method involved changing the location of actuators from one sampling point to another. In doing so, the intermediate points in-between two sampling points were left unexplored. To address this issue, linear interpolation functions can be incorporated in the optimization, where the actuators can be placed in between the sampling points as well. Leaving out the intermediate points between the sampling points might involve missing out on a possible optimum value of the actuator location. Also, by incorporating the interpolation functions, the problem statement can be converted to an optimization problem. The optimization problem will include placement of actuators using a gradient search method as implemented in Chapter 2.

3. Computational time associated with actuator placement

   The results obtained from the brute force method involved an exhaustive search wherein each and every combination of actuator locations were evaluated. The time taken to generate the results was around 11 minutes. In this case, 2 actuators per half were placed. In the case where 3 actuators per half are to be placed, the brute force method takes-up 61 minutes. This exhaustive method might prove beneficial in developing an idea of the results that can be expected, but this method takes long computational time thereby increasing the computational cost of the problem. The time duration taken in placement of 2 and 3 actuators per half was done in a 2-dimensional domain. If this method was to be implemented in a 3-dimensional setting, then it might take up huge computational space and put undue strain on the system. This issue can be solved by using optimization search techniques, where the optimizer will perform gradient search method depending on flatness objective of choice.

4. Number of multiple optimum actuator locations

   Figure 3.17a and Figure 3.17b indicates multiple possible actuator location combinations. This might lead to multiple outcomes when an optimization algorithm is incorporated for the problem. There might also be a case wherein the results generated are based on the local optimum. In order to generate a unique solution of the problem statement, an additional constraint must also be incorporated while defining the problem. This constraint will enable the solver to generate a single output for the optimization problem.

5. Effect of force on local and global flatness

   The LSF and MZ plots demonstrate the flatness property of the surface when the actuators are assigned a fixed force magnitude. Each of the actuators in the model performs

either pushing or pulling action on the structure. The force of the actuator with varying locations tends to generate a moment on the structure which affects the local and global flatness. The nature of the contour plots and the location of the optimum will change when the exhaustive search method is carried out for different actuator force values. To find the optimum force for each of the actuators, along with the actuator location, the actuator force must also be taken as a variable during optimization.

6. Selection of objective function for optimization

   For an optimization problem, the definition of objective function will be based on either local surface flatness optimization (LSF) or on global flatness optimization (MZ). However, the LSF algorithm involves scanning of the deformed surface from multiple starting points and then taking the absolute maximum value of the absolute maximum values as the LSF score. This makes the definition of sensitivities complex, thereby making local flatness objective tedious for implementation. Also, the LSF plot consists of sharp peaks at some of the sampling points. This causes difficulties in defining sensitivities of the function, leading to complexities in optimization.

G CONCLUSION

This chapter focused on estimation of flatness property of a deformed surface. The estimation was based on the results obtained from a local (LSF) and a global (MZ) scanning algorithm. The deformed surface of a wafer table was chosen as a case study wherein the surface was subject to self-weight deformations along with a 2^{nd} order deformation being superimposed on its top surface. For estimation of local flatness, the dimension of the scanning slit play a critical role in estimating the LSF score. For a deformation with set number of sampling points, it was observed that a smaller slit will have less sampling points to contain during a scanning iteration. This would mean that the alignment of the slit will be better as compared to the one with a larger slit dimension. Therefore, the smaller the dimension of the slit, the smaller is the LSF deformation error. Another important aspect which affects the local scanning errors is the nature of the deformation curve. It is observed that, as the deformation becomes of a higher order nature, the LSF scanning error increases thereby increasing the overlay errors during lithography process.

In order to reduce the errors in the wafer table, the deformations must be corrected by incorporating actuators under the deformed structure. The results presented include generation of a range of optimum values for MZ values and LSF scores obtained from a brute force method. It was observed that, for a particular actuator force, the LSF error ranged from 1 nm to 6 nm depending on the location of the force. This influence was also seen on the MZ value of the deformation. Also, it was observed that the magnitude of self-weight sag of the structure was very less as compared to the superimposed deformation. Therefore, the flatness correction was mainly dominated by the actuator forces. It can be further concluded that, by varying the actuator forces along the domain, the scanning error of the deformation can be improved. This proves the influence of the actuator force on the local and global flatness of a deformed surface. The location and the magnitude of the force can be found by defining a gradient based optimization problem which includes improvement of flatness property of the structure. The LSF algorithm involves taking the absolute maximum value of the absolute maximum values as the LSF score, resulting in sharp peaks in the LSF plot at some of the sampling points. This causes difficulties in defining sensitivities of the function, leading to complexities in optimization. Due to the complexities in defining LSF as an objective, global flatness should be considered as a point of focus and must be defined as the objective function.

The scanning of the surface and estimation of the errors was done in a 2-dimensional domain. However this algorithm can also be realized in a 3-dimensional setting wherein, the scanning can be done along the X and Y-directions simultaneously. This estimation of surface error and scanning of the surface in a 3-dimensional domain is subjected to future work.

4

ACTUATOR PLACEMENT OPTIMIZATION

This chapter is a combination of Chapter 2 and Chapter 3. It includes the implementation of an optimization algorithm to minimize the deformations in a wafer table. This is achieved by the placement of actuators and by defining their force properties. The first section contains an overview of the chapter in accordance with ASML case study. The second section includes the definition of interpolation function applied in the optimization using actuator location and actuator force as variables. The third and fourth section includes the definition of the actuator optimization objective and constraint functions, along with the definition of their respective sensitivities. The chapter then concludes with the results obtained, choice of parameters, followed by the optimal positioning of actuators, their discussion, and then the conclusion on the results.

A CASE STUDY - ASML

The photolithography machines manufactured at ASML expose the reticle mask using Deep ultraviolet (DUV) or Extreme ultraviolet (EUV) light and then further transfer the mask's pattern on a silicon wafer. One of the key components that play a vital role in determining the precision of an ASML lithography machine is the wafer table of the system. Its role is to load the silicon wafer in a stress-free environment and keep the wafer in place during the whole lithography process. The friction provided by the wafer table is an important aspect in positioning the wafer in place. Apart from the friction contact, flatness of the wafer table determines the precision of the entire machine. In order to understand the factors affecting the precision of lithography systems, it is important to have a good understanding of the surface flatness. Accurate flatness estimation of the top surface enables precise interpretation and reliable modeling of the system.

In this chapter, the top surface deformations of the wafer table will be corrected in the sub-nanometer range. The correction will be based on first estimating the flatness of the top surface and then placing actuators in appropriate locations to improve it. The scanning will be based on the algorithms explained in Chapter 3. The implementation will undergo defining the problem statement of flatness correction using an optimization technique. The optimization problem involves making a choice between optimizing global flatness (MZ value) or local flatness (LSF score) as the objective for flatness correction. Local/site flatness and global flatness of the surface will be calculated based on LSF score and MZ value respectively. After scanning, the flatness of the system can be interpreted from the values obtained through local and global scanning. These estimated flatness values are to be minimized by the placement of push-pull type piezoelectric actuators under the wafer table. The optimization involves considering actuator location and actuator force as design variables. The results illustrated in Chapter 3, Section E include the effect of actuator location on the LSF score and MZ value of the surface. However, this implementation represented results obtained through brute force exhaustive search wherein every possible combination of actuator location was explored. The results obtained included assuming a constant actuator force, and also leaving the intermediate actuator location unexplored. All these drawbacks and limitations of the results from the previous chapter can be addressed by incorporating gradient-based optimization.

The optimizer incorporated in this optimization is MMA, as implemented in Chapter 2. The

limitations discussed in Chapter 3, Section F are all addressed in this chapter. The MMA optimizer incorporated involves minimization of MZ value of the surface as the global flatness is taken into consideration. As mentioned in Chapter 3 - Section C, the LSF algorithm involves undertaking the absolute maximum value from absolute maximum values that are obtained through least square fit function. This makes the definition of the sensitivities for optimization a complex task. Apart from that, Figure 3.13 involves sharp error peaks wherein the errors at the nodes are defined. These sharp peaks lead to complications in defining the differentiation function. Due to complexities in defining the sensitivities of LSF, the MZ value is chosen as the optimization objective. As compared to the brute force results, the inclusion of an optimizer will involve obtaining an optimum global flatness value thereby having an added advantage of reduced computational time. Along with the reduced computational time, the issue of multiple optima can be solved by incorporating a constraint on the problem. The constraints incorporated are on the eigenfrequency of the structure and the actuator forces. Along with the actuator location as a variable, the actuator forces are also added to the list of variables, thereby enabling the algorithm to find the best combination to attain the optimum. The actuators incorporated in the design domain are piezoelectric push-pull type actuators. In this optimization, the actuator force is bounded between -100 N (pull force) and $+100$ N (push force).

B SHAPE FUNCTION

The wafer table structure is modelled in a plane-strain FEM domain where the entire structure is sub-divided into discrete elements. Figure 3.17 includes contour plots wherein every possible actuator position was evaluated with their corresponding effect on LSF score and MZ value. This was done by changing the actuator position from one node to another. However, the positioning of actuators in intermediate points between any two nodes was left unexplored. In order to find the optimum surface flatness, the optimization includes placement of actuators between two nodes and interpolating the actuator forces to the 2 adjacent nodes. The interpolations play a vital role in the optimization as it provides the sensitivity information to the optimizer. This interpolation of actuator force is done by the implementation of shape functions.

The shape function is a function which interpolates the solution between the discrete values obtained at the mesh nodes. Figure 4.1 represents a single element illustrating the interpolation of forces along the nodes. The nodes of the element k are represented by p and r. Node q represents the location at which the actuator force b^q_{act} acts.

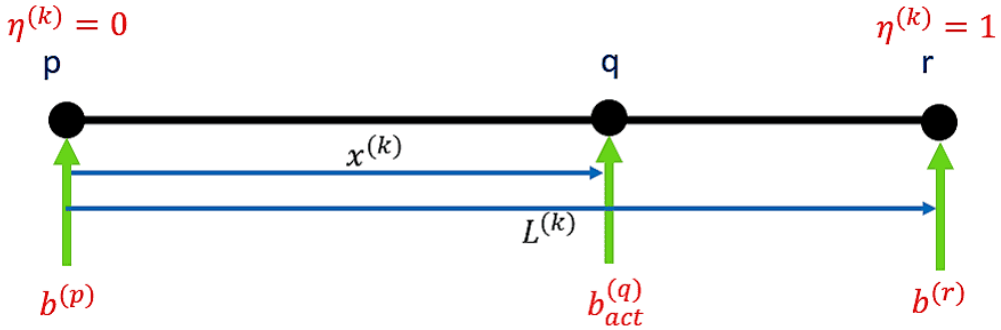

Figure 4.1: Linear interpolation of actuator force

Since node q is the intermediate point in between node p and node r, the distribution of actuator force from node q to nodes p and r is done using linear interpolation functions. Here, x^k represents a position of node q, and the L^k represents the length of the element. The forces at nodes p and r can be expressed using natural coordinates η as represented in Equation 4.1.

$$\eta^{(k)} = \frac{x^k}{L^k} \tag{4.1}$$

Where the forces at nodes p and r are formulated as:

$$b^{(p)} = (1 - \eta^{(k)})b^{q}_{act} \quad \text{and} \quad b^{(r)} = \eta^{(k)}b^{q}_{act}; \quad 0 \leq \eta \leq 1 \tag{4.2}$$

where $\eta^{(k)} = 0$ corresponds to the starting point of the element, at node p, and $\eta^{(k)} = 1$ corresponds to the end point of the element, at node r. In this thesis, the shape functions are implemented as they provide sensitivity information about the actuator location and actuator forces that act as the design variables. The sensitivity formulations of the functions are represented in Equation 4.3.

$$\frac{\delta \mathbf{g}(x^k)}{\delta x^k} = \frac{\delta \mathbf{g}(x^k)}{\delta \eta^k}\frac{\delta \eta^k}{\delta x^k} \tag{4.3}$$

Here, $\mathbf{g}(x^k)$ can represent actuator stiffness/actuator force and can be expressed using the natural coordinates. These expressions make it easier to integrate and differentiate without having to take into account the size and shape of the element as much.

C PROBLEM FORMULATION

The optimization problem formulation includes the minimization of the MZ value obtained from placement of actuators along the surface. The optimization consists of actuator locations and actuator force as the design variable. The actuator force is bounded having a maximum push force of $+100$ N and a maximum pull force of -100 N. The optimization problem formulation is represented in Equation 4.4.

$$\begin{aligned} &\min_{\mathbf{l},\mathbf{F},F_m} \quad \text{MZ} \\ &\text{subject to: } \frac{\omega_{min}}{\omega_1(\mathbf{l})} - 1 \leq 0 \\ &\qquad (\textstyle\sum_{i=1}^{n} F_i) + F_m = 0; \quad -100 \leq (\mathbf{F}, F_m) \leq 100 \end{aligned} \tag{4.4}$$

where n denotes number of actuators, $\mathbf{l}$ denotes a vector containing location of the actuators actuators, $\mathbf{F}$ denotes the actuator forces, and F_m denotes the force of the middle actuator. As represented in Equation 3.1, the MZ value is defined as the distance between the maximum deformation value and the minimum deformation value. However, while formulating the objective function for an optimization problem, the MZ value is defined by implementing a p-norm aggregation function. The primary motive of implementing a p-norm aggregation function is its ability to converge to the maximum value of the data set [17]. The p-norm aggregation function overestimates the maximum value by attempting to find the distance between the calculated value and the maximum value in the sampling data, thereby controlling the distance during the convergence of the function [18]. The formulation of the objective function is shown in Equation 4.5. Here $\mathbf{u}$ denotes the displacement of sampling points. The wafer table gets displaced due to the actuator forces. In order to correctly implement the MZ value, it is necessary that the maximum and minimum sampling point deformation is known. This is done by overestimating the maximum of the deformation and underestimating the minimum of the deformation.

$$\begin{aligned} \tilde{\mathbf{u}} &= S \cdot \mathbf{u} \\ \text{MZ} &= \left(\textstyle\sum_{i=1}^{k} \tilde{u}_i^{p}\right)^{\frac{1}{p}} - \left(\textstyle\sum_{i=1}^{k} \tilde{u}_i^{-q}\right)^{\frac{-1}{q}} \end{aligned} \tag{4.5}$$

where k denotes number of sampling points on the surface, $\tilde{\mathbf{u}}$ denotes the scaled displacement of sampling points, S denotes the scaling factor, and p and q denotes the power of the p-norm aggregation function for overestimation and underestimation respectively. The outcome obtained from the p-norm aggregation function is defined as the minimum zone value. In the p-norm function, larger values of p and q result in smaller variation in distance between the calculated value and the actual value. In order to find the best suited value, the error of the function was

checked wherein the value of p and q were varied ranging from 2 to 150. Having lower values of the norm results in high errors in the final objective function. As the value of norm crosses 40, there is numerical underflow observed, wherein the the value of the objective function is lower than the systems capability of handling. In this optimization, the deformation of a point is in the order of nanometers, and as the optimization cycles iterates, its value further drops down. Therefore, in this optimization, the deformations were scaled by 10^8 and the p-norm error was further reduced with high values of the power (p and q). However, if the values of the power were increased further, the error obtained decreased but the sensitivity of the function becomes non-smooth with high fluctuations. Therefore, to maintain a balance between the sensitivity and the error, the choice of the power value is an important aspect in the objective function. In this implementation, the value of p and q was assigned as 36. During optimization, the optimal solution is found by continually modifying the design until the minimum value objective function is computed, while it satisfies the constraint equations. The two constraints imposed on the optimization are:

1. **Eigenfrequency Constraint**
   The eigenfrequency constraint is applied to the fundamental eigenfrequency such that the first non-rigid body frequency must be greater than 1250 Hz. The representation of the constraint in negative null form is as shown in Equation 4.6.

$$\frac{\omega_{min}}{\omega_1(\mathbf{1})} - 1 \leq 0 \tag{4.6}$$

   where ω_1 is the first non-rigid body mode eigenfrequency of the structure. The stiffness of the system is of the order 10^8 N/m and the weight of the wafer table is 1.5 kg. From this data, the frequency of the structure should be around 1250 Hz. Therefore, the value of ω_{min} is assigned the value of $2\pi 1250$ rad/s.

2. **Force Constraint**
   The optimum global flatness value of the structure can be obtained by optimizing for the force of actuators along with their placement. In order to achieve this, an equality constraint on actuator force is applied in the optimization. The wafer table must be in static equilibrium at all times. Therefore, the summation of all the actuator forces must be zero. If it is not the case the structure will not be in static equilibrium and will be accelerating in a particular direction. The formulation of the constraint is as shown in Equation 4.7. In this formulation, gravitational force is ignored as the effect of that force is very less as compared to the actuator forces.

$$(\sum_{i=1}^{n} F_i) + F_m = 0; \quad -100 \leq (\mathbf{F}, F_m) \leq 100 \tag{4.7}$$

   The implementation of this constraint is done by converting it in two negative null form formulations. The equations are represented as:

$$\begin{gathered} (\textstyle\sum_{i=1}^{n} F_i) + F_m \leq e; \quad (\textstyle\sum_{i=1}^{n} F_i) + F_m \geq -e \\ \frac{(\sum_{i=1}^{n} F_i) + F_m}{e} - 1 \leq 0 \\ \frac{-\left\{(\sum_{i=1}^{n} F_i) + F_m\right\}}{e} - 1 \leq 0 \end{gathered} \tag{4.8}$$

   In Equation 4.8, the summation of actuator forces is bounded between $-e$ and $+e$, wherein e is assigned a very small value (in this optimization e = 0.1). The reason for this bounding is to convert the equality constraint in negative null form. By applying this conversion, the single equality constraint is converted into 2 inequality constraints. Here, the constraint on $+e$ is called force constraint on upper bound and that on $-e$ is called force constraint on lower bound.

The design variables are normalized in the optimization and the value of the variables is bounded between 0 and 1. In the case of actuator location the normalization was straight forward where 0 represents the minimum value and 1 represents center of the wafer table. Since, symmetric deformation curves are superimposed on the wafer table, the maximum value of the actuator

position is the center of the wafer table. The force of the actuator is also normalized from 0 to 1, where 0 represent pulling force ($-F_{max}$) and 1 is the pushing force (F_{max}) of the actuator. The actuator force implementation is formulated in Equation 4.9.

$$F_a = (2(f) - 1)F_{max} \tag{4.9}$$

where F_a represents actuator force, f represents the force normalization value from 0 to 1, and $F_{max} = 100$ N is the maximum force of the actuator. If the value of f is assigned 0.5 the actuator will not apply any force. Therefore, in this optimization, the state, $f = 0.5$ is the starting point of the actuators force as a variable.

D SENSITIVITY ANALYSIS

This section includes formulation of the sensitivities associated in this optimization. As shown in Figure 3.16, the actuators are represented as spring members. This section also includes the sensitivity of the p-norm function and also the sensitivities associated with actuators with respect to its location.

1. P-norm function

   The MZ value of the wafer table is calculated using a p-norm aggregation function. The formulation of the objective is represented in Equation 4.5. The sensitivity of the p-norm function (P) is formulated as:

$$\frac{\delta f}{\delta \tilde{u}_i} = \frac{\delta f}{\delta P} \cdot \frac{\delta P}{\delta \tilde{u}_i} \quad \forall i \in \{1, ..., n\}$$

$$\frac{\delta f}{\delta \tilde{u}_i} = \frac{\delta f}{\delta P} \cdot \frac{\delta \left(\sum_{i=1}^{n} \tilde{u}_i^p \right)^{\frac{1}{p}}}{\delta \tilde{u}_i}$$

$$\frac{\delta f}{\delta \tilde{u}_i} = \frac{\delta f}{\delta P} \cdot \left(\tilde{u}_i \right)^{p-1} \left(\sum_{i=1}^{n} \tilde{u}_i^p \right)^{\frac{1-p}{p}}$$

   Here, f is the final objective function, and $\tilde{u}_i$ represents the deformation of the n sampling points.

2. Actuator properties

   The sensitivity of the actuators is dependent on the interpolation function mentioned in Equation 4.3. The sensitivity formulation is explained taking a reference of Figure 4.2.

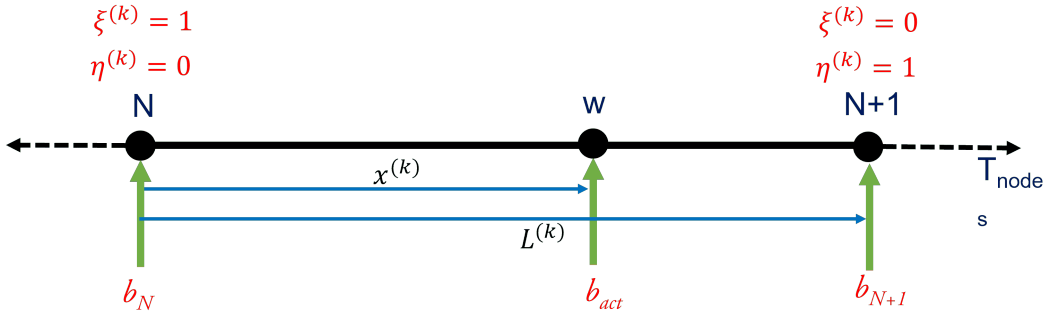

Figure 4.2: Actuator force distribution

Here w denotes the actuator location, b_{act} denotes the actuator force at w, N and $N+1$ denote the interpolating points, η and ξ represent the natural co-ordinates, T denotes the total number of nodes, $\mathbf{g}$ represents the actuator property (actuator force/stiffness), and f represents the final objective function. The formulation of sensitivity of actuator property sensitivity based on the change of location (x) is represented as:

$$\frac{\delta f}{\delta x} = \frac{\delta f}{\delta \mathbf{g}} \cdot \frac{\delta \mathbf{g}}{\delta x}$$

$$\frac{\delta f}{\delta x} = \sum_{i=1}^{T} \frac{\delta f}{\delta g_i} \cdot \frac{\delta g_i}{\delta x}$$

$$\frac{\delta \mathbf{g}}{\delta x} = \left[0,0,0,...,\frac{\delta g_N}{\delta x},\frac{\delta g_{N+1}}{\delta x},...,0,0,0\right]$$

$$\frac{\delta f}{\delta x} = \frac{\delta f}{\delta g_N} \cdot \frac{\delta g_N}{\delta x} + \frac{\delta f}{\delta g_{N+1}} \cdot \frac{\delta g_{N+1}}{\delta x}$$

$$\frac{\delta f}{\delta x} = \frac{\delta f}{\delta g_N} \cdot \left\{\frac{\delta g_N}{\delta \eta} \cdot \frac{\delta \eta}{\delta x}\right\} + \frac{\delta f}{\delta g_{N+1}} \cdot \left\{\frac{\delta g_{N+1}}{\delta \xi} \cdot \frac{\delta \xi}{\delta x}\right\}$$

The forces on the nodes denoted by g_N and g_{N+1} are represented in terms of actuator force b_{act} as:

$$\frac{\delta f}{\delta x} = \frac{\delta f}{\delta g_N} \cdot \left\{\frac{\delta \eta b_{act}}{\delta \eta} \cdot \frac{\delta \eta}{\delta x}\right\} + \frac{\delta f}{\delta g_{N+1}} \cdot \left\{\frac{\delta \xi b_{act}}{\delta \xi} \cdot \frac{\delta \xi}{\delta x}\right\}$$

Now the natural coordinates η and ξ are represented in terms of distance of the actuator force location as:

$$\frac{\delta f}{\delta x} = \frac{\delta f}{\delta g_N} \cdot \left\{b_{act} \cdot \frac{\delta \frac{L-x}{L}}{\delta x}\right\} + \frac{\delta f}{\delta g_{N+1}} \cdot \left\{b_{act} \cdot \frac{\delta \frac{x}{L}}{\delta x}\right\}$$

$$\frac{\delta f}{\delta x} = \frac{\delta f}{\delta g_N} \cdot \left\{b_{act} \cdot \frac{-1}{L}\right\} + \frac{\delta f}{\delta g_{N+1}} \cdot \left\{b_{act} \cdot \frac{1}{L}\right\}$$

$$\frac{\delta f}{\delta x} = \frac{b_{act}}{L}\left\{\frac{\delta f}{\delta g_{N+1}} - \frac{\delta f}{\delta g_N}\right\}$$

This formulation can also be translated when interpolating the stiffness of the actuator. The sensitivity of the actuator stiffness is represented as:

$$\frac{\delta f}{\delta x} = \frac{K_{act}}{L}\left\{\frac{\delta f}{\delta g_{N+1}} - \frac{\delta f}{\delta g_N}\right\}$$

Where K_{act} is the stiffness of the actuator.

E RESULTS

Based on the formulation of the global flatness function as per Equation 4.5, a MZ value minimization has been carried out. The motive of this optimization is to minimize the deformations in the wafer table subjected to self weight sagging and superimposed deformation curves. The optimization involves implementation of eigenfrequency and force constraints to the problem. The design domain of the structure is represented in Figure 3.16. It includes finding the optimum location and force of the actuators thereby taking them as the design variables.

The four deformations imposed on the wafer table are; 1) 2^{nd} order - Parabola (Bowl), 2) 2^{nd} order - Inverted Parabola (Umbrella), 3) Cosine function, 4) Inverted cosine function. The equations of the curves are represented in Table 4.1, where n denotes the number of sampling points, y_{max} is

the maximum deformation amplitude, and y denote the y deformation amplitude depending on the corresponding x values.

Curvature type	Equation of the curvature
2^{nd} order - Parabola (Bowl)	$y = y_{max}(\frac{x}{R})^2$
2^{nd} order - Inverted parabola (Umbrella)	$y = y_{max} - y_{max}(\frac{x}{R})^2$
Cosine function	$y = \frac{y_{max}}{2} - \frac{y_{max}}{2}\ cos(\frac{2\pi x}{D})$
Inverted cosine function	$y = \frac{y_{max}}{2} + \frac{y_{max}}{2}\ cos(\frac{2\pi x}{D})$

Table 4.1: Equations of the deformation curves

The optimization included undertaking placement of 2 actuators per half and 1 actuator in the center. Therefore, there are 5 actuators in total wherein the location and force of the actuators in one half is same as that to the other. In total there exist 5 variables in the optimizations, 3 being the actuator forces and 2 are the actuator location. As mentioned in Section A, the location of the center actuator remains constant throughout the optimization and is optimized only for its force (F_m). The design variables are illustrated in Table 4.2.

Variable name	Symbol
Actuator 1 location	l_1
Actuator 2 location	l_2
Actuator 1 force	F_1
Actuator 2 force	F_2
Center actuator force	F_m

Table 4.2: Definition of optimization variables - 2 actuators per half

The optimization was carried out by implementing the respective objective and constraint functions using the MMA solver. Each of the 4 deformations were superimposed on the wafer table separately and the results obtained are shown in Figure 4.3, Figure 4.4, Figure 4.5, and Figure 4.6. These figures represent the optimization carried out when the wafer table was subjected to 2^{nd} order - Parabola (Bowl), 2^{nd} order - Inverted Parabola (Umbrella), Cosine, and Inverted cosine deformation curves respectively.

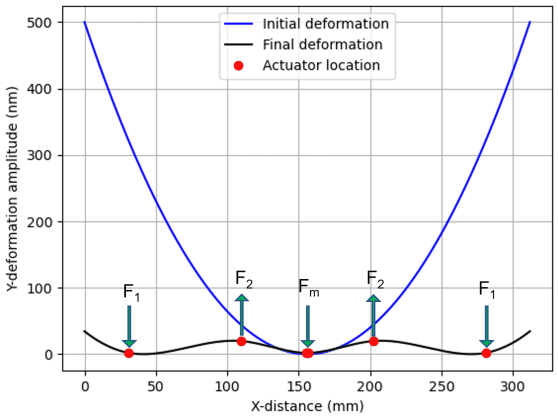

(a) Deformation Initial v/s Final

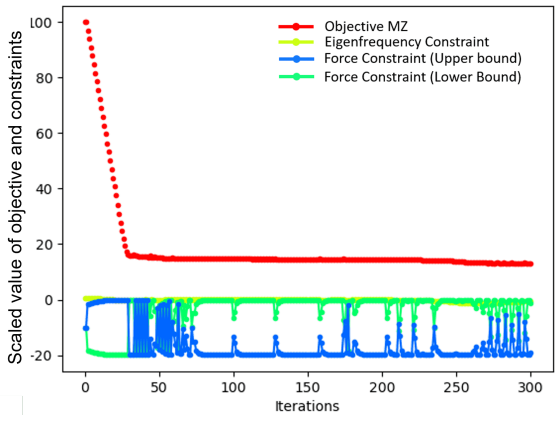

(b) Actuator optimization convergence - Bowl deformation

Figure 4.3: Optimization results - 2^{nd} order - Parabola (Bowl)

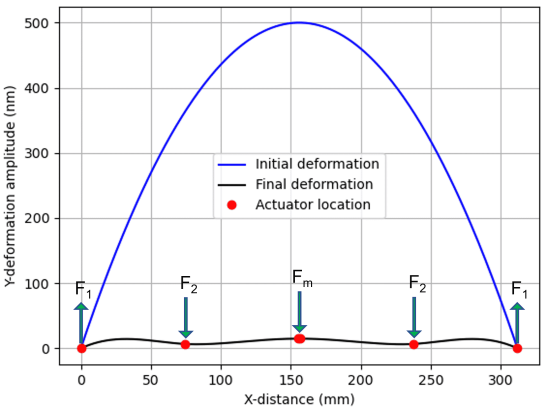

(a) Deformation Initial v/s Final

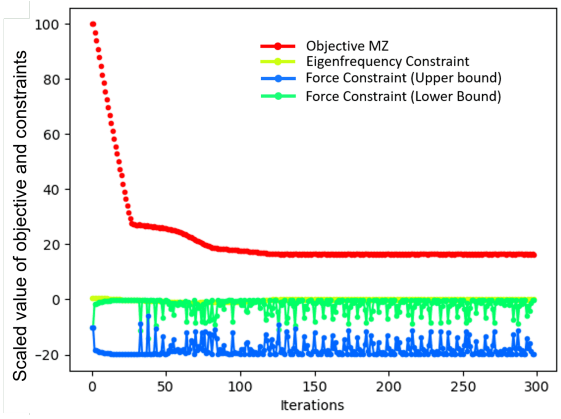

(b) Actuator optimization convergence - Umbrella deformation

Figure 4.4: Optimization results - 2^{nd} order - Inverted parabola (Umbrella)

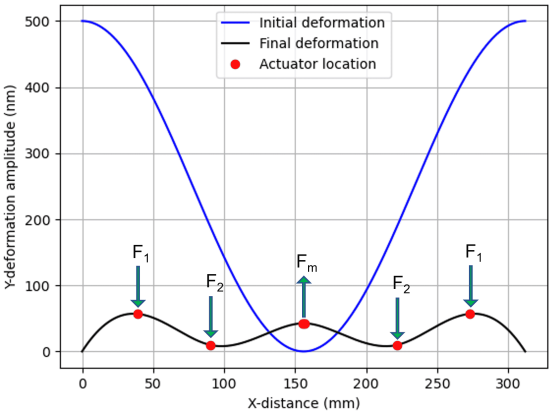

(a) Deformation Initial v/s Final

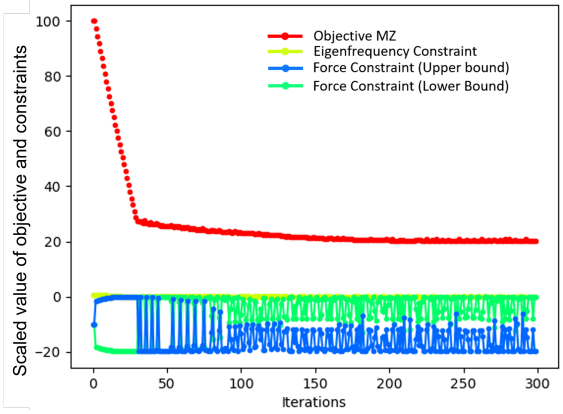

(b) Actuator optimization convergence - Cosine deformation

Figure 4.5: Optimization results - Cosine function

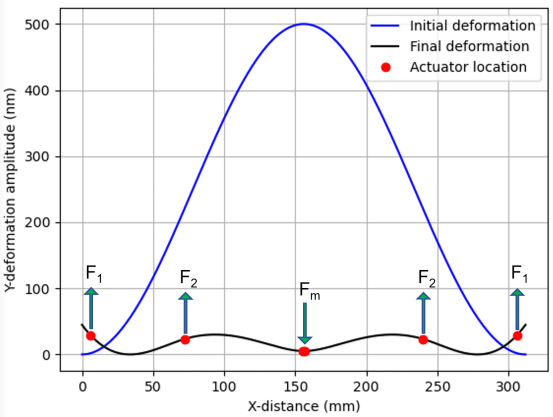

(a) Deformation Initial v/s Final

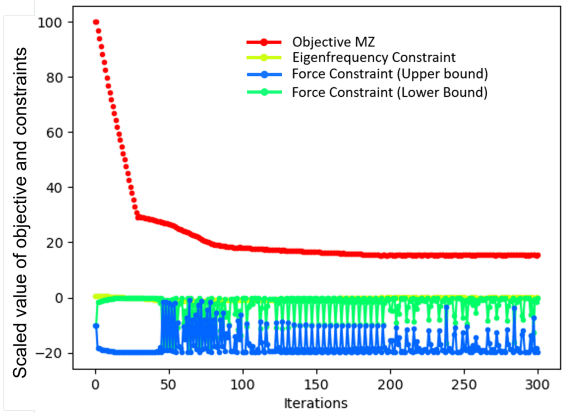

(b) Actuator optimization convergence - Inverted Cosine deformation

Figure 4.6: Optimization results - Inverted cosine function

The results illustrated in Figure 4.3a, Figure 4.4a, Figure 4.5a, and Figure 4.6a represents the deformations of the wafer table. The initial deformation corresponds to addition of self-weight

sag and superimposition of deformation curve. The figures show the initial and final deformation of the wafer table when the actuators are placed at the optimum location and act with optimum force. Figure 4.3b, Figure 4.4b, Figure 4.5b, and Figure 4.6b represents the convergence plots of the deformations. The plots demonstrating the change in the design variables are available in Appendix C. The equations tabulated in Table 4.1 show that the Bowl and Cosine curve have maximum deformation at the edges. Whereas, the Umbrella and Inverted cosine curve have maximum deformation at the center. These differences in curve types were implemented to check, how the optimization behaves for center versus edge deformation. In the implementation, the initial MZ value for all deformations is 500 nm. The results obtained in Figure 4.3, Figure 4.4, Figure 4.5, and Figure 4.6 are quantified in tabular form shown in Table 4.3. The table also shows the initial and final LSF score of the deformation.

Deformation	l_1	l_2	F_1	F_2	F_m	**MZ**	**LSF** (nm)	
	(mm)	(mm)	(N)	(N)	(N)	(nm)	Initial	Final
Bowl	31.07	109.57	−30.09	41.64	−11.64	34.420	2.199	2.157
Umbrella	0.31	74.55	34.05	−24.69	−9.42	14.924	2.232	1.769
Cosine	39.30	90.63	−7.99	−42.29	50.18	57.115	5.138	4.954
Inv. Cosine	6.61	72.58	13.09	30.87	−44.06	44.792	5.075	4.831

Table 4.3: Optimum values - (2 actuators per half)

The results show that the optimum MZ value of Bowl and Cosine deformation is greater than that of Umbrella and Inverted cosine respectively. The MZ values represented in the table represent the exact MZ value. It can be observed that controlling a deformation curve with maximum deformation along the edges is difficult as compared to a curve with center deformation. Taking the center axis of the wafer table as the reference point, for edge based deformation curves the optimizer generally tries to place one actuator at the edge with a suitable force. While doing so, the center part which consists of minimum deformation tends to deteriorate thereby making the optimizer place the second actuator close to the reference point. This enforces the optimizer to converge to a local optimum. This is not the case for Umbrella and Inverted cosine deformation, wherein the maximum deformation is at the center of the wafer table. During optimization of the center-based deformation curves, during initial iterations the optimizer tries to place the actuator somewhere in the mid-region and as the optimization converges, the actuator location is shifted more towards the edge. This behaviour can be verified through the plots showing the change in the design variables throughout the optimization. The plots are available in the Appendix C. From the results, it is observed that one actuator is placed at the edge where the deformation is minimum and the other actuator gets placed in a region approximately between the wafer edge and the reference point. From the results obtained for Umbrella and Inverted cosine deformation, it would be difficult to comment on the global convergence, since no information is available about it. A thorough investigation is further required to comment on the local/global convergence of Umbrella and Inverted cosine deformation. However, based on the MZ value obtained for these deformations, it can be assumed that the optimum actuator locations for these deformations are in the vicinity of the global optimum or have converged to the best local optimum. From Table 4.3, it can be seen that after optimization there is a decrease in the LSF score which inherently reduces local scanning error. However, the dependency of local scanning error on global flatness needs to undergo further examination to reach a conclusion.

In order to estimate the effect of number of actuators on the surface deformations, an optimization with 3 actuators per half was implemented. In this optimization, 7 actuators in total were involved wherein the location and force conditions of the actuators remained same as previous optimization with 5 total actuators. In this optimization, there existed 7 variables in the optimizations, 4 being the actuator forces and 3 are the actuator location. The location of the center actuator remains constant throughout the optimization and is optimized only for its force. The results obtained are shown in Figure 4.7. The optimization variables are tabulated in Table 4.4.

Variable name	Symbol
Actuator 1 location	l_1
Actuator 2 location	l_2
Actuator 3 location	l_3
Actuator 1 force	F_1
Actuator 2 force	F_2
Actuator 3 force	F_3
Middle actuator force	F_m

Table 4.4: Definition of optimization variables - 3 actuators per half

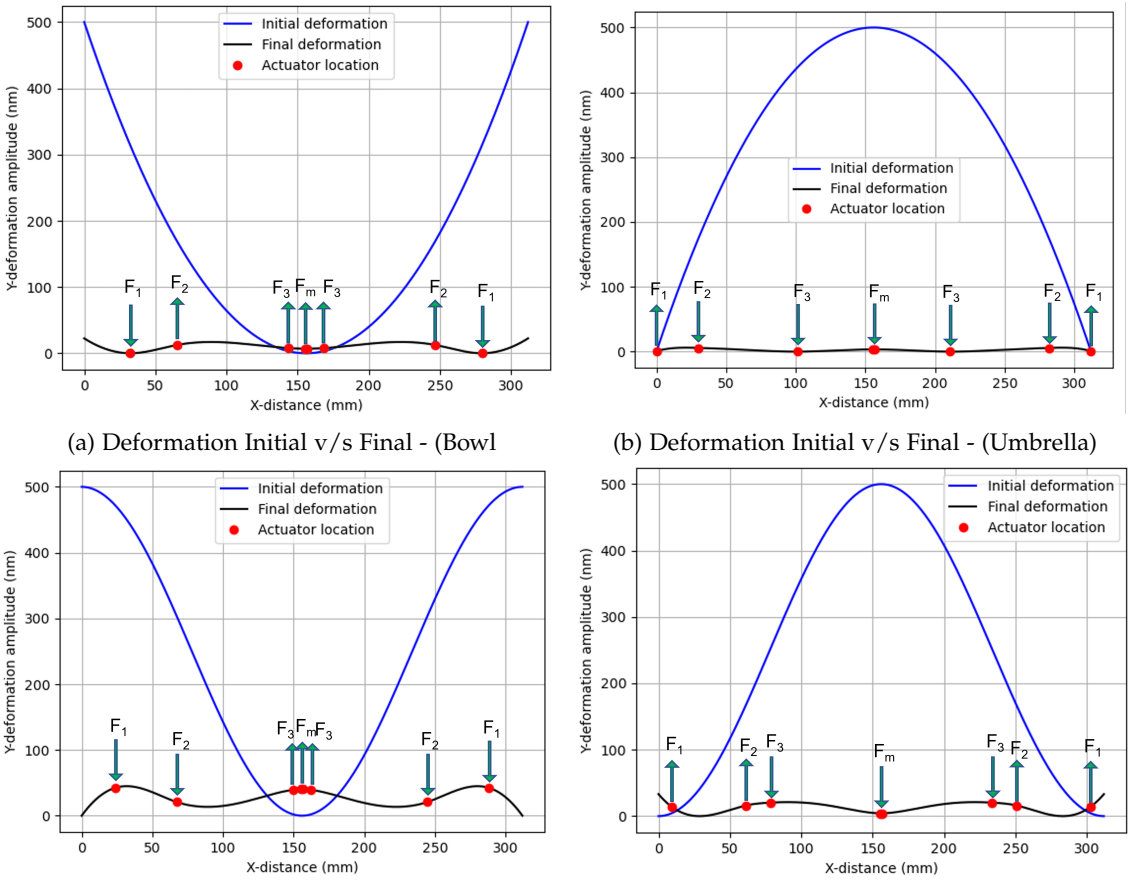

(a) Deformation Initial v/s Final - (Bowl

(b) Deformation Initial v/s Final - (Umbrella)

(c) Deformation Initial v/s Final - (Cosine)

(d) Deformation Initial v/s Final - (Inverted cosine

Figure 4.7: Optimization results - 3 actuators per half

The results illustrated in Figure 4.7a, Figure 4.7b, Figure 4.7c, and Figure 4.7d represents the deformations of the wafer table. The results obtained in Figure 4.7 are quantified in tabular form shown in Table 4.5.

Deformation	l_1 (mm)	l_2 (mm)	l_3 (mm)	F_1 (N)	F_2 (N)	F_3 (N)	F_m (N)	**MZ** (nm)	**LSF** (nm)
Bowl	32.66	65.79	143.25	−40.75	23.94	8.66	8.06	22.50	2.177
Umbrella	0.76	30.03	101.59	41.46	−6.91	−24.60	−10.03	6.176	1.469
Cosine	24.18	67.70	149.99	−9.18	−53.02	23.91	38.18	44.917	4.492
Inv. Cosine	9.49	61.58	78.26	4.19	59.23	−24.74	−38.74	33.144	4.847

Table 4.5: Optimum values - (3 actuators per half)

The results obtained in Table 4.3 and Table 4.5 show that as the number of actuators increase, the MZ value decreases thereby improving the global flatness of the surface. The results also show that, the optimizer tends to place one of the actuator in the area where the deformation is low i.e. in the case of Bowl and Cosine, one actuator is placed very close to the center of the wafer table (l_3) and in the case of Umbrella and Inverted cosine one actuator is stationed at the edge (l_1). Also, the results show that the local flatness value (LSF score) does not depend on the global flatness value (MZ value).

This section included the results obtained from the optimization for flatness correction of a deformed wafer table. It was observed that for the edge based deformation curves the chances of convergence to a bad local optima is quite high. Whereas in the case of center based deformation curves, the MZ value obtained is comparatively low than that of the other curves and the convergence is towards a good local optima which lies in the vicinity of the global optimum. One primary reason of the local convergence is the selection of starting point of the optimization. Therefore, it needs an analysis wherein the behaviour of the MZ value for all 4 deformations is studies by changing the starting point of the optimization.

F EFFECT OF STARTING POINT ON OPTIMIZATION

From the results obtained in the previous section, it is observed that in the case of edge based deformation curves there are high chances of the optimizer to converge to a local optima. This behaviour of convergence is highly dependent on the selection of starting point of the optimization. When defining an optimization problem, it is of utmost importance to define an appropriate starting point from which it is possible to go to a good local optimum. Generally, in problems with multiple design variables and multiple possible starting points, it becomes very difficult to find an ideal starting point from which the optimizer is expected to converge to a better solution.

In order to check the effect of starting point on the actuator placement problem, multiple optimizations were run from different combination of starting points. Through this investigation, it was observed that, in the case of edge based deformation curves, the optimizer always converged to a local optimum and kept cycling around that point. The results obtained form the investigations are shown in Figure 4.8.

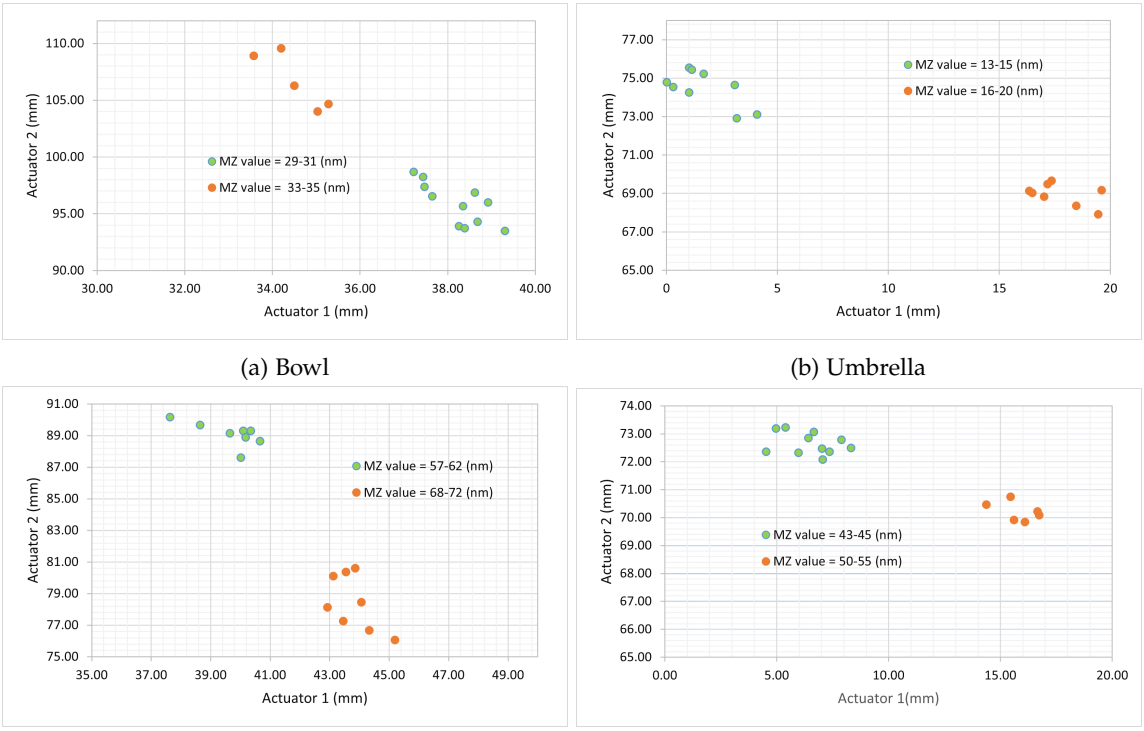

(a) Bowl

(b) Umbrella

(c) Cosine

(d) Inverted Cosine

Figure 4.8: Effect of starting point on global flatness (2 actuators per half)

The plots illustrate the final actuator locations along with their MZ values when the optimization was performed by changing the starting points from 0.0 to 1.0 in the increments of 0.1. It can be observed that each of the deformation curve consists of 2 local optimum. Based on the data collected it was observed that the normalized starting point of (0.1, 1.0) proved a better option and hence was chosen as the starting point for all the deformation curves. This selection of starting point was based on data compiled through multiple test runs of the optimization. However, if the number of actuators are increased then it becomes cumbersome to investigate through this technique. Therefore, there needs exploration of methods that involves a holistic approach in determining a suitable starting point for such problems with high dimensions.

Similar to 2 actuators per half, an investigation of selection of starting point was performed in 3 actuators per half case as well. The investigations revealed that the initial starting point of second and third actuator should not be very close to each other. This causes the optimizer to converge to a bad local optimum. For instance, if the initial point was assigned as (0.1, 0.9, 1.0) or (0.1, 0.2, 1.0) the MZ value obtained was the worst of all. Therefore, based on the observed pattern, a starting point of (0.1, 0.4, 1.0) was selected for 3 actuators per half case.

After defining a suitable starting point and performing individual deformation optimization, there is an important aspect that needs to be focused on. The actuators are to be placed between the intermediate body and the wafer table. The results tabulated in Table 4.3 and in Table 4.5 show different optimum actuator positions for different type of deformations. However, in an intermediate body, the location of actuators are fixed and therefore it is necessary to find the optimum location of actuators which adheres to all types of deformations and maintain the global flatness of the surface. Inorder to achieve this, an analysis was performed wherein the location of the actuators are to be fixed and the forces of the actuators are considered as the design variables. This analysis is performed in order to get an estimation of the optimum actuator locations on the intermediate body. Further, a combined optimization problem was defined wherein all the four deformation curves were considered at once and the optimum actuator locations and forces were found.

G ACTUATOR POSITIONING FOR ALL DEFORMATION TYPES

In this section, the optimum location of actuators on the intermediate body are to be found. This includes referring data of optimum actuator locations tabulated in Table 4.3 and in Table 4.5. All of the 4 deformation curves produce total 8 actuator locations for 2 actuators per half and 3 actuators per half cases. In this section, an analysis is performed wherein the optimum actuator locations obtained previously are kept constant and all the deformations are evaluated for their global flatness by having actuator forces as the design variables. Which means each of the actuator locations will be evaluated for all the 4 deformation curves. This analysis will be done for all 8 actuator locations and the corresponding effect on global flatness will be evaluated. In each of the optimization, the actuator location value obtained from the previous optimizations are fixed and all four deformation curves undergo optimization for that one location with their actuator force as the optimization variable. This analysis is performed to check the convergence of some of the deformations to a local optima and to get an estimation of a better optimum actuator location. After performing this analysis, a combined optimization problem is defined wherein the global flatness of the wafer table will be optimized considering all the deformation curves at once.

Initially the analysis of 2 actuators per half is performed. The parameters are defined in Table 4.6.

Reference	**Deformation**	**Actuator** 1 **-** l_1 **(mm)**	**Actuator** 2 **-** l_2 **(mm)**
A	Bowl	31.07	109.57
B	Umbrella	0.31	74.55
C	Cosine	39.30	90.63
D	Inv. Cosine	6.61	72.58

Table 4.6: Properties of piezoelectric actuators - Fixed actuator positions

Table 4.6 represents the optimum location of actuators for Bowl, Umbrella, Cosine, and Inverted cosine deformations. The optimum actuator locations obtained from previous optimizations are referred as A, B, C, and D respectively. For each of the location reference, an optimization is carried out by taking actuator forces as design variables. It is done to study the influence of each of the location reference on MZ value of each of the curves. For example, at location reference A the optimization was carried out by superimposing the wafer table with Bowl, Umbrella, Cosine, and Inverted cosine deformations. This is implemented for each location (A, B, C, and D). The results obtained from this analysis are represented in Figure 4.9. The value of actuator forces obtained from the analysis are available in Appendix C.

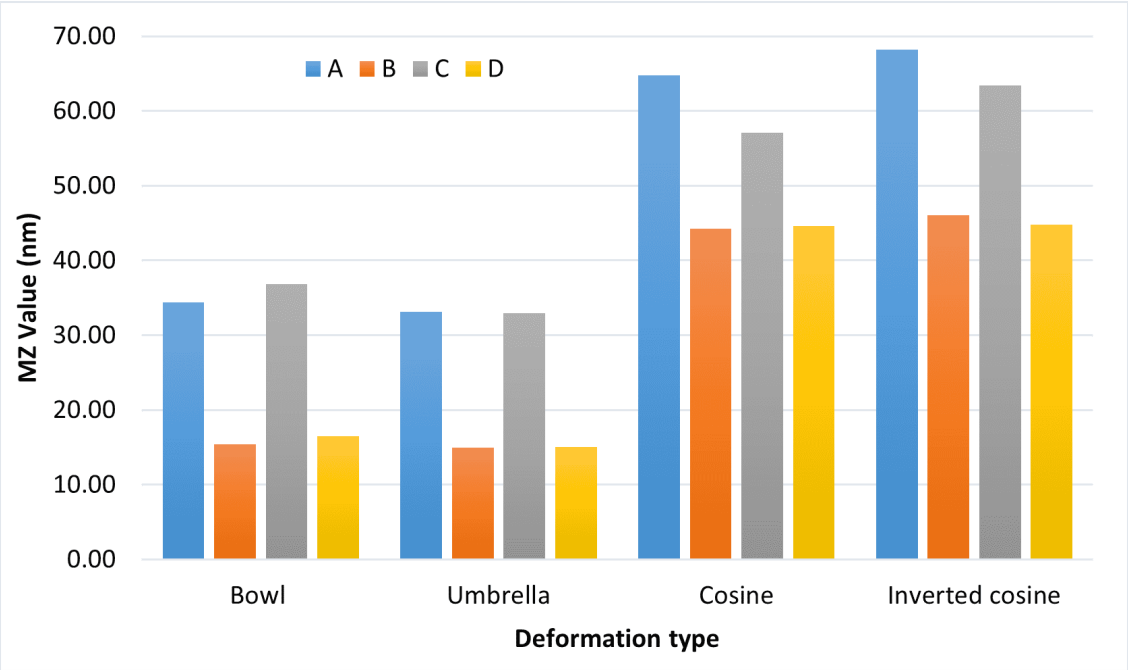

Figure 4.9: Effect of actuator location on MZ value

The bar plot show that, out of the 4 location references, location B and D as ideal actuator locations for all the deformations with least MZ value. In the case of edge deformation curves (Bowl and Cosine), location B and D give better results as compared to their respective optimum. This confirms their convergence to a local optimum. In the case of center deformation curves (Umbrella and Inverted Cosine), their respective optimum location proves best to attain global flatness. From the results obtained it can be observed that the values of actuator location at reference point B and D are very close to each other and prove to be as ideal actuator position on intermediate body. Therefore, from the analysis it can be concluded that, in the case of 2 actuators per half the optimum actuator location must be around:

Actuator	**Location (mm)**
Actuator 1	0 to 5
Actuator 2	74 to 79

Table 4.7: Expected optimum actuator locations

Table 4.7 represents the expected range of optimum from the analysis performed. In order to verify the results obtained, a combined optimization is performed wherein all four deformation curves are considered in a single optimization problem. In this optimization, the objective and the constraints remain the same and consists of 14 design variables. The design variables are 2 actuator locations which remain common for all deformation and 12 actuator forces (3 forces per deformation F_1, F_2, and F_m). Here, there is a common actuator location for all the 4 deformation curves along with the individual actuator forces that are all simultaneously optimized. The optimization routine follows the same procedure as the previous one. The only difference here is that, since it involves 4 deformation curves, there exists 4 MZ values after each iteration. In order to defined a single objective for optimization, a p-norm (p = 36) is taken of those 4 values and the final obtained value is defined as the objective function. The results obtained from this optimization is shown in Figure 4.10.

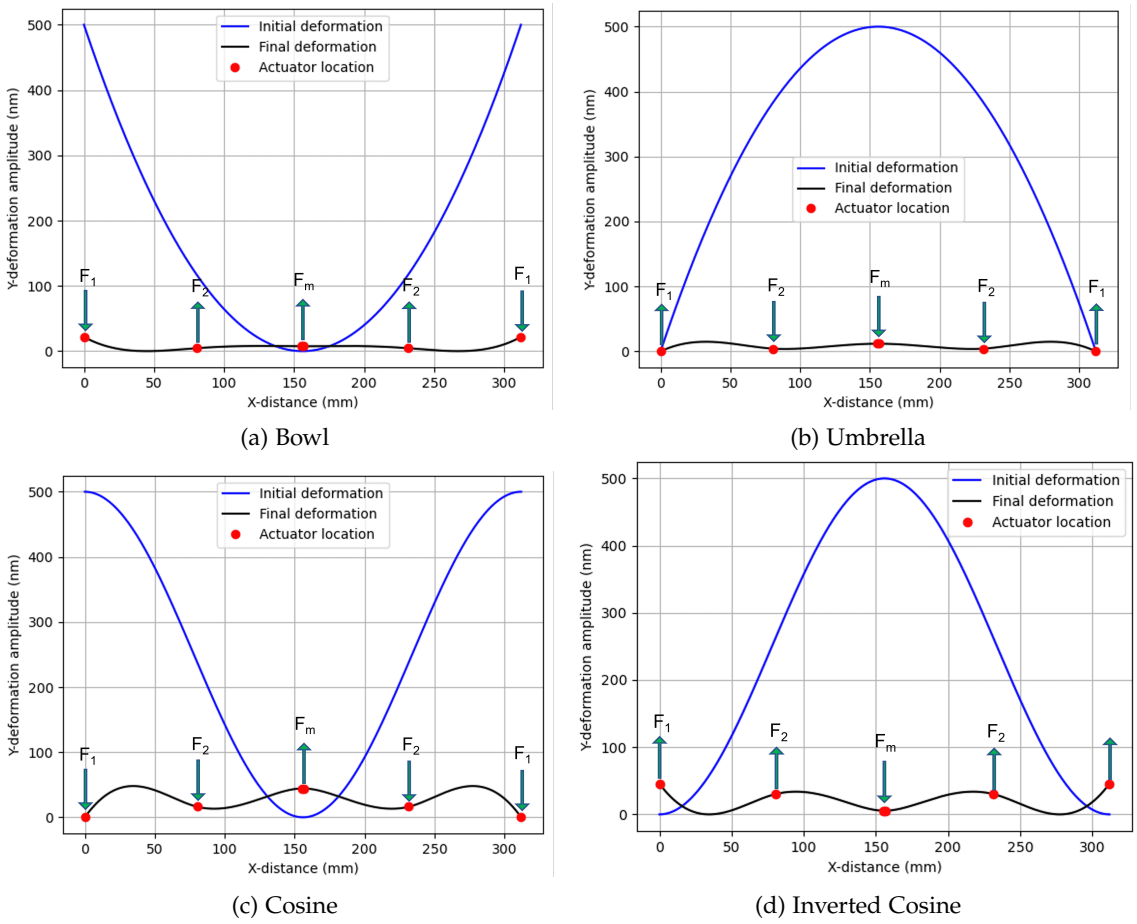

(a) Bowl

(b) Umbrella

(c) Cosine

(d) Inverted Cosine

Figure 4.10: Optimization results - Combined deformation (2 actuators per half)

The results obtained are tabulated in Table 4.8.

Deformation	l_1 (mm)	l_2 (mm)	F_1 (N)	F_2 (N)	F_m (N)	**MZ** (nm)	**LSF** (nm)
Bowl	0.00	80.40	−29.67	18.82	10.85	21.829	1.722
Umbrella			34.46	−26.29	−8.25	14.896	1.784
Cosine			−14.82	−32.04	46.76	48.00	4.784
Inv. Cosine			17.89	28.34	−46.33	45.779	4.679

Table 4.8: Optimum values - (2 actuators per half)

The results obtained from the combined optimization verify the analysis data in Table 4.7. The optimum actuator locations are around the expected range. The MZ values of all the deformations are also close to the expected range. In the case of Umbrella and Inverted cosine, the MZ value match their individual outcome. Whereas in the case of Bowl and Cosine, the MZ value of the deformation has improved from their initial case and march the values obtained in reference location *B* and *D*.

A similar analysis and optimization was implemented with 3 actuators per half case as well. For 3 actuators per side, the definition of parameters is tabulated in Table 4.9.

Reference	Deformation	Actuator1 - l_1 (mm)	Actuator2 - l_2 (mm)	Actuator3 - l_3 (mm)
X	Bowl	32.66	65.79	143.25
Y	Umbrella	0.76	30.03	101.59
Z	Cosine	24.18	67.70	149.99
W	Inv. Cosine	9.49	61.58	78.26

Table 4.9: Properties of piezoelectric actuators - fixed actuator position

Table 4.9 represents the optimum location of actuators for Bowl, Umbrella, Cosine, and Inverted cosine deformations. Each of the location results are referred as X, Y, Z, and W respectively. Based on the actuator positions, their corresponding effect on the global flatness MZ value is represented in Figure 4.11.

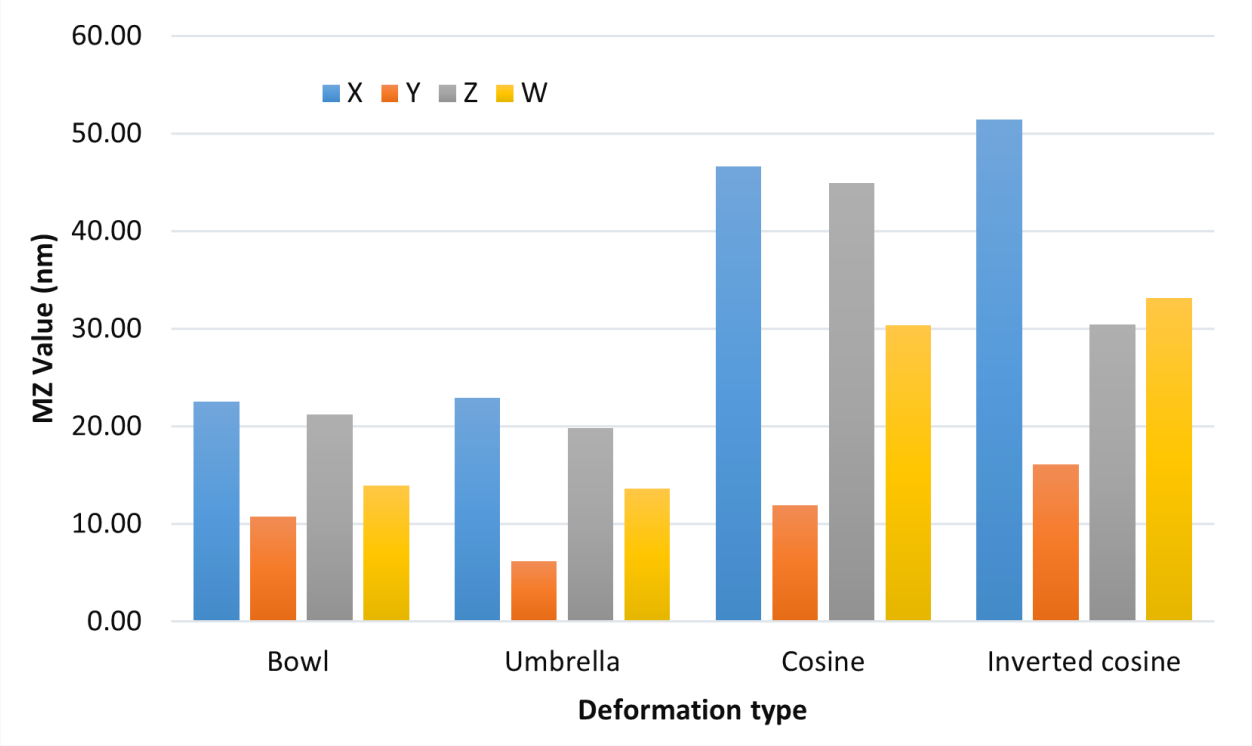

Figure 4.11: Effect of actuator location on MZ value

The bar plot show that location Y as ideal actuator location which gives lower MZ value for all the deformations. In the case of edge deformation curves (Bowl and Cosine), location Y gives better results as compared to their respective optimum. This confirms their convergence to local optimum. In the case of Umbrella deformation its respective optimum proves best to attain global flatness. However, in the case of Inverted cosine, the optimum for Umbrella deformation proves a better option. As compared to the case of 2 actuators per half, it was expected that the actuator locations obtained for Inverted cosine case would be the best for it, but that was not the case. Therefore, from the analysis it can be concluded that, in the case of 3 actuators per half the optimum actuator location must be around:

Actuator	Location (mm)
Actuator 1	0 to 5
Actuator 2	27 to 32
Actuator 3	98 to 103

Table 4.10: Expected optimum actuator locations

Table 4.10 represents the expected range of optimum from the analysis performed. In order to verify the results obtained, a combined optimization problem similar to previous one is defined wherein all four deformation curves are considered all at once. In the case of 3 actuators per half, there exists 19 design variables, 3 common actuator locations, 16 actuator forces (4 per deformation). The results obtained from this optimization is shown in Figure 4.12.

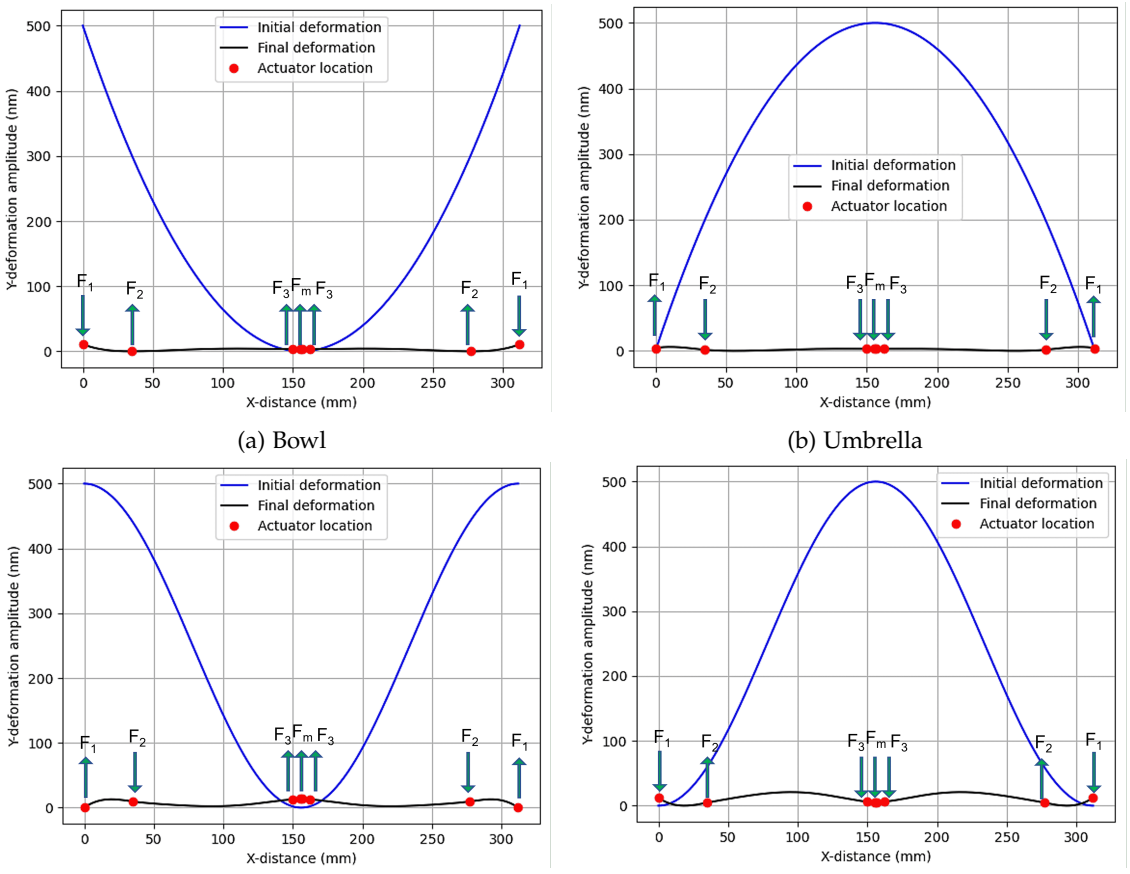

(a) Bowl

(b) Umbrella

(c) Cosine

(d) Inverted Cosine

Figure 4.12: Optimization results - Combined deformation (3 actuators per half)

The results obtained are tabulated in Table 4.11.

Deformation	l_1 (mm)	l_2 (mm)	l_3 (mm)	F_1 (N)	F_2 (N)	F_3 (N)	F_m (N)	**MZ** (nm)	**LSF** (nm)
Bowl	0.17	35.64	149.62	−36.68	2.21	20.33	14.13	10.826	1.565
Umbrella				46.08	−13.33	−22.28	−10.50	6.037	1.369
Cosine				6.19	−68.23	23.95	38.01	13.274	3.802
Inv. Cosine				−1.31	62.43	−27.15	−34.00	20.934	3.857

Table 4.11: Optimum values - (3 actuators per half)

The results obtained from the combined optimization provide different actuator locations as compared to the values in Table 4.10. Out of the 3 optimum actuator locations, l_1 and l_2 are in the expected range or very close to it but location l_3 does not match the expected analysis data. When compared with data in Figure 4.11 reference Y positions, it can be seen that the MZ values of Bowl, Umbrella and Cosine are in the expected range and are very close to the data obtained but the Inverted Cosine deformation is slightly compromised with a variation of around 5 nm. The values obtained from the optimization are as a result of convergence to the best local optima. Upon multiple trials by changing the starting points it was observed that in all instances the problem converged to a l_3 value in the range of $145 - 150$ only. One possible reason for the local convergence of the solution might be due to the high dimensional nature of the problem. In the case of 3 actuators per half there are 19 design variables that define the final optimum. Therefore, there are high chances for the problem to converges to a local solution. From this verification it can be observed that the obtained MZ values from the optimization and the analysis are very close to each other but the value of one of the design variable (l_3) is very different than expected. This means that the optimization problem has two or more local optima that can be closest to the global optimum. However, the phenomena of local convergence observed in this case is subject to further exploration which can be done by comparing the results by optimizing the same problem using Genetic Algorithm (GA).

This section included further implementations of actuator optimization. The primary aim of carrying out the experimentation was to find the best possible actuator locations on an intermediate body. The location of the actuators must be such the actuators must be able to correct wafer table subjected to any form of deformation. The results show that, as the number of actuators increase the deformation of the surface is better corrected thereby ensuring optimum global surface flatness.

H DISCUSSION

Based on the results obtained from the optimization and the analysis performed, following factors influenced the nature of the results and must be taken into consideration.

1. Edge deformation v/s Center deformation

   The optimization performed included 4 deformation curves that are categorized as edge based deformation and center based deformation. From the results obtained it is observed that the edge based deformation curves always converge to a local optimum. This is due to difficulty in controlling the edges of the wafer table. In the case of center based deformation, the Umbrella curve always converged to the best optimum and gave the ideal MZ value as compared to the other curves. However, the optimum actuator locations of Inverted cosine curve were very close to the value of Umbrella deformation in the case of 2 actuators per half, but in the case of 3 actuators per half actuator 3 converged to a different value. This resulted in the global flatness of the Inverted curve in that case being compromised.

2. Selection of starting point

   The selection of starting point play a critical role in the outcome of the optimization. From the results obtained in Section F it is observed that each of the deformation curves consists of 2 local optima. These local optima are the one which are known to us as per the investigation done through multiple runs by changing the initial starting points. There needs further exploration and a holistic approach in defining the starting point for such problems with high number of design variables. Since no information of the global optimum is known, results obtained in the case of 2 actuators per half it can be concluded that the optimum actuator locations are in the vicinity of the global optima parameters. However in the case of 3 actuators per half the number of design variables increase resulting in increased dimension of the optimization problem. Therefore the chances of the problem converging to a local optimum becomes higher.

3. Convergence to local optimum

   The results from the individual optimizations in Section E when compared with the analysis performed in Section G and it was found that in the case of edge based deformation curves the optimizer converged to a local optimum. This was also observed when the data from the analysis was compared with the 3 actuator per half combined optimization results. The results show convergence to a different optimum location value of l_3 in Table 4.10 as compared to the value obtained in Table 4.11. This variation in the optimum results occur due to convergence of the solution to a local optima. There needs to be further investigation on the choice of optimizer to solve this problem.

4. Effect of number of actuators

   The results obtained from the combined optimization show that as the number of actuators increases, the chances of the optimization to converge to a local optimum increases. This effect of local convergence can be seen from the results of 3 actuators per half case wherein, the estimated values of the design variables obtained in Table 4.10 are different as compared to Table 4.11. This is due to increase in the number of actuators resulting in the increase in number of design variables. However, in both cases the value of the objective function is in similar range, which means that one optimization problem can have multiple best local optimum. There needs further investigation on the nature of the optimization when the number of actuators are further increased and the effect that it will have when this case study is considered in 3D.

I CONCLUSION

This chapter focused on flatness correction of a deformed surface. The correction involved considering a wafer table of a wafer stage system. The wafer table analysis was through a case study from ASML lithography machines. The surface deformations were corrected by incorporating piezoelectric actuators under the wafer table. The flatness estimation of the wafer table was achieved by incorporating an optimization involving global flatness (MZ value) correction as an objective function.

In this chapter, global flatness was considered over local flatness errors. The choice of global flatness as an objective was due to the ease in definition of its sensitivities. In the case of local flatness, the definition of sensitivities is quite complex, since it includes deriving sensitivities of absolute maximum obtained from absolute maxima which were calculated from multiple least square fits. Therefore, global flatness was chosen over local flatness as the objective for actuator placement optimization.

The results obtained by placement of actuators indicated different optima for each of the deformation curves. The results show that the selection of starting point play a critical role in defining the outcome of the optimization. Also, it was observed that the chances of edge based deformation to converge to a local optima were higher than that of center based deformation. Based on the results obtained, an analysis for optimum location of actuators under the wafer table was made considering each of the four deformations and estimating the optimum actuator locations. The optimum actuator location range obtained from this analysis was then verified by implementing a combined optimization. The results obtained showed that in the case of 2 actuators per half the convergence can be considered fairly close to the global optimum. However in the case of 3 actuators per half, the dimension of the problem was very large (19 design variables) which caused one of the design variable to converge to a different value than the expected range. However, the optimization results lead to fairly good global flatness values, a further investigation on the incorporation of a robust algorithm or a stochastic optimization technique is needed that has the capability to handle high dimensional problem. The future scope of actuator placement can also be extended to other deformation curves thereby making the actuators susceptible in correcting all types of deformations.

5

CONCLUSION AND RECOMMENDATIONS

This chapter involves the conclusions drawn from the research conducted in the previous chapters. The conclusions drawn in this chapter are based on the results obtained in achieving the goal of designing a short stroke wafer stage system. The final section of this chapter involves recommendations for future work and the possible investigation of topics encountered during the conduct of this research.

A CONCLUSION

The research presented in this thesis revolved around the design of a short stroke wafer stage system of a lithography machine. The objective of the research involved the design of an intermediate body using topology optimization, scanning for the deformation errors on the wafer table, and defining the actuator positions on the intermediate body. The topology optimization involved incorporating a density-based approach using the SIMP method. A gradient-based optimization was performed by incorporating the MMA optimizer. Next, the scanning of a deformed surface involved recording errors using a global scanning algorithm (MZ) and a local scanning algorithm (LSF). The scanning algorithms were implemented on a deformed wafer table and the effect of surface resolution on the scanning errors was studied. Finally, an optimization problem was formulated to reduce the scanning errors of the wafer table. The reduction in errors involved incorporating piezoelectric actuators under the wafer table. The optimization involved undertaking the location and force of actuators as the design variables. Based on the research conducted, from each of the three sub-tasks mentioned, the following conclusions are drawn:

1. **Topology optimization of intermediate body**

   The results obtained by implementing weighted sum multi-objective formulation involved encountering scaling issues. Also, this method involves assigning weights to the objective functions. The choice of weights assignment depended on the designer which largely affects the outcome of the optimization. The scaling and optimization of two objectives; in this thesis - compliance and eigenfrequency resulted in stagnation in the values of the individual objectives in a specific weight range. This occurs due to differences in the order of magnitudes of the individual objective functions resulting in the effect of one of the objective not affecting the outcome of the optimization. Therefore, the weighted multi-objective approach was converted to a single objective approach using the ϵ-constraint method. Further investigation is required to study the effect of different multi-objective optimization formulations on the outcome of the optimization design of the structure. Also, better scaling strategies can be incorporated that would better define the final objective. Apart from that, it was also observed that an intermediate body of mass 8 kg might be better as compared to the current 6.5 structure. However, the selection will be based on the transmissibility of disturbances from the long stroke system.

2. **Surface deformation scanning algorithms**

   The flatness of a deformed surface can be estimated by 2 types of scanning; 1) Global scanning, 2) Local scanning. In the case of global scanning, a peak to base value defined the flatness of the surface. In the case of a local scan, the value of scanning errors depends on the size of the scanner. The smaller the scanner, the less are the sampling points to contain, the better is the alignment and the lower is the LSF score. The definition of the flatness property of a surface depends on the scanning value obtained from either scanning method. However, the global scanning methods provide a better outlook of the deformation of the surface, since they considered the entire surface at once. The local scanning algorithm (LSF) explained in this thesis involved a complex procedure. Also, the LSF algorithm provided a non-smooth error plot with sharp peaks thereby making it complex to define its sensitivity. Therefore, while defining an optimization problem function, the objective must be to focus on the global scanning of the surface with the local scanning value in the hindsight. After getting an estimation of the surface fatness, an attempt to rectify the deformations was done by placing piezoelectric actuators under the wafer table. The rectification largely depended on the force exerted by the actuators.

3. **Actuator placement optimization for deformation correction**

   Global flatness value (MZ value) was chosen as an objective function over local flatness value (LSF score) due to the complexities in defining the sensitivities of the scanning algorithm. During the decision on the number of actuators to involve for flatness correction, a center actuator was also stationed. The center actuator proves beneficial in providing stability to the structure, thereby enhancing its eigenfrequency and also assisting in reducing the global deformation value. The case of a perfectly flat surface can be achieved by placing an infinite number of actuators under the surface, however, practically this is not feasible. An optimum flat surface is dependent on the number of actuators. More the actuators, better is the overall flatness of the surface. The results obtained from the combined optimization showed that the deformations were 95 % corrected and the flatness of the surface was improved. The interpolation function incorporated provided better results (MZ value = 21.829 nm) in comparison to the nodal point forces from the brute force method (MZ value = 24.876 nm). From the optimization for individual deformation curves, it was observed that the edge-based deformations always converged to a local optimum. Further analysis proved that each of the deformation curves consists of 2 known local optima which depended on the choice of the starting point. This makes the selection of starting point extremely critical. The results obtained from the optimizations were analyzed by implementing a combined optimization for 2 actuators per half and 3 actuators per half cases. The results obtained from these optimizations showed that in the former case the convergence can be assumed very close to the global optimum as the optimum actuator value were very close to the expected range. However, in the case of 3 actuators per half, it was seen that one of the actuators was placed at a different location than expected. One of the reasons for this behaviour is the high dimension of the problem (19 design variables). Therefore, further investigation is required in the choice of the optimizer such that the optimization can converge to a global optimum.

In this thesis, the implementation of the concepts were done on a wafer table of a lithography machine. The research conducted in this thesis and the optimization problem defined can be translated to any structure that is deformed from its initial state. The actuator optimization can be implemented in correcting the deformations of such deviated structure.

B RECOMMENDATIONS

The results obtained in the design of a short stroke wafer stage system involving design of intermediate body and deformation corrections are subject to further investigations. The investigations mainly include implementations, wherein the definition of a combined optimization and the

reduction in computational time can be the primary inhibitors for extension of the problem to a 3-dimensional setting.

- **Topology optimization of intermediate body**
  The results obtained from the optimization involved converting a multi-objective problem to a single objective problem. It might be interesting to investigate other multi-objective formulations, thereby also extending the research to check the design outcome when the multi-objective problem is defined with some other optimizer. In this thesis, the design was subject to static boundary conditions. It might be interesting to further evaluate the design by defining it in a dynamic domain subjected to external vibrations. Apart from the investigations associated with the problem formulation, the current optimization can also be extended to a 3-dimensional domain.

- **Surface scanning & error quantification**
  The extension of the LSF algorithm to 3D might be an interesting aspect in understanding the effect of the algorithm on the local errors when compared with the results obtained in 2D. Being a complex algorithm in implementation, it is important to investigate the changes in the scanning error when the incrementors are removed and the scanning is dependent purely based on the dimension of the scanning slit.

- **Actuator placement optimization for deformation correction**
  This research focused on superimposing the surface with deformations that were symmetric along their axis. Therefore, it might be interesting to investigate the outcome of the optimization when asymmetric curves are superimposed on the surface. One possible issue that might be encountered in asymmetric curves is the generation of moments on the structure. In the case of asymmetric curves, the criteria of moment balancing will come picture. It might be worthwhile to define a problem where this factor is taken care of. Another important aspect to focus on is the implementation of the interpolation function. In this application, the interpolation was done between two sampling points. This can be further extended by interpolating the actuator properties to 4 or more sampling points. This might also assist in solving the local optima issues.

- **Choice of the optimizer**
  It is seen that the results of the optimization are based on the convergence to a local optimum. The optimization can be further investigated by incorporating other optimizer like the implementation of genetic algorithm or a particle swarm approach. It might be interesting to check the convergence of the problem and the handling of such high dimension problem when it is optimized with genetic algorithms.

- **Actuator placement optimization in 3D**
  The extension of actuator optimization in 3D remains an interesting and challenging area of implementation and research. The extension in 3D can be coupled with superimposing other deformation curve types. The reference of other deformation curves could be taken from Zernike polynomials.

- **Combined optimization - Intermediate body + Actuator placement**
  The entire thesis revolved around the design of a short stroke system. The sub-problems involved in the main research goal were analyzed and studied separately. In actuator optimization the intermediate body was considered to be infinitely stiff. Therefore, the effect of stiffness of the intermediate body on actuator location was not being explored. It will be interesting to combine the approaches studied in this thesis to one big optimization problem wherein the problem definition would include design of an intermediate body along with the placement of the actuators. This recommendation will include implementation both in 2D and 3D.

Bibliography

[1] A. Suleman, E. Prasad, R. Blackow, D. Waechter. "Smart Structures — an Overview". In: *Smart Structures:Applications and Related Technologies* (2001), pp. 3–16. DOI: 10.1007/978-3-7091-2686-8_1.

[2] M.M.A. Steur. "Design of an active wafer clamp for wafer machines". PhD thesis. Technische Universiteit Eindhoven - Mechanical Engineering, Nov. 2017. ISBN: 978-90-386-4360-1.

[3] K. Tahara, H. Matsuoka, N. Morioka, H. Tsunaki, M. Kannaka, T. Kita. "Determination of silicon wafer site flatness using dual heterodyne interferometers with sub-nanometer precision". In: *Review of Scientific Instruments* 91 (6 June 2020). DOI: 10.1063/1.5143534.

[4] M. Bendsoe and O. Sigmund. *Topology Optimization - Theory, Methods and Applications.* Springer Berlin, Heidelberg, 2004. DOI: 10.1007/978-3-662-05086-6.

[5] O. Sigmund. "On the usefulness of non-gradient approaches in topology optimization". In: *Springer Verlag* 43 (2011), pp. 589–596. DOI: 10.1007/s00158-011-0638-7.

[6] K. Svanberg. "The method of moving asymptotes—a new method for structural optimization". In: *International Journal for Numerical Methods in Engineering* 24 (2 1987). DOI: 10.1002/nme.1620240207.

[7] G. Rozvany. "The SIMP method in topology optimization - Theoretical background, advantages and new applications". In: *8th Symposium on Multidisciplinary Analysis and Optimization* (2000). DOI: 10.2514/6.2000-4738.

[8] M.Sotola, P. Marsalek, D. Rybansky, M. Fusek, D. Gabriel. "Sensitivity analysis of key formulations of topology optimization on an example of cantilever bending beam". In: *Symmetry* 13 (4 2021). DOI: 10.3390/sym13040712.

[9] R. T. Marler, J. S. Arora. "The weighted sum method for multi-objective optimization: new insights". In: *Structural and Multidisciplinary Optimization* 41 (2010), pp. 853–862. DOI: 10.1007/s00158-009-0460-7.

[10] Z. D. Ma, H. C. Cheng and N. Kikuchi. "Structural design for obtaining desired eigenfrequencies by using the topology and shape optimization method". In: *Computing Systems in Engineering* 5 (1 1994). DOI: 10.1016/0956-0521(94)90039-6.

[11] G. Mavrotas. "Effective implementation of the -constraint method in Multi-Objective Mathematical Programming problems". In: *Applied Mathematics and Computation* 213 (2 July 2009), pp. 455–465. DOI: 10.1016/J.AMC.2009.03.037.

[12] J. Du, N. Olhoff. "Topological design of freely vibrating continuum structures for maximum values of simple and multiple eigenfrequencies and frequency gaps correction". In: *Structural and Multidisciplinary Optimization* 34.6 (2007), pp. 545–545. DOI: 10.1007/s00158-007-0167-6.

[13] H. Takeishi, S.V. Sreenivasan. "Nanoimprint system development and status for high volume semiconductor manufacturing". In: *Alternative Lithographic Technologies VII* 9423 (2015). DOI: 10.1117/12.2087017.

[14] K. T. Turner, S. Veeraraghavan, J. K. Sinha. "Predicting distortions and overlay errors due to wafer deformation during chucking on lithography scanners". In: *Journal of Micro/Nanolithography, MEMS, and MOEMS* 8 (4 Oct. 2009), p. 043015. DOI: 10.1117/1.3247857.

[15] K. Tahara, H. Matsuoka, N. Morioka, and M. Kannaka. "Site flatness measurement system with an accuracy of sub-nanometer order for silicon wafer". In: *R and D: Research and Development Kobe Steel Engineering Reports* 65.2 (2015), pp. 87–91.

[16] H. Shu, C. Zou, J. Chen, and S. Wang. "Research on Micro/Nano Surface Flatness Evaluation Method Based on Improved Particle Swarm Optimization Algorithm". In: *Frontiers in Bioengineering and Biotechnology* 9 (Dec. 2021), p. 1108. DOI: 10.3389/fbioe.2021.775455.

[17] E. Fernández, F. Fernández, M. Collet, H. Tsunaki, P. Alarcón, A. Alarcón, S. Bauduin, P. Duysinx. "An aggregation strategy of maximum size constraints in density-based topology optimization". In: *Structural and Multidisciplinary Optimization* (Nov. 2019). DOI: 10.1007/s00158-019-02313-8.

[18] M. Zhang, Y. Yang, H. Zhang , D. Zhang , F. Shen. "L2,p-norm and sample constraint based feature selection and classification for AD diagnosis". In: *Neurocomputing* 195 (2016), pp. 104–111. DOI: https://doi.org/10.1016/j.neucom.2015.08.111.

A

APPENDIX:TOPOLOGY OPTIMIZATION

This appendix contains calculation of the maximum weight of the intermediate body. It also includes the change in compliance of the structure when the thickness of the wafer table is assigned a different value. Finally a discussion on scaling issues associated with multi-objective formulation is included.

Calculation of m_{max}

In this thesis the maximum weight of the intermediate (m_{max}) was assigned as 6.4 kg. This value depended largely on the choice of the thickness of the wafer table which was taken as 7 mm in the optimization. From Equation 2.4 and the total weight condition, the weight of the intermediate body is calculated as follows:

$$\frac{WT + W}{InB} = \frac{1}{4}$$
$$WT + InB \approx 8$$

Here taking standard values of a 300 mm diameter silicon wafer. The weight of the wafer (W) is assigned as 0.125 gram.

$$\frac{8 - InB + 0.125}{InB} = \frac{1}{4}$$
$$InB \approx 6.5 \text{ kg}$$

Wafer table thickness v/s Compliance

The thickness of the wafer table can be ranged from 5 mm to 10 mm. The change in the compliance of the intermediate body depending on the change in the wafer table thickness is shown in Table

Wafer table thickness (mm)	Compliance (m/N)
5	7.775×10^{-7}
6	9.766×10^{-7}
7	1.162×10^{-6}
8	1.434×10^{-6}
9	1.697×10^{-6}
10	1.998×10^{-6}

Table A.1: Effect of wafer table thickness on the compliance of the structure

Issues in weighted sum approach

The initial problem formulation of the structural optimization included implementation of weighted sum multi-objective approach. The weighted sum approach is the most commonly used approach for multi-objective formulation. However, there exists some issues in this approach which largely influence the outcome of the optimization. The issues encountered are as follows:

1. Dependency on the weights

   As represented in Figure 2.4, the value of compliance and eigenfrequency changes as per the assigned weight. This assignment of weight is as per the priority that the designer decides. If the objective priority information is not known to the designer it might lead to improper distribution of weights leading to biased sampling.

2. Scaling issues

   Figure 2.4 also represents the range of compliance and eigenfrequency values. In this optimization both the objectives were scaled and then added using the weighted sum approach. However, it can be seen that the compliance value are 10^2 higher than the eigenfrequency values. This means that if the compliance values are scaled from 0 to 100, then the eigenfrequency values must be scaled from 0 to 1. This would result in the compliance objective dominating the final multi-objective formulation.

B

APPENDIX:LSF

This appendix contains The LSF error plots and the LSF error extract plot of all the deformations mentioned in Chapter 3. The plots included in this Appendix resemble the error extracts for 310 mm diameter wafer table.

LSF plots

Cosine deformation

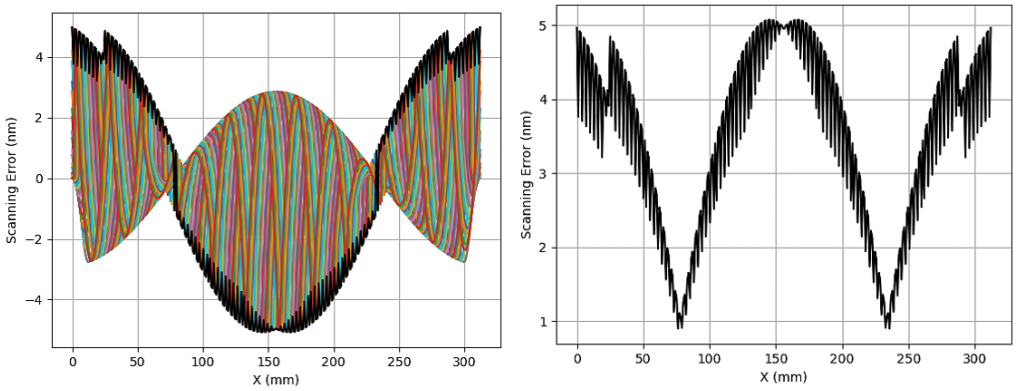

(a) LSF scanning error plot (b) LSF error extract

Figure B.1: LSF plots - Cosine deformation | *LSF score: 5.0751 nm*

Bowl deformation

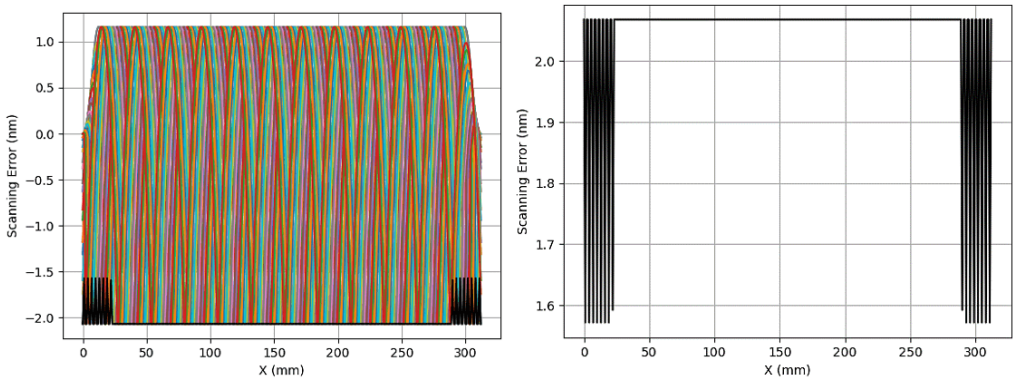

(a) LSF scanning error plot (b) LSF error extract

Figure B.2: LSF plots - Bowl deformation | *LSF score: 2.0678 nm*

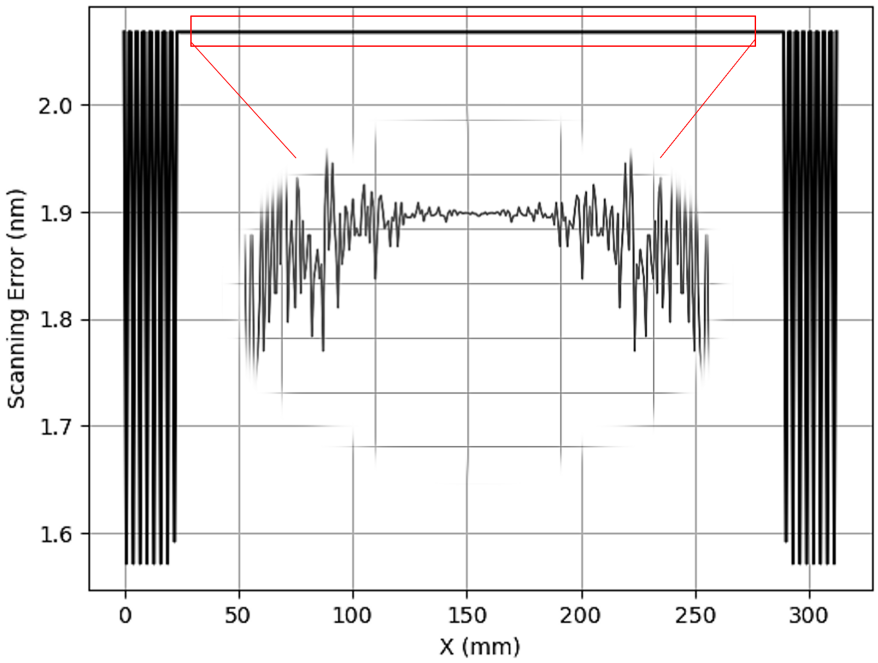

Figure B.3: Error plot of mid region - Bowl

3^{rd} order deformation

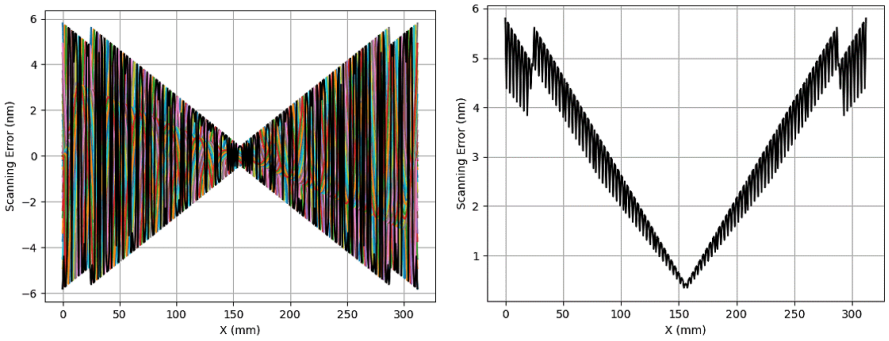

(a) LSF scanning error plot (b) LSF error extract

Figure B.4: LSF plots - 3^{rd} order deformation | *LSF score: 5.7964 nm*

4^{th} order deformation

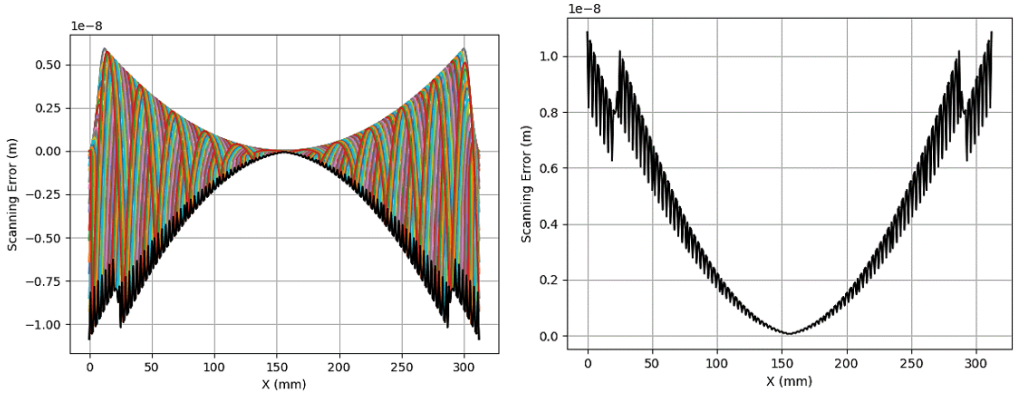

(a) LSF scanning error plot (b) LSF error extract

Figure B.5: LSF plots - 4^{th} order deformation | *LSF score: 10.8458 nm*

C

APPENDIX: ACTUATOR OPTIMIZATION

This appendix contains the optimization plots for 2 actuators per half and 3 actuators per half cases. The plots show the variation in the design variables as the optimization converges. Furthermore, this appendix includes the actuator forces obtained from the analysis performed in Chapter 4 - Section G.

Plots - 2 actuators per half

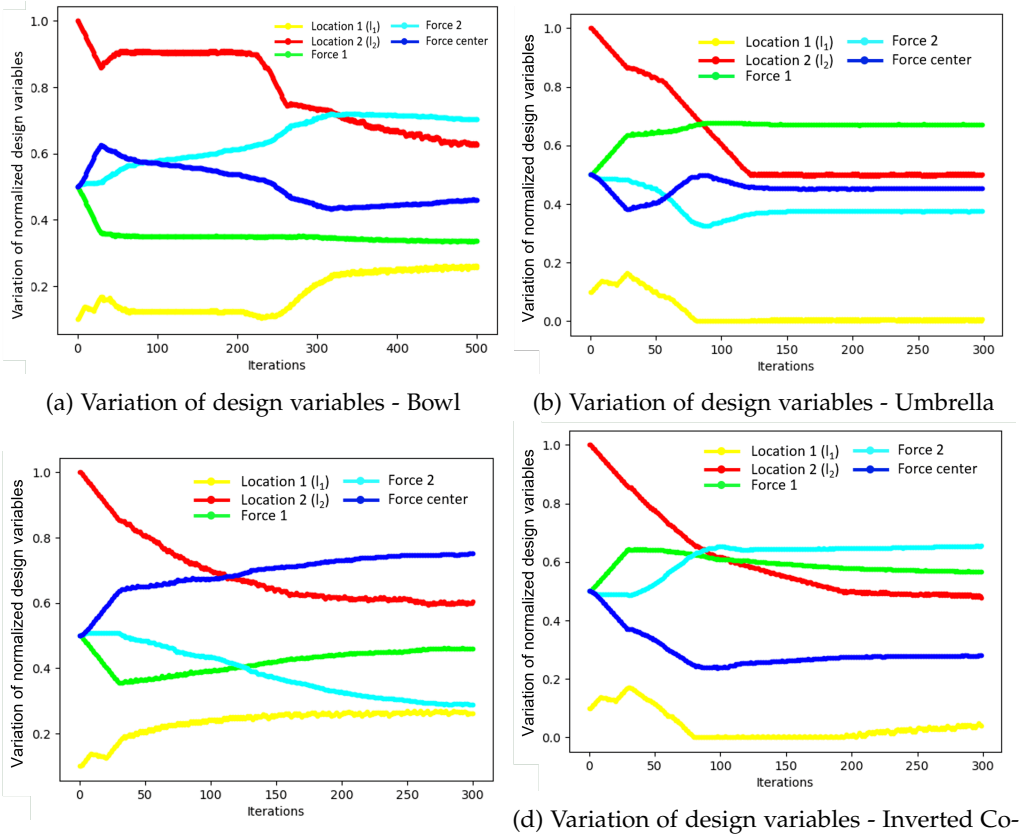

(a) Variation of design variables - Bowl

(b) Variation of design variables - Umbrella

(c) Variation of design variables - Cosine

(d) Variation of design variables - Inverted Cosine

Figure C.1: Variation of design variables during optimization - 2 actuators per half

Plots - 3 actuators per half

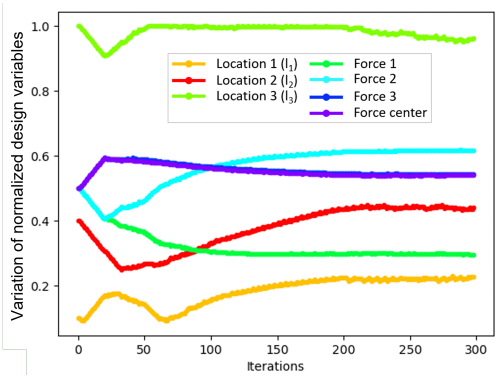

(a) Variation of design variables - Bowl

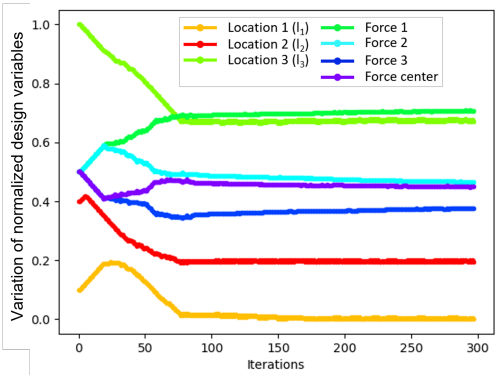

(b) Variation of design variables - Umbrella

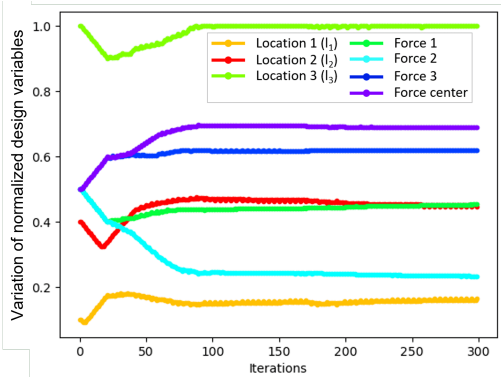

(c) Variation of design variables - Cosine

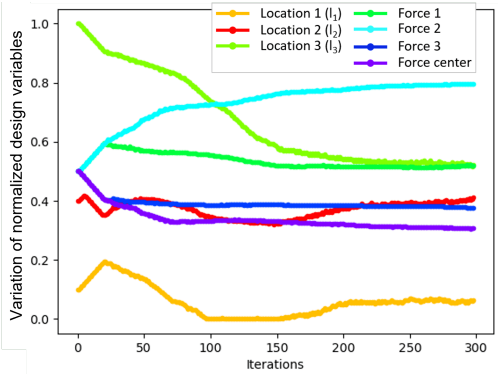

(d) Variation of design variables - Inverted Cosine

Figure C.2: Variation of design variables during optimization - 3 actuators per half

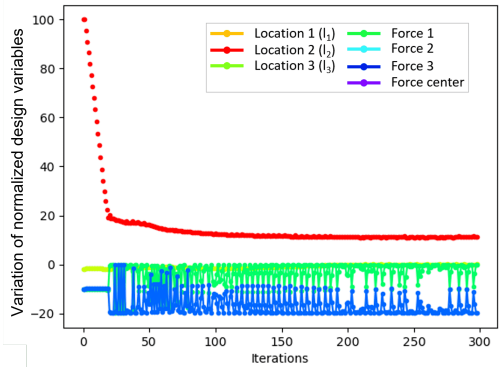

(a) Convergence - Bowl

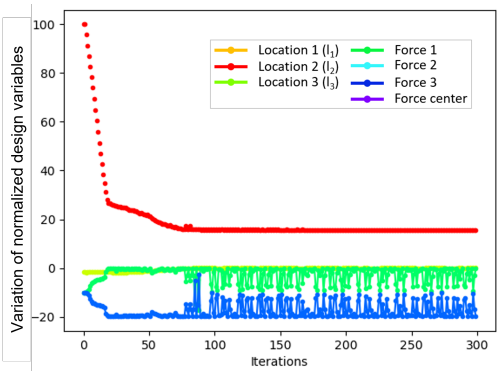

(b) Convergence - Umbrella

Figure C.3: Convergence plots - 3 actuators per half

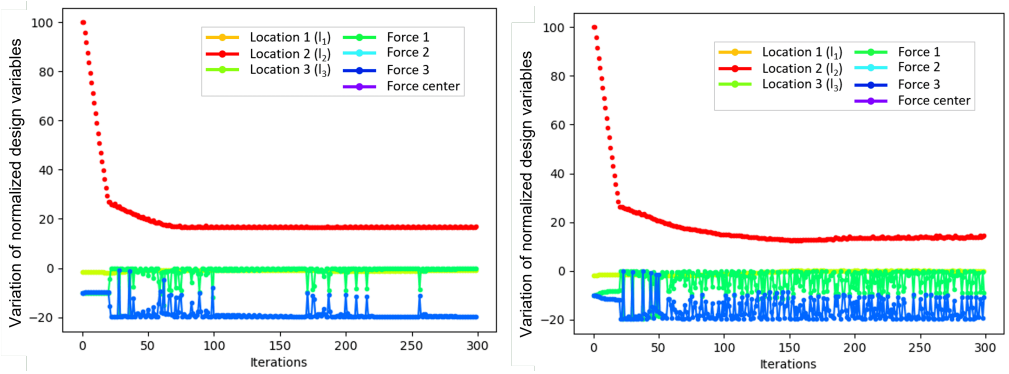

(a) Convergence - Cosine

(b) Convergence - Inverted Cosine

Figure C.4: Convergence plots - 3 actuators per half

Analysis Data - 2 actuators per half

Bowl

Reference	l_1 (mm)	l_2 (mm)	F_1 (N)	F_2 (N)	F_m (N)	**MZ** (nm)	**LSF** (nm)
A	31.07	109.57	−30.09	41.64	−11.64	34.420	2.157
B	0.31	74.55	−30.14	20.44	9.60	15.424	1.692
C	39.30	90.63	−32.83	38.03	−5.29	37.858	2.216
D	6.61	72.58	−29.18	20.42	8.66	16.535	1.908

Table C.1: Obtained values of the design variables - Bowl

Umbrella

Reference	l_1 (mm)	l_2 (mm)	F_1 (N)	F_2 (N)	F_m (N)	**MZ** (nm)	**LSF** (nm)
A	31.07	109.57	−29.25	43.35	−13.99	34.420	2.157
B	0.31	74.55	34.05	−24.69	−9.42	14.924	1.769
C	39.30	90.63	−29.47	31.54	−1.96	32.978	2.054
D	6.61	72.58	32.76	−23.46	−9.40	15.059	1.929

Table C.2: Obtained values of the design variables - Umbrella

Cosine

Reference	l_1 (mm)	l_2 (mm)	F_1 (N)	F_2 (N)	F_m (N)	**MZ** (nm)	**LSF** (nm)
A	31.07	109.57	−18.07	−55.87	73.85	64.825	5.044
B	0.31	74.55	−12.27	−32.20	44.37	44.235	4.736
C	39.30	90.63	−7.99	−42.29	50.18	57.115	4.954
D	6.61	72.58	−9.75	−33.73	43.39	44.648	4.852

Table C.3: Obtained values of the design variables - Cosine

Inverted cosine

Reference	l_1 (mm)	l_2 (mm)	F_1 (N)	F_2 (N)	F_m (N)	**MZ** (nm)	**LSF** (nm)
A	31.07	109.57	−17.70	−51.03	68.84	68.175	4.980
B	0.31	74.55	15.66	29.30	−45.07	44.043	4.643
C	39.30	90.63	−6.03	−46.19	52.32	63.434	4.980
D	6.61	72.58	13.09	30.87	−44.06	43.792	4.831

Table C.4: Obtained values of the design variables - Cosine

Analysis Data - 3 actuators per half

Bowl

Reference	l_1 (mm)	l_2 (mm)	l_3 (mm)	F_1 (N)	F_2 (N)	F_3 (N)	F_m (N)	**MZ** (nm)	**LSF** (nm)
X	32.66	65.79	143.25	−40.75	23.94	8.66	8.06	22.50	2.177
Y	0.76	30.03	101.59	35.24	−2.87	−22.087	−10.17	10.76	1.543
Z	24.18	67.70	149.99	−36.56	16.88	11.31	8.26	21.24	2.126
W	9.49	61.58	78.26	33.53	−18.09	−7.43	−7.90	13.938	1.976

Table C.5: Analysis Data - 3 actuators per half

Umbrella

Reference	l_1 (mm)	l_2 (mm)	l_3 (mm)	F_1 (N)	F_2 (N)	F_3 (N)	F_m (N)	**MZ** (nm)	**LSF** (nm)
X	32.66	65.79	143.25	−38.383	22.84	10.29	5.34	22.911	2.054
Y	0.76	30.03	101.59	41.46	−6.91	−24.60	−10.03	6.176	1.469
Z	24.18	67.70	149.99	−36.66	19.30	12.38	5.074	19.825	2.057
W	9.49	61.58	78.26	35.18	−20.00	−4.47	−10.79	13.627	1.974

Table C.6: Analysis Data - 3 actuators per half

Cosine

Reference	l_1 (mm)	l_2 (mm)	l_3 (mm)	F_1 (N)	F_2 (N)	F_3 (N)	F_m (N)	**MZ** (nm)	**LSF** (nm)
X	32.66	65.79	143.25	−0.56	−60.81	29.51	31.77	46.651	4.954
Y	0.76	30.03	101.59	17.84	−70.55	17.71	34.89	11.889	3.593
Z	24.18	67.70	149.99	−9.18	−53.02	23.91	38.18	44.917	4.492
W	9.49	61.58	78.26	0.01	−83.24	51.68	31.47	30.382	4.824

Table C.7: Analysis Data - 3 actuators per half

Inverted Cosine

Reference	l_1 (mm)	l_2 (mm)	l_3 (mm)	F_1 (N)	F_2 (N)	F_3 (N)	F_m (N)	**MZ** (nm)	**LSF** (nm)
X	32.66	65.79	143.25	−0.41	−58.17	27.645	31.04	51.462	4.980
Y	0.76	30.03	101.59	12.02	−66.95	20.80	34.21	16.106	3.656
Z	24.18	67.70	149.99	−2.022	−76.48	43.13	35.42	30.435	4.830
W	9.49	61.58	78.26	4.19	59.23	−24.74	−38.74	33.144	4.847

Table C.8: Analysis Data - 3 actuators per half